COMBATING INFECTION AND PROMOTING HEMOCOMPATIBILITY IN MEDICAL DEVICES USING ANTIFOULING AND NITRIC OXIDE RELEASING STRATEGIES

by

PRIYADARSHINI SINGHA

(Under the Direction of Hitesh Handa)

ABSTRACT

Implanted medical devices, such as catheters, vascular grafts, and stents face critical challenges even as they are used in several thousand patients each year. The implanted materials are subjected to fundamentally critical challenges caused by thrombosis and infections. While thrombosis can cause subsequent device-failure accompanied by embolism and even deaths; a device that is not able to provide anti-infection properties can easily be contaminated through the microflora present on the skin of the patient and cause devastating problems such as bloodstream infections. 1.7 million cases of hospital-acquired infections in the U.S. alone cause approximately 99,000 deaths annually. These complications contribute to an annual expenditure of $28.4 to $33.8 billion in direct medical costs. Thus, these numbers have warranted a plethora of research to combat medical device associated thrombosis and infection. While an assortment of prevention methods has been researched and designed to create antithrombotic and antimicrobial materials, the search for the elusive ideal material that can provide a robust biocompatible environment remains active.

Among the front runners in this quest for biocompatibility is the small endogenous gaseous molecule, nitric oxide (NO). It is a unique molecule that can offer both antimicrobial

and antithrombotic properties to the material that it is incorporated in. Nitric oxide's multi mechanism-based antimicrobial strategies can be bactericidal towards the commonly found nosocomial pathogens *Staphylococcus aureus*, *Pseudomonas aeruginosa*, and *Escherichia coli* etc., and the antithrombotic properties have been known to be effective in both *in vitro* and *in vivo* environments for catheters and extracorporeal circulation. However, NO releasing materials cannot repel proteins, which are the most important biomacromolecules involved in biocompatibility for long term applications. Without antifouling properties, the surfaces can be easily fouled over time with proteins and start the coagulation cascade or allow resistant bacteria to settle down on the material's surface. This dissertation serves as a study to improve upon various NO releasing materials' biocompatibility properties by coupling it with different antifouling strategies, thus paving the way towards a biocompatible environment for improved functioning of the medical device.

INDEX WORDS: Hemocompatible, biocompatible, antimicrobial, nitric oxide, antifouling, medical devices

COMBATING INFECTION AND PROMOTING HEMOCOMPATIBILITY IN MEDICAL DEVICES USING ANTIFOULING AND NITRIC OXIDE RELEASE STRATEGIES

by

PRIYADARSHINI SINGHA

BE, M.V.J. College of Engineering, India, 2012

MS, University of California-Irvine, 2014

A Dissertation Submitted to the Graduate Faculty of The University of Georgia in Partial Fulfillment of the Requirements for the Degree

DOCTOR OF PHILOSOPHY

ATHENS, GEORGIA

2019

COMBATING INFECTION AND PROMOTING HEMOCOMPATIBILITY IN MEDICAL DEVICES USING ANTIFOULING AND NITRIC OXIDE RELEASE STRATEGIES

by

PRIYADARSHINI SINGHA

Major Professor:	Hitesh Handa
Committee:	Vincent J. Starai
	Eric Freeman

Electronic Version Approved:

Suzanne Barbour
Dean of the Graduate School
The University of Georgia
May 2019

DEDICATION

This dissertation is dedicated to my parents for providing me the opportunities in which I could choose my dreams and for believing in me during the darkest days. You are the reason that I have been able to go this far and have the courage to always strive for the best. All of this has been worth it.

ACKNOWLEDGEMENTS

First and foremost, I would like to thank my mentor and friend, Dr. Hitesh Handa. From the first day in Athens, you made me realize that a place so far from home could become your second home. In research and personal growth, you are a perfect example of a person who can be disciplined, kind, and achieve so much by being humble. Your approachable demeanor has made it possible for me to have conversations regarding research, career, and personal experiences. Being a dreamer is easy but being a realist dreamer like you can only be learned from mentors. Thank you for being an honest and a supporting mentor! I know we will always be rooting for each other.

I would like to convey my past- and present lab members particularly Marcus Goudie, Sean Hopkins, Joel Mansfield, Jennie McCarty, Lori Estes, Mark Garren for working with me with a true team spirit and sharing some enjoyable moments outside lab. Finding friends among competing lab members is uncommon and you have been consistently there for me throughout my graduate studies at UGA.

Next, I would like to thank Dr. Jason Locklin, for introducing me to the Riverbend South Research building and taking me under his wing when I joined UGA in 2015. Even though we parted ways as co-advisor and mentee, your insightful advice on research has helped me throughout my Ph.D. I would also like to thank Locklin lab members: Qiaohong Liu, Li Chen, and Karson Brooks for training me on the fundamental characterization techniques in polymer chemistry.

I would like to thank my committee members, Dr. Vincent J. Starai and Dr. Eric Freeman. Your support for my Ph.D. research has been invaluable and your individual strengths as faculty members inspires me to continue research in academia and hope to someday be a faculty member too.

I would like to extend my thanks to Dr. Elizabeth Brisbois. Your hard work and diligence inspire me to have hopes on becoming a faculty member. I am glad that we have enjoyed some good times outside research at the many conferences we have been to. Talking about your experiences as you grew from being a Ph.D. candidate to a Postdoctoral researcher and now a faculty member at UCF has helped me learn the dynamics of different universities.

I would like to express my gratitude to all the collaborators for my research: Dr. Sudipta Seal and his lab, Dr. A. I. Batchinsky and his lab, Dr. V.J. Starai and Emma Brannon. I have learned about research outside of nitric oxide and medical device coatings because of you.

To all the staff members: Margaret Sapp, Patsy Adams, Ellen King – thank you for all the administrative help! My course requirements and lab supply for research would not be sorted without you.

A big thank you to Dr. James Warnock, Dr. Lawrence Hornak, and Dr. Donald Leo for providing the leadership at a time when the College of Engineering is growing tremendously fast. Without your support, we would all be lost researchers.

I would like to express my gratitude to my sister, Nandini Singha and my significant other, Tadeusz McMahon. You have both helped me look at and enjoy life outside of research. As Ph.D. students, we sometimes become so invested in work that we forget to experience some of the intangible joys in life. Hiking and road tripping with both of you has helped relieve so much of the stress!

TABLE OF CONTENTS

Page

LIST OF TABLES

Page

LIST OF FIGURES

Page

CHAPTER 1

INTRODUCTION AND LITERATURE REVIEW

Introduction

Despite decades of research and development to create an ideal hemocompatible and antimicrobial biomaterial, researchers are still far from conquering the critical problem. Hemocompatibility is the term to describe a material that does not illicit any adverse reactions when in contact with blood. Adverse reactions include thrombosis and fouling of the device leading to occlusion. It is one of the most important criteria for successful clinical applications of biomaterials.[1] The term antimicrobial on the other hand is given to a material that can either prevent the adhesion of microbes on its surface (i.e. antifouling) or kill the microbes (i.e. bactericidal).[2] It is also important to note here that the term antifouling is for a surface that can prevent adhesion of any kind of biomacromolecule including proteins, blood cells, and bacteria. Therefore, fouling is the common problem that leads to thrombosis and infections and is currently the most common cause of complications in clinical settings. According to the Centers for Disease Control and Prevention, an estimated 687,000 healthcare-associated infections were reported in U.S. acute care hospitals in 2015 which led to approximately 72,000 deaths. Every day, about one in 31 patients have at least one HAI. While these numbers have fallen slightly over the years, the cost and number of deaths from HAIs is still significantly high.

The following sections introduce and provide literature review of the two categories of biomaterials that can reduce the instances of infection and thrombosis: i) nitric oxide (NO) releasing materials ii) passive antifouling strategies.

Nitric oxide releasing materials

Awarded as the "Molecule of the Year" in 1992 by the American Association for the Advancement of Science, nitric oxide (NO) has been studied since the 1980s, as an important signaling molecule for various physiological and pathological functions.[3] This announcement was followed by a flurry of experiments and discoveries which led to the 1998 Nobel Prize in Physiology or Medicine to be awarded to Robert Furchgott, Louis Ignarro and Ferid Murad.[4] It was the first gas to be discovered as a biological messenger molecule and continues to surprise scientists with its potential applications. Nitric oxide is a free radical stable gas that is known to potentially inhibit platelet aggregation, promote angiogenesis, cause vasodilation, act as a neurotransmitter and an antimicrobial, and also have wound healing properties.[5] Thus, proving that the small gas molecule is highly diffusible in the biological milieu.[6]

It has been understood that NO is physiologically produced via the enzymatic sequential oxidation of L-arginine by nitric oxide synthases (NOS) in endothelial cells (Figure 1.1). Once produced, it diffuses to the smooth muscle and subsequently binds to the heme iron on guanylate cyclase to activate it. Thus, performing its function as a vasodilator.[7] This production increases during infections via the catalytic activity of inducible nitric oxide synthase (iNOS or NOS2) and gives the characteristic of an antimicrobial to NO. There are 3 known isoforms of NOS found in mammals and 1 found in several bacterial species.[8, 9] For the purpose of this dissertation, we will focus only on the NO produced via catalytic activity of endothelial NOS (eNOS or NOS3) and iNOS. As discussed above, eNOS is responsible for vasodilation. The production of NO via eNOS is Ca^{2+} dependent and increases with increased Ca^{2+} or sometimes in response to Ca^{2+} independent stimuli like shear stress. This Ca^{2+} dependent eNOS release provides a basal release of NO. The iNOS enzyme is constitutively expressed only in the presence of inflammation and

therefore its production indicates either the presence of infection or autoimmune disorders. Thus, iNOS is released by the immune system and cardiovascular system for immune defense activities.

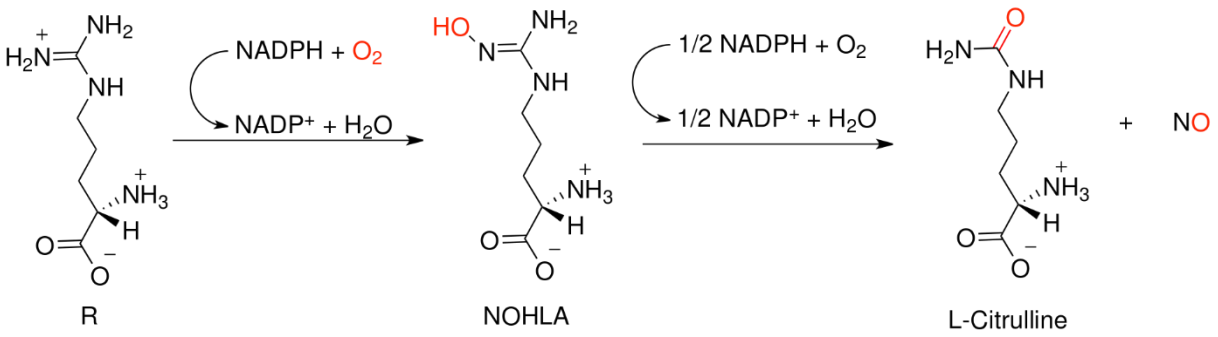

Figure 1.1: Endogenous NO production via enzymatic oxidation of L-arginine to N^{ω}-hydroxy-L-arginine (NOHLA) and then to L-Citrulline.

Originally known as the endothelium derived relaxing factor (EDRF), Radomski *et al*., Azuma *et al*., and Furlong *et al.* examined the role of NO as a vasodilator and inhibitor of platelet aggregation in 1987.[10-13] However, before it was demonstrated by Palmer *et al.* that the amount of NO released by the vascular endothelium accounted for the properties of the EDRF and thus NO was EDRF, Furchgott had demonstrated the function of EDRF as a vasodilator.[14, 15] This role of NO as an inhibitor of platelet aggregation is mediated via activation of guanylase cyclase by the production of NO and subsequent increased production of cyclic guanosine monophosphate (cyclic GMP). Radomski *et el.* studied the mechanism by activating the L-arginine-NO pathway through the introduction of platelets to aggregating agents and thus demonstrating that stimulation of the platelets led to a 100-fold increase in the resting

concentration of Ca^{2+} and this sharp increase in Ca^{2+} is what causes the production of NO by eNOS.[10, 11]

Nitric oxide released by iNOS has been found to have antimicrobial activity against a host of microbes including bacteria, viruses, fungi, and protozoa.[16] The enzyme iNOS is present in a host of immune cells especially macrophages and is activated in the presence of infection or inflammation and unlike NO produced by eNOS, this production is less susceptible to feedback inhibition by NO so that NO can be continually produced to defend against microbes.[17] Some of the potential antimicrobial mechanisms of NO include (Figure 1.2): i) nitrosation of thiols to alter protein function and catalyze disulfide bond formation ii)Reaction with cellular iron or iron-sulfur centers to inactivate essential enzymes iii) Reaction with superoxides to produce peroxynitrites which are highly reactive and toxic molecules to microbes iv) React directly with DNA and thus causes deamination and/or crosslinking of DNA.[16] Thus, due to NO's ability to diffuse through cellular membranes, it can do severe damage to microbial cells through nitrosative and oxidative stress.[17]

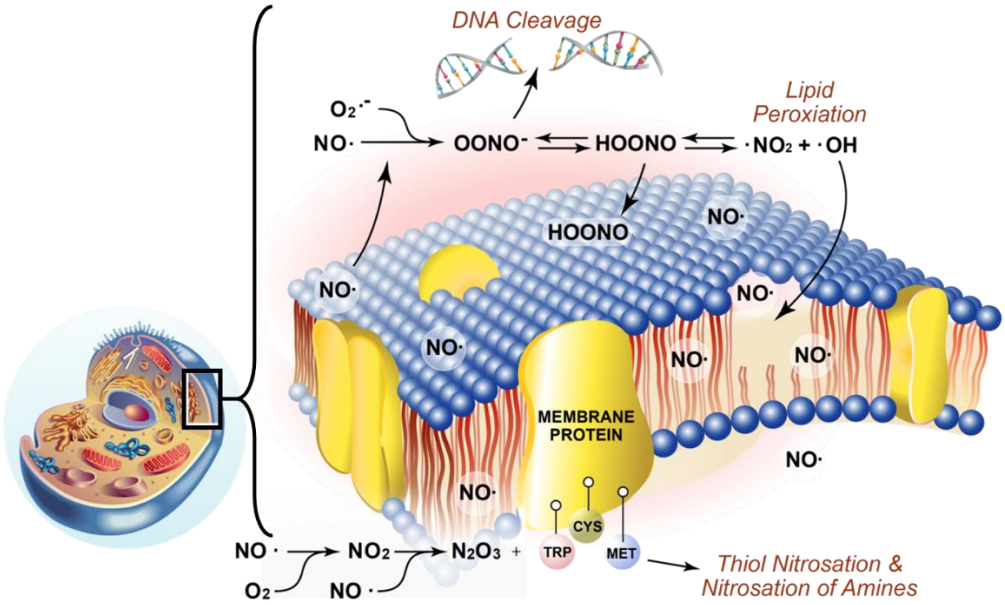

Figure 1.2: Antimicrobial mechanisms of nitric oxide

Being a fast-reacting free radical gas means that NO needs to be stored in stable conditions for it to be produced for various applications for different periods of time. Therefore, a way to mitigate this problem is to synthesize NO donors that can donate NO through thermal or photochemical self-decomposition (*S*-nitroso-*N*-acetylpenicillamine, diazeniumdiolate, oximes), enzymatic oxidation (N-hydroxyguanidines), and reaction with acids, alkalis, metals, or thiols (organic nitrates, nitrites, and syndnonimines). Some of the commonly used donors in biomaterials for both antithrombotic and antimicrobial functions include *S*-nitrosothiols (S-nitroso-*N*-acetylpenicillamine (SNAP), S-nitrosoglutathione (GSNO)) and diazeniumdiolated dibutylhexanediamine (DBHD/N_2O_2) (Figure 1.3).

In the last few years, numerous biomaterials with the potential to release NO for a myriad of applications have been developed. Most account for antithrombotic, antimicrobial, and wound healing applications.[18-32] Some of the most significant developments in antithrombotic and antimicrobial applications of NO releasing polymers include studies done with SNAP, GSNO and DBHD/N_2O_2 as NO donors.[33]

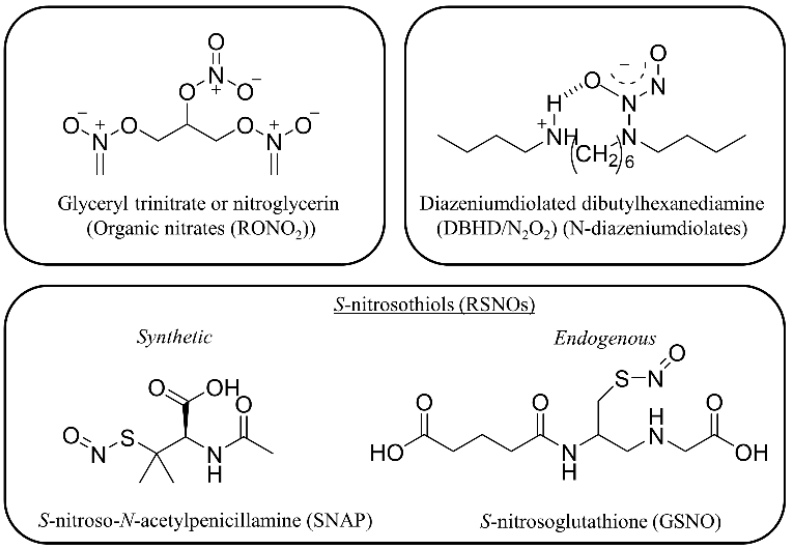

Figure 1.3: Commonly studied NO donors

The Meyerhoff group has studied several diazeniumdiolate-doped polymeric films for their NO-releasing potential.[26, 27, 34, 35] DBHD/N_2O_2 is a lipophilic NO donor that releases NO spontaneously through proton or thermal driven mechanisms.[27] While hydrophobic films were successfully doped with DBHD/N_2O_2 to release NO, the by-products increased the pH in the organic polymer phase and turned off NO production before the NO payload was used up.[36] This problem was solved by another study in which Handa *et al.* used ester-capped poly(lactide-co-glycolide) (PLGA) as an additive within plasticized poly (vinyl chloride) (PVC) films containing DBHD/N_2O_2 to sustain NO release by maintaining a steady pH state.[27] This study also demonstrated the attenuation of activation of platelets and reduction in clot formation in an *in vivo* extracorporeal circulation (ECC) model.

S-nitroso-*N*-penicillamine (SNAP) is a synthetic *S*-nitrosothiol that has gained prominence in the last few years.[25, 29, 30, 32, 37-41] SNAP decomposes in the presence of heat, light, or metal ions (copper) to release NO and a FDA-approved by-product, NAP.[42] While previously thought to be unstable and not useful for biological applications, SNAP has been successfully used to immobilize and develop NO-releasing materials with a capacity of up to 4 months of consistent NO release.[43] SNAP doped materials have also been found to be resilient during sterilization with hydrogen peroxide vapors, ethylene oxide gas, and ultraviolet light exposure.[39] NO release from SNAP-doped polymers have been found to be effective for both *in vitro* and *in vivo* antimicrobial and antithrombotic applications.[25, 29, 30, 32, 37, 38, 40, 41, 44]

In summary, NO releasing materials have great potential to be used for various applications and can be hugely successful as therapeutics for critical medical devices coatings, thus acting as an effective drug to prevent infection and promote hemocompatibility for combination products.

Passive antifouling strategies

While a bactericidal agent and platelet aggregation inhibitor like NO provides several beneficial functions, an active strategy cannot provide an antifouling surface that prevents adhesion of biomacromolecules. A surface that is fouled even by a few biomacromolecules like proteins, can attract platelets and bacteria over time, thus reducing its efficacy as an antimicrobial and antiplatelet material.[32] For instance, *Staphylococcus aureus* has a surface-bound protein called fibronectin binding protein A that binds to blood proteins fibronectin and fibrinogen and promote bacterial infection.[45] Additionally, fibrinogen is one of the main promoters of coagulation, allowing platelets to bind and aggregate and thus causing surface-induced thrombogenesis.[46] Thus, developing strategies to resist non-specific protein adsorption is key to achieving longer term antimicrobial and biocompatible systems of medical implants (Figure 1.4).[47]

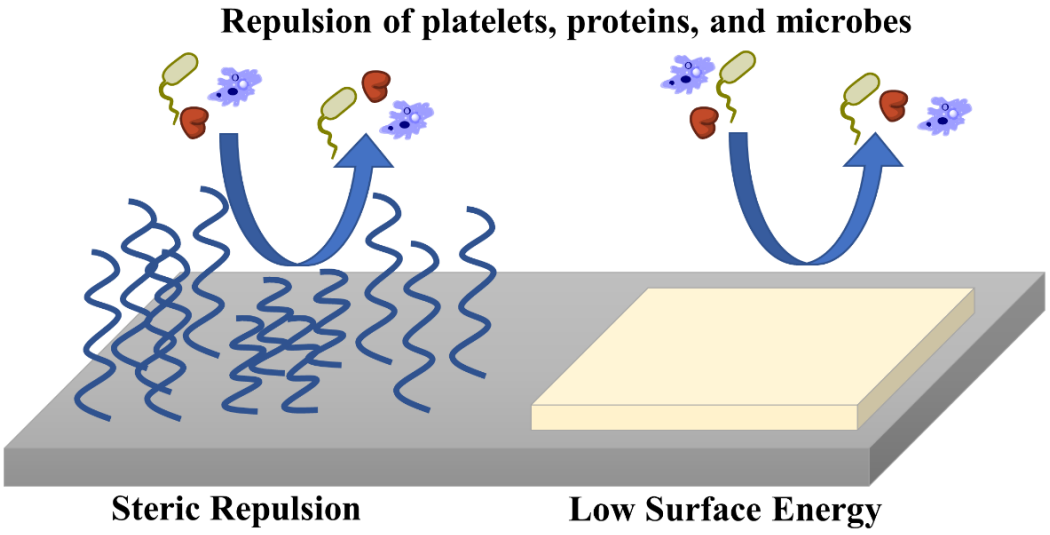

Figure 1.4: Most common antifouling strategies: steric repulsion and low surface energy.

Low Surface Energy

Defined by the Baier curve, which demonstrates the correlation between relative adhesion of fouling biomacromolecules and energy of the surface, a low surface energy surface achieves antifouling properties by having a critical surface energy of 22-24 mN/m.[48] This means that for surfaces with this surface energy, it is favorable for water to re-wet the surface in an aqueous system after biomacromolecules are removed as less energy is needed. Most low energy surface materials tend to be hydrophobic polymers like poly(tetrafluoroethylene) (PTFE), and poly(dimethylsiloxane) (PDMS).[49, 50] These polymers have been extensively researched due to their robust nature and attractive properties like chemical and thermal stability, along with bioinertness.[47] However, despite initial successes for both of these materials, they still suffer from irreversible, and non-specific protein adhesion.[51, 52]

Since the hydrophobic surfaces tended to have major drawbacks, more strategies like superhydrophobic and omniphobic surfaces have been introduced based on the concept of low surface energy.[31, 53-56] While superhydrophobic surfaces have lower surface energy, omniphobic surfaces have the least surface energy.[57] Surface topography or roughness can also contribute to antifouling nature of the material. Superhydrophobic properties have been found to significantly reduce the attachment of biomacromolecules.[53-55, 58, 59] In 2014, Leslie *et al.* published their findings on development of a bioinspired, omniphobic coating for anti-biofilm and antithrombotic applications.[56] This coating was able to stay stable under blood flow conditions and also remain patent for 8 hours *in vivo* without any anticoagulation. Developments like these show promise for short term applications and reduction of the use of systemic anticoagulants, thereby reducing complications arising from blood-contacting devices.

Hydration layer and Steric Repulsion

When hydrophilic materials attract water to the surface (and demonstrate excellent wetting properties demonstrated through low contact angles), a tightly correlated hydration layer is formed on the surface through hydrogen bonding and/or ionic solvation. This hydration layer creates a physical and energetic barrier that prevents proteins and bacteria from binding to the surface since these interactions become thermodynamically unstable.[2, 60] Steric repulsion, the mechanism behind hydration layers, is the compression of long polymer chains that yield repulsive forces to prevent protein adhesion.[61] The most commonly studied antifouling materials in this category include polyethylene glycol (PEG), SAM-OEG, POEGMA, and polyzwitterionic surfaces (polyMPC, polyCBMA, polySBMA).[62-71]

Hydrophilic materials have poor mechanical properties due to their high water uptake, so they have been recently coated or immobilized onto other substrates to improve their antifouling efficacy and stability.[72, 73] Some of the commonly researched hydrogel-based antifouling polymers include PEG, poly(vinyl alcohol), poly(hydroxymethyl acrylate), and poly(ethylene oxide).[62, 74-82] However, despite successful repulsion of proteins, these surfaces still show some degree of platelet adhesion when used *in vivo*.[83]

A zwitterion is a neutral molecule containing both a positive and a negative charge. If the summation of the charges remains neutral, there can be more than one positive and negative charge on the molecule. Zwitterionic polymers fall under the category of antifouling materials with electrostatic and steric repulsion characteristics. Like hydrophilic coatings, zwitterions also form hydration layers but through tight electrostatic interactions unlike the comparatively loose Van der Waals' force of hydrophilic coatings. The zwitterionic hydration layers are formed by hydrogen bonding between the groups on the zwitterion and water molecules at the coating

interface. The charge neutral characteristic of a zwitterionic polymer allows it to form a hydration shell/layer around the polymer via electrostatic interactions.[84] This acts as a barrier against foulants because the hydration layer does not allow proteins to settle down on the surface of the device which otherwise would promote bacterial adhesion. This barrier is known to be denser and thicker than the hydration shell formed by PEG. Compared with the directional arrangement of water molecules in the hydration shell formed via hydrogen bonds in case of PEG, the dipole arrangement of water molecules in the hydration shell formed via electrostatic interactions by zwitterionic molecules are closer to free water. This makes the zwitterionic materials superior to PEG-based materials in repelling biological foulants and more biocompatible.[85] The second mechanism of antifouling by zwitterionic polymers is steric hindrance. When the foulants encounter zwitterionic polymer chains, compressing the excluded volume of and lowering their motility, the system Gibbs free energy increases. So the polymer chains tend to recover to the swelling state and stop the foulants from getting in touch with the surface.[77] Three of the most commonly studied are phosphorylcholines, sulfobetaines and carboxybetaines (Figure 1.5).[86] They are typically presented as pendant groups bound to polymethacrylate or polyacrylamide backbones. The structural versatility granted to zwitterionic coatings due to the ability to attach different functional groups to these polymers gives them an advantage over other polymers used for biological applications.[87]

The antifouling nature of zwitterions has been known for a long time and they have been studied for a variety of medical device coatings. One of the first antifouling zwitterionic materials to be investigated were phosphorylcholine containing polymers. Zwaal *et al.* found that erythrocytes have an asymmetric lipid bilayer membrane which makes their inner surface of the membrane thrombogenic but gives anti-thrombogenic properties to the outer surface [88]. The

outer side of the membrane is composed majorly of phosphatidylcholine, a zwitterionic molecule. Chapman *et al.* found that negatively charged phospholipids were thrombogenic and phosphorylcholine containing surfaces were not. This study attracted interest in the antifouling and biocompatible properties of zwitterionic materials and was termed biomembrane mimicry or biomimicry, in which the surfaces of material behaved like membranes and repelled attachment of biomacromolecules. Two groups have been instrumental in spearheading the research in 2-methacryloyloxyethyphosphorylcholines (MPC), Nakabayashi and Ishihara [89, 90] in Japan and Chapman [91, 92] in UK. The group in Japan specializes in copolymers of MPC with butyl methacrylate (C4, MPC-*co*-BMA) while the group in UK focuses on copolymers of MPC with n-dodecyl methacrylate (C12, MPC-*co*-DMA). Both polymers have reliable antifouling properties.[93-95] Due to their poor mechanical properties these polymers are not suitable as the base material for medical devices, but they have been exploited as surface coatings.[1]

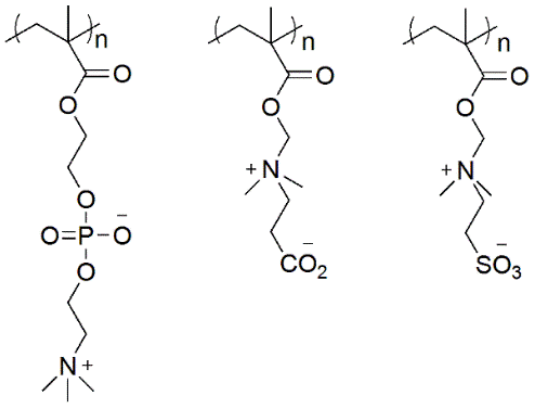

Figure 1.5: Structures of some commonly used zwitterionic polymers for antifouling surfaces.

[1] Two paragraphs on zwitterion coatings and Figure 1.5 have been reproduced from:
Singha, P., Locklin, J., Handa, H. 2017 "A review of the recent advances in antimicrobial coatings for urinary catheters" . Acta Biomaterialia
Reprinted with permission of the publisher

Conclusion

Several strategies have been developed in the last few decades to combat the critical challenges of infections and thrombosis in medical implants. Some of the major developments in the field of fabricating antifouling and antimicrobial surfaces have been with the following strategies: biocide-release, contact activity, steric repulsion and low surface energy. Antifouling surfaces can significantly increase the biocompatibility of the surface by reducing protein attachment and consequent events. However, to truly achieve biocompatibility, it is essential to have a surface that can repel proteins and kill any bacteria that comes close to the material as without a bactericidal agent the surface can get fouled over time and bacteria can attach to even a small number of proteins on the surface. For this reason, the combination of an antimicrobial surface with an antifouling surface can be beneficial and have better biocompatibility chances.

Organization of the dissertation

This dissertation details the research and development of biomaterials that possess antimicrobial and antithrombotic properties with the utilization of both passive and active strategies. The NO releasing polymer, acting as the biocide-releasing and anti-coagulating surface, is combined with passive strategies including hydrophilic and polyzwitterionic polymers to give biocompatibility characteristics to the biomaterials. The remaining of the dissertation is organized as follows:

Chapter 2 investigates the catalytic and additive antimicrobial effects of zinc oxide nanoparticles on NO-releasing polyurethanes. It demonstrates the beneficial effects of a mammalian friendly metal ion that increases antimicrobial efficacy. This is achieved by topcoating a 10 wt.% zinc oxide nanoparticle containing polymer on a NO-releasing polymer.

Chapter 3 demonstrates that a hydrophilic polymer as a topcoat can act as an antifouling layer and prevent protein adhesion while at the same time enhance NO-release and antimicrobial characteristics of a hydrophobic polymer.

Chapter 4 describes the development of an active release strategy in which immobilized NO donors act as a source of long-term NO release while at the same time providing an antifouling surface. This material provides a solution for drawbacks of passive strategies in which surface fouling can impede their function as antifouling surfaces. The antifouling surface in this case itself acts as a source of the bactericidal agent, NO.

Chapter 5 investigates the immobilization of a biomimetic layer of antifouling hydrophobin on NO releasing polymers. Hydrophobins are a group of proteins that are only expressed by filamentous fungi and can change a hydrophilic surface to a hydrophobic surface and vice versa. Thus, by depositing hydrophobins on hydrophobic NO releasing polymers, a hydrophilic surface is obtained that can resist protein, platelet, and bacterial adhesion.

Chapter 6 demonstrates a facile method used to photo-crosslink a polyzwitterion to a NO-releasing polymer. Polyzwitterions are one of the most effective antifouling polymers available currently. However, coating hydrophobic polymers with polyzwitterions is difficult due to the extremely high wetting properties of polyzwitterions. In this chapter, the study demonstrates a quick and easy method to crosslink polyzwitterions to NO-releasing hydrophobic polymers. The *in vitro* characteristics of the hybrid material are demonstrated.

Chapter 7 explores the *in vivo* characterization of the materials developed in Chapter 6 by fabricating vascular catheters. It establishes the *in vitro* characteristics previously seen on a week-long model of bioreactor studies for antimicrobial efficacy and rabbit model for thrombus formation and inflammation.

Chapter 8 offers conclusions based on the dissertation work and outlines future directions researchers may pursue based on the strategies for biocompatibility developed in this work.

References

1. M. Weber, H. Steinle, S. Golombek, L. Hann, C. Schlensak, H. P. Wendel and M. Avci-Adali, *Frontiers in bioengineering and biotechnology*, 2018, **6**, 99-99.
2. P. Singha, J. Locklin and H. Handa, *Acta Biomaterialia*, 2017, **50**, 20-40.
3. D. Koshland, 1992, **258**, 1861-1861.
4. T. Raju, *Journal*, 2000.
5. A. W. Carpenter and M. H. Schoenfisch, *Chem Soc Rev*, 2012, **41**, 3742-3752.
6. J. R. L. Jr, 2015, **1**, null.
7. A. J. Gow, 2006, **3**, 150-152.
8. D. J. Stuehr, *Biochimica et Biophysica Acta (BBA) - Bioenergetics*, 1999, **1411**, 217-230.
9. I. Gusarov, M. Starodubtseva, Z.-Q. Wang, L. McQuade, S. J. Lippard, D. J. Stuehr and E. Nudler, 2008, **283**, 13140-13147.
10. M. W. Radomski, R. M. Palmer and S. Moncada, *Br J Pharmacol*, 1987, **92**, 639-646.
11. M. Radomski, R. Palmer and S. J. B. j. o. p. Moncada, 1987, **92**, 181-187.
12. H. Azuma, M. Ishikawa and S. J. B. j. o. p. Sekizaki, 1986, **88**, 411-415.
13. B. Furlong, A. Henderson, M. Lewis and J. J. B. j. o. p. Smith, 1987, **90**, 687-692.
14. R. M. Palmer, A. Ferrige and S. J. N. Moncada, 1987, **327**, 524.
15. R. F. Furchgott, *J Circulation research*, 1983, **53**, 557-573.
16. M. A. De Groote and F. C. Fang, *Clinical Infectious Diseases*, 1995, **21**, S162-S165.
17. D. O. Schairer, J. S. Chouake, J. D. Nosanchuk and A. J. Friedman, *Virulence*, 2012, **3**, 271-279.

18. K. A. Mowery, M. H. Schoenfisch, J. E. Saavedra, L. K. Keefer and M. E. Meyerhoff, *Biomaterials*, 2000, **21**, 9-21.

19. G. W. Charville, E. M. Hetrick, C. B. Geer and M. H. Schoenfisch, *Biomaterials*, 2008, **29**, 4039-4044.

20. B. V. Worley, K. M. Schilly and M. H. Schoenfisch, *Molecular Pharmaceutics*, 2015, **12**, 1573-1583.

21. L. Yang, X. Wang, D. J. Suchyta and M. H. Schoenfisch, *Bioconjugate Chemistry*, 2017, DOI: 10.1021/acs.bioconjchem.7b00537.

22. F. S. Schanuel, K. S. Raggio Santos, A. Monte-Alto-Costa and M. G. de Oliveira, *Colloids and Surfaces B: Biointerfaces*, 2015, **130**, 182-191.

23. H. Nurhasni, J. Cao, M. Choi, I. Kim, B. L. Lee, Y. Jung and J.-W. Yoo, *International journal of nanomedicine*, 2015, **10**, 3065-3080.

24. M. Champeau, V. Póvoa, L. Militão, F. M. Cabrini, G. F. Picheth, F. Meneau, C. P. Jara, E. P. de Araujo and M. G. de Oliveira, *Acta Biomaterialia*, 2018, **74**, 312-325.

25. E. J. Brisbois, H. Handa, T. C. Major, R. H. Bartlett and M. E. Meyerhoff, *Biomaterials*, 2013, **34**, 6957-6966.

26. H. Handa, E. J. Brisbois, T. C. Major, G. M. Annich, M. E. Meyerhoff and R. H. Bartlett, 2013.

27. H. Handa, E. J. Brisbois, T. C. Major, L. Refahiyat, K. A. Amoako, G. M. Annich, R. H. Bartlett and M. E. Meyerhoff, *Journal of Materials Chemistry B*, 2013, **1**, 3578-3587.

28. H. Handa, T. C. Major, E. J. Brisbois, K. A. Amoako, M. E. Meyerhoff and R. H. Bartlett, *Journal of Materials Chemistry B*, 2014, **2**, 1059-1067.

29. E. J. Brisbois, R. P. Davis, A. M. Jones, T. C. Major, R. H. Bartlett, M. E. Meyerhoff and H. Handa, *Journal of Materials Chemistry B*, 2015, **3**, 1639-1645.

30. E. J. Brisbois, T. C. Major, M. J. Goudie, R. H. Bartlett, M. E. Meyerhoff and H. Handa, *Acta Biomaterialia*, 2016, **37**, 111-119.

31. M. J. Goudie, J. Pant and H. Handa, *Scientific Reports*, 2017, **7**, 13623.

32. M. J. Goudie, P. Singha, S. P. Hopkins, E. J. Brisbois and H. Handa, *ACS Applied Materials & Interfaces*, 2019, DOI: 10.1021/acsami.8b16819.

33. B. Wu, B. Gerlitz, B. W. Grinnell and M. E. Meyerhoff, *Biomaterials*, 2007, **28**, 4047–4055.

34. W. Cai, J. Wu, C. Xi and M. E. Meyerhoff, *Biomaterials*, 2012, **33**, 7933-7944.

35. H. Handa, M. E. Meyerhoff, R. H. Bartlett, E. J. Brisbois and L. Refahiyat, *Journal*, 2013.

36. M. M. Batchelor, S. L. Reoma, P. S. Fleser, V. K. Nuthakki, R. E. Callahan, C. J. Shanley, J. K. Politis, J. Elmore, S. I. Merz and M. E. J. J. o. m. c. Meyerhoff, 2003, **46**, 5153-5161.

37. E. J. Brisbois, H. Handa, T. C. Major, R. H. Bartlett and M. E. Meyerhoff, 2013.

38. Y. Wo, Z. Li, E. J. Brisbois, A. Colletta, J. Wu, T. C. Major, C. Xi, R. H. Bartlett, A. J. Matzger and M. E. Meyerhoff, *ACS Applied Materials & Interfaces*, 2015, **7**, 22218-22227.

39. M. J. Goudie, E. J. Brisbois, J. Pant, A. Thompson, J. A. Potkay and H. Handa, *International Journal of Polymeric Materials and Polymeric Biomaterials*, 2016, **65**, 769-778.

40. Y. Wo, E. J. Brisbois, J. Wu, Z. Li, T. C. Major, A. Mohammed, X. Wang, A. Colletta, J. L. Bull, A. J. Matzger, C. Xi, R. H. Bartlett and M. E. Meyerhoff, *ACS Biomaterials Science & Engineering*, 2017, **3**, 349-359.

41. Y. Wo, Z. Li, A. Colletta, J. Wu, C. Xi, A. J. Matzger, E. J. Brisbois, R. H. Bartlett and M. E. Meyerhoff, *Composites Part B: Engineering*, 2017.

42. M. J. Goudie, E. J. Brisbois, J. Pant, A. Thompson, J. A. Potkay and H. Handa, *International journal of polymeric materials*, 2016, **65**, 769-778.

43. S. P. Hopkins, J. Pant, M. J. Goudie, C. Schmiedt and H. Handa, *ACS Applied Materials & Interfaces*, 2018, **10**, 27316-27325.

44. J. Pant, M. J. Goudie, S. P. Hopkins, E. J. Brisbois and H. Handa, *ACS Applied Materials & Interfaces*, 2017, **9**, 15254-15264.

45. L. Piroth, Y.-A. Que, E. Widmer, A. Panchaud, S. Piu, J. M. Entenza and P. Moreillon, 2008, **76**, 3824-3831.

46. D. P. Mikhailidis, M. A. Barradas, A. Maris, J. Y. Jeremy and P. Dandona, *Journal of clinical pathology*, 1985, **38**, 1166-1171.

47. Z. K. Zander and M. L. Becker, *Journal*, 2017.

48. C. M. Magin, S. P. Cooper and A. B. Brennan, *Materials Today*, 2010, **13**, 36-44.

49. M. Gabriel, K. Niederer, M. Becker, C. M. Raynaud, C.-F. Vahl and H. Frey, *Bioconjugate Chemistry*, 2016, **27**, 1216-1221.

50. S. Xue, C. Li, J. Li, H. Zhu and Y. Guo, *Journal of Membrane Science*, 2017, **524**, 409-418.

51. F. Liu and D. Grainger, 2017.

52. H. Zhang and M. Chiao, *Journal of Medical and Biological Engineering*, 2015, **35**, 143-155.

53. X. Hou, X. Wang, Q. Zhu, J. Bao, C. Mao, L. Jiang and J. Shen, *Colloids and Surfaces B: Biointerfaces*, 2010, **80**, 247-250.

54. C. Y. Loo, P. M. Young, W. H. Lee, R. Cavaliere, C. B. Whitchurch and R. Rohanizadeh, *Acta Biomater*, 2012, **8**, 1881-1890.

55. E. J. Falde, S. T. Yohe, Y. L. Colson and M. W. Grinstaff, *Biomaterials*, 2016, **104**, 87-103.

56. D. C. Leslie, A. Waterhouse, J. B. Berthet, T. M. Valentin, A. L. Watters, A. Jain, P. Kim, B. D. Hatton, A. Nedder, K. Donovan, E. H. Super, C. Howell, C. P. Johnson, T. L. Vu, D. E. Bolgen, S. Rifai, A. R. Hansen, M. Aizenberg, M. Super, J. Aizenberg and D. E. Ingber, *Nat Biotech*, 2014, **32**, 1134-1140.

57. A. Deshmukh, C. Boo, V. Karanikola, S. Lin, A. P. Straub, T. Tong, D. M. Warsinger and M. Elimelech, *Energy & Environmental Science*, 2018, **11**, 1177-1196.

58. J. Weber, S. Schewe and B. Berg, *Journal*, 2007.

59. W. L. Storm, J. Youn, K. P. Reighard, B. V. Worley, H. M. Lodaya, J. H. Shin and M. H. Schoenfisch, *Acta Biomaterialia*, 2014, **10**, 3442-3448.

60. P. Singha, J. Pant, M. J. Goudie, C. D. Workman and H. Handa, *Biomaterials Science*, 2017, DOI: 10.1039/C6BM00948D.

61. S. Chen, L. Li, C. Zhao and J. Zheng, *Polymer*, 2010, **51**, 5283-5293.

62. C.-G. Gölander, J. N. Herron, K. Lim, P. Claesson, P. Stenius and J. Andrade, in *Poly (ethylene glycol) Chemistry*, Springer, 1992, pp. 221-245.

63. H. Chen, Y. Zhang, D. Li, X. Hu, L. Wang, W. G. McClung and J. L. Brash, *Journal of Biomedical Materials Research Part A*, 2009, **90A**, 940-946.

64. J. Jin, W. Jiang, J. Yin, X. Ji and P. Stagnaro, *Langmuir*, 2013, **29**, 6624-6633.

65. K. M. Kovach, J. R. Capadona, A. S. Gupta and J. A. Potkay, *Journal of Biomedical Materials Research Part A*, 2014, **102**, 4195-4205.

66. X. Lin, K. Fukazawa and K. Ishihara, *ACS Appl Mater Interfaces*, 2015, **7**, 17489-17498.

67. S. Guo, D. Jańczewski, X. Zhu, R. Quintana, T. He and K. G. Neoh, *Journal of Colloid and Interface Science*, 2015, **452**, 43-53.

68. K. A. Amoako, H. S. Sundaram, A. Suhaib, S. Jiang and K. E. Cook, *Advanced Materials Interfaces*, 2016, **3**, 1500646-n/a.

69. A. Venault, C.-W. Huang, J. Zheng, A. Chinnathambi, S. A. Alharbi, Y. Chang and Y. Chang, *International Journal of Polymeric Materials and Polymeric Biomaterials*, 2016, **65**, 65-74.

70. V. B. Damodaran and N. S. Murthy, *Biomaterials Research*, 2016, **20**, 18.

71. M. He, K. Gao, L. Zhou, Z. Jiao, M. Wu, J. Cao, X. You, Z. Cai, Y. Su and Z. Jiang, *Acta Biomaterialia*, 2016, **40**, 142-152.

72. J. Kopecek, *Biomaterials*, 2007, **28**, 5185-5192.

73. M. Mihajlovic, M. Staropoli, M.-S. Appavou, H. M. Wyss, W. Pyckhout-Hintzen and R. P. Sijbesma, *Macromolecules*, 2017, **50**, 3333-3346.

74. M. Beija, Y. Li, A. B. Lowe, T. P. Davis and C. Boyer, *European Polymer Journal*, 2013, **49**, 3060-3071.

75. Q. An, F. Li, Y. Ji and H. Chen, *Journal of Membrane Science*, 2011, **367**, 158-165.

76. E. Poverenov, M. Shemesh, A. Gulino, D. A. Cristaldi, V. Zakin, T. Yefremov and R. Granit, *Colloids and surfaces. B, Biointerfaces*, 2013, **112**, 356-361.

77. S. Jeon, J. Lee, J. Andrade and P. De Gennes, *Journal of Colloid and Interface Science*, 1991, **142**, 149-158.

78. S. Jeon and J. Andrade, *Journal of Colloid and Interface Science*, 1991, **142**, 159-166.

79. J. Andrade, V. Hlady and S.-I. Jeon, *Polymeric Materials: Science and Engineering*, 1993, 60-61.

80. J. H. Lee, H. B. Lee and J. D. Andrade, *Progress in Polymer Science*, 1995, **20**, 1043-1079.

81. X. Qin, K. Chen, L. Cao, Y. Zhang, L. Li, X. J. C. Guo and S. B. Biointerfaces, 2017, **155**, 408-414.

82. L. Shen, H. Wang, Y. Zhang, R. Li, B. Fabien, G. Yu, H. Lin, B.-Q. J. S. Liao and P. Technology, 2018, **207**, 83-91.

83. G. R. Llanos and M. V. J. J. o. b. m. r. Sefton, 1993, **27**, 1383-1391.

84. S. Chen, J. Zheng, L. Li and S. Jiang, *Journal of the American Chemical Society*, 2005, **127**, 14473-14478.

85. R. Bernstein, S. Belfer and V. Freger, *Environmental science & technology*, 2011, **45**, 5973-5980.

86. J. L. Harding and M. M. Reynolds, *Trends Biotechnol*, 2014, **32**, 140-146.

87. L. Mi and S. Jiang, *Angewandte Chemie International Edition*, 2014, **53**, 1746-1754.

88. R. Zwaal, P. Comfurius and L. Van Deenen, 1977.

89. M. Kojima, K. Ishihara, A. Watanabe and N. Nakabayashi, *Biomaterials*, 1991, **12**, 121-124.

90. T. Ueda, H. Oshida, K. Kurita, K. Ishihara and N. Nakabayashi, *POLYMER JOURNAL-TOKYO-*, 1992, **24**, 1259-1259.

91. J. A. Hayward and D. Chapman, *Biomaterials*, 1984, **5**, 135-142.

92. R. l. R. Bird, B. Hall, D. Chapman and K. Hobbs, *Thrombosis research*, 1988, **51**, 471-483.

93. Y. Iwasaki, K. Kurita, K. Ishihara and N. Nakabayashi, *Journal of Biomaterials Science, Polymer Edition*, 1995, **6**, 447-461.

94. K. Ishihara, H. Nomura, T. Mihara, K. Kurita, Y. Iwasaki and N. Nakabayashi, 1997.

95. G. Cheng, Z. Zhang, S. Chen, J. D. Bryers and S. Jiang, *Biomaterials*, 2007, **28**, 4192-4199.

CHAPTER 2

ZINC-OXIDE NANOPARTICLES ACT CATALYTICALLY AND SYNERGISTICALLY WITH NITRIC OXIDE DONORS TO ENHANCE ANTIMICROBIAL EFFICACY[2]

[2] Singha, P., Workman, C.D., Pant, J., Hopkins, S.P., Handa, H. 2019. *Journal of Biomedical Materials Research Part A.*

Reprinted here with permission of the publisher

Abstract

The development of infection resistant materials is of substantial importance as seen with an increase in antibiotic resistance. In this project, the nitric oxide (NO)-releasing polymer has an added topcoat of zinc oxide nanoparticle (ZnO-NP) to improve NO-release and match the endogenous NO flux ($0.5 – 4 \times 10^{-10}$ mol cm^{-2} min^{-1}). The ZnO-NP is incorporated to act as a catalyst and provide the additional benefit of acting synergistically with NO as an antimicrobial agent. The ZnO-NP topcoat is applied on a polycarbonate-based polyurethane (CarboSil) that contains blended NO donor, *S*-nitroso-*N*-acetylpenicillamine (SNAP). This sample, SNAP-ZnO, continuously sustained NO release above 0.5×10^{-10} mol cm^{-2} min^{-1} for 14 days while samples containing only SNAP dropped below physiological levels within 24 hours. The ZnO-NP topcoat improved NO release and reduced the amount of SNAP leached by 55% over a 7-day period. ICP-MS data observed negligible Zn ion release into the environment, suggesting longevity of the catalyst within the material. Compared to samples with no NO-release, the SNAP-ZnO films had a 99.03% killing efficacy against *Staphylococcus aureus* and 87.62% killing efficacy against *Pseudomonas aeruginosa*. A cell cytotoxicity study using mouse fibroblast 3T3 cells also noted no significant difference in viability between the controls and the SNAP-ZnO material, indicating no toxicity towards mammalian cells. The studies indicate that the synergy of combining a metal ion catalyst with a NO-releasing polymer significantly improved NO-release kinetics and antimicrobial activity for device coating applications.

Introduction

One of the most common problems with implanted medical devices is the increased susceptibility of the patients to infections.[1] Infections attributed to medical devices, otherwise known as healthcare associated infections (HAIs), have led to various complications like

increased healthcare costs, medical device failure, and unnecessary deterioration in a patient's health.[2] While the Centers for Disease Control and Prevention estimates that 1 out of every 25 hospitalized patients is affected, HAIs are increasingly linked to mortality and morbidity.[3] Some of the most common types of HAIs include catheter associated urinary tract infections, surgical site infections, and bloodstream infections. The need to prevent and control HAIs is evident; such infections can be transmitted between different healthcare facilities and their prevention can result up to $31.5 billion in medical cost savings.[3]

While infection can be managed using several strategies, prevention of infections by anti-fouling and antimicrobial materials for medical devices has been studied extensively.[4] Although some of the most successful strategies include both active and passive agents, active agents are most widely studied due to their higher rate of success in preventing infections in the long term as passive surfaces can be fouled over time. Passive materials such as polyethylene glycol, zwitterionic polymers and other hydrophilic polymers are unable to kill the pathogens themselves and can also be fouled over time through settling of other biomacromolecules, which in turn can attract microbes. Therefore, agents such as silver nanoparticles (Ag-NPs), antibiotics, chlorhexidine, triclosan, quaternary ammonium ions, antimicrobial peptides, and nitric oxide (NO) have been studied widely.[5]

The often-miraculous roles of NO in several biological applications, ranging from nerve signals to gut functions, have been studied aggressively since 1992 when it was awarded the "Molecule of the Year" by The American Association for the Advancement of Science. Since NO's half-life is very short in physiological conditions, NO is transported in the form of endogenous *S*-nitrosothiols (RSNOs, e.g. *S*-nitrosoglutathione (GSNO), *S*-nitrosoalbumin, *S*-nitrosocysteine).[6] *S*-nitrosothiols degrade to release NO and form a disulfide.[7] However, over the

last two decades, NO release from both endogenous and synthetic donors has also been studied for the purpose of antimicrobial medical device coatings and wound healing applications.[5, 8-14] While NO donors like N-diazeniumdiolates have been researched extensively, their disadvantages include low NO release, cytotoxicity towards mammalian cells, and by-products that are not approved by the FDA.[15-17] Similar to GSNO, *S*-nitroso-*N*-acetylpenicillamine (SNAP) is another RSNO, but is synthetic and has a longer shelf-life with increased NO donor capacity in polymers.[18, 19] SNAP has been studied extensively in different polymers and thus is a well-characterized NO donor with the least cytotoxicity towards mammalian cells since the release of NO leads to FDA approved by-products.[20]

Zinc oxide is another antimicrobial but it is already commercially used and is known to have less cytotoxicity towards mammalian cells while having similar antibacterial effects at the same concentration when compared to other commonly used antimicrobial metal ions such as copper and silver.[21] It inhibits the growth of dental caries-related bacteria, *Streptococcus mutans*, *Actinomyces viscosus*, *Lactobacillus casei*, *Staphylococcus aureus (S. aureus)*, and *Candida albicans.*[22] Zinc oxide nanoparticles (ZnO-NPs) have been found to inhibit growth and cause loss of cell viability in *Escherichia coli (E. coli)* and *S. aureus* at concentrations ranging from as low as 1 mM up to 3.4 mM. The same concentrations also had minimal effects on primary human T cell viability.[23] Metal ions with high affinity for sulfur like Zn ions tend to inhibit glycolysis within microorganisms by oxidizing thiols groups in essential glycolytic enzymes. Coupled with low toxicity towards mammalian cells, ZnO-NPs are a good example of metal ion nanoparticles that are required in low concentrations for higher antimicrobial effects.[24]

As of yet, no studies have been conducted to demonstrate the increased antimicrobial activity of biomaterials that contain *both* NO releasing properties and ZnO-NP coated surfaces.

The hybrid material fabricated in this study containing both ZnO-NP and NO donor capacity will serve two purposes: 1) provide a synergistic effect of antimicrobial properties by combining different mechanisms of bactericidal properties exhibited by NO and ZnO -NPs, and 2) the catalytic release of NO in the presence of a ZnO-NP topcoat.

While the enhanced biological effects of NO releasing materials have been studied with metal ions like iron and copper,[25-27] and polyurethane/metal organic framework composite materials,[28] the catalytic effects of a much more mammalian cell friendly metal ion, ZnO-NPs, has not been studied *until now*. In the past, the effect of Zn^{2+} on its ability to generate NO from SNAP has been studied using a Zn wire and a solution for *in vivo* biodegradable bare stent and has been found to elevate NO release.[29] However, the enhanced biological effects including increased antimicrobial activity and lower cytotoxic effects of ZnO-NPs on NO releasing polymers have not been studied.

As discussed herein, we have attempted to fabricate, study, and demonstrate the catalytic and antimicrobial properties of a hybrid material SNAP-ZnO (Figure 2.1). The base polymer used for the fabrication was CarboSil, a thermoplastic silicone-polycarbonate-urethane (TSPCU, DSM Biomedical). It is a biocompatible and biostable polymer that is thromboresistant in nature and can be processed using different techniques. ZnO-NPs were topcoated on the NO-releasing polymer to enhance infection resistant properties of potential medical coatings. Different concentrations of ZnO-NPs were dispersed in previously established concentrations of NO-releasing polymer topcoats and studied for leaching properties of SNAP. Once the lowest leaching (highest SNAP storage) combination is determined, the hybrid sample is then used to investigate synergistic properties of NO and ZnO-NP in antimicrobial and cytotoxicity studies. Studies for up to 14 days of elevated NO release and 24-hour antimicrobial effects have been

presented. Along with proof of antimicrobial efficacy of the material, cytotoxic studies are performed to ensure mammalian cell friendly nature of the final product.

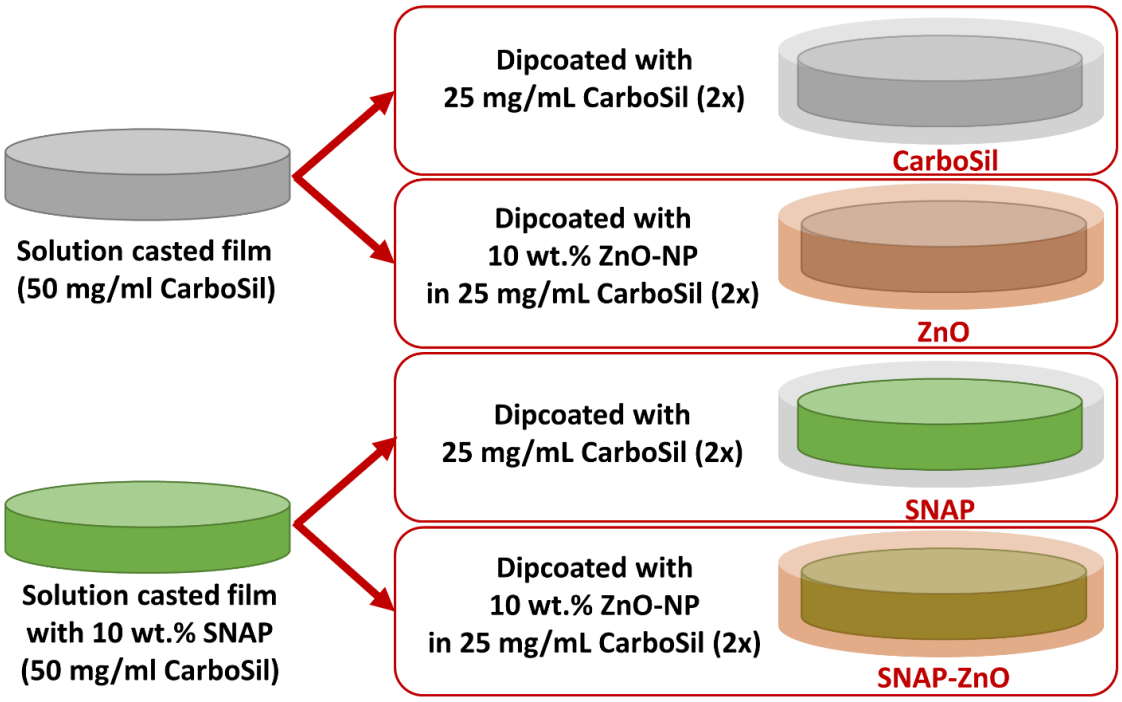

Figure 2.1: Fabrication process of four main tested samples in antimicrobial and cytotoxicity tests: CarboSil, ZnO, SNAP, and SNAP-ZnO

Materials and Methods

Materials

CarboSil® 2080A UR STPU (referred to as CarboSil hereon) was acquired from DSM Biomedical Inc. (Berkeley, CA). Anhydrous tetrahydrofuran (THF), *N*-acetyl-*D*-penicillamine (NAP), sodium nitrite ($NaNO_2$), concentrated sulfuric acid (H_2SO_4), phosphate buffered saline (PBS), ZnO-NPs, cell counting kit-8 and ethylenediamine tetraacetic acid (EDTA) were obtained from Sigma Aldrich (St. Louis, MO). Concentrated hydrochloric acid (conc. HCl), and methanol

were bought from Fisher-Scientific (Hampton, NH). CarboSil™ 2080A (CarboSil) was obtained from DSM Biomedical Inc. (Berkeley, CA). Gram-positive *Staphylococcus aureus* (ATCC 6538) and Gram-negative *Pseudomonas aeruginosa* (ATCC 27853, *P. aeruginosa*) were originally obtained from American Type Culture Collection (Manassas, VA). Milli-Q filter was used to obtain deionized (DI) water for all the aqueous solution preparations. Nitrogen and oxygen gas cylinders were purchased from Airgas (Kennesaw, GA). LB Agar (LA), Miller and Luria broth (LB), Lennox were purchased from Fischer BioReagents (Fair Lawn, NJ).

Synthesis of S-nitroso-N-acetyl-penicillamine (SNAP)

The protocol for the synthesis of SNAP was followed from a previously reported method with slight modifications.[30] Briefly, 2M HCl and 2M H_2SO_4 were added to a beaker containing a 1:1 mixture by volume of methanol and water, followed by an equimolar ratio of NAP and $NaNO_2$. The solution was stirred for 30 minutes then moved to an ice bath to facilitate the precipitation of the SNAP crystals. After 6 hours, the crystals were collected via vacuum filtration and dried for 24 hours. The entire process and crystals obtained were shielded from light throughout the entire duration of the experiment.

Fabrication of ZnO-NP loaded-NO Releasing Films

The bulk of the films were made using solvent casting method and top coats were added using dip coating (both techniques have been previously described and published).[30, 31] Briefly, SNAP films were prepared by dissolving CarboSil in THF for a final concentration of 50 mg ml^{-1}. CarboSil is a polycarbonate-based polyurethane that contains a silicone segment and is marketed by DSM. It has been used previously by our and other groups and has been found to have stable NO-releasing properties when incorporated with SNAP.[30-32] (Exact properties are not public knowledge but all details are available on the company's website.) When CarboSil was

fully dissolved, 10 wt.% SNAP was added to the solution. The solution was then poured into a Teflon™ mold and left to dry in the dark, overnight. Dried films were cut into circular disks with diameters of 8 mm. Then, various solutions of 25 mg ml^{-1} of CarboSil were prepared separately (containing 0, 1, 5, and 10 wt.% ZnO-NP). The circular films were top coated twice with the prepared solution containing 0, 1,5 or 10 wt.% ZnO-NP by dipping the films in the solution and allowing 10 minutes of drying between coats. The ZnO-NP used was purchased from Sigma-Aldrich. The size of the ZnO-NP was specified as <50nm in size and >97% purity. All films were allowed 24 hours to fully dry before being used for experiments.

Following is a table (Table 2.1) for all the compositions used along with the sample names.

Table 2.1: Composition for each sample.

Sample Fabrication		
SAMPLE NAME	**BASE FILM**	**TOPCOAT**
CarboSil	50 mg/ml CarboSil	2 dips of 25 mg/ml CarboSil solution
ZnO-1	50 mg/ml CarboSil	2 dips of 25 mg/ml CarboSil solution containing 1 wt.% ZnO-NP
ZnO-5	50 mg/ml CarboSil	2 dips of 25 mg/ml CarboSil solution containing 5 wt.% ZnO-NP
ZnO	50 mg/ml CarboSil	2 dips of 25 mg/ml CarboSil solution containing 10 wt.% ZnO-NP
SNAP	50 mg/ml CarboSil with 10 wt.% SNAP	2 dips of 25 mg/ml CarboSil solution
SNAP-ZnO-1	50 mg/ml CarboSil with 10 wt.% SNAP	2 dips of 25 mg/ml CarboSil solution containing 1 wt.% ZnO-NP
SNAP-ZnO-5	50 mg/ml CarboSil with 10 wt.% SNAP	2 dips of 25 mg/ml CarboSil solution containing 5 wt.% ZnO-NP
SNAP-ZnO	50 mg/ml CarboSil with 10 wt.% SNAP	2 dips of 25 mg/ml CarboSil solution containing 10 wt% ZnO-NP

SNAP Leaching Analysis

Prepared circular films were tested for leaching of SNAP using UV-Vis spectrophotometry. The SNAP leached into the PBS used to soak the films was measured by detecting the absorbance at 340 nm wavelength (maximum absorbance for S-nitroso bond in SNAP) at various time points over 7 days. Samples were weighed before applying the topcoats to determine the amount of SNAP initially present. After application of topcoats, films were soaked in PBS (with EDTA) at 37°C for the duration of the study. Measurements were compared to a calibration curve.

Energy-dispersive X-ray spectroscopy

Scanning electron microscopy (SEM, FEI Teneo, FEI Co.) fitted with a large detector Energy dispersive X-ray spectroscopy (EDS, Oxford Instruments) system was employed at an accelerating voltage of 10.00 kV to examine the presence and elemental mapping of SNAP and ZnO-NP particles throughout the surfaces fabricated.

Nitric Oxide Release Measurements

Chemiluminescence of NO release from SNAP-ZnO films versus the SNAP films was measured using a Siever's Nitric Oxide Analyzer (NOA) (Boulder, CO). Films containing SNAP (both with and without ZnO coatings) were measured for their NO release. Each sample was placed in an amber reaction cell containing PBS buffer at 37°C. EDTA was added to this PBS buffer as a chelating agent and prevent any catalytic release of NO by free metal-ions in the solution. Nitrogen gas was bubbled through the solution to purge NO from the solution. Sweep gas carried the purged NO to the detection chamber, where it was measured in PPB. Samples were measured from the NOA on days 0, 1, 3, 5, and 7. Between measurements samples were kept in PBS buffer in a 37°C incubator.

Inductively Coupled Plasma – Mass Spectroscopy (ICP-MS)

To measure the amount of metal-ion nanoparticles (ZnO in this case) in the sample leachates for the duration of the study, an ICP-MS study was conducted using a VG ICP-MS Plasma Quad 3 instrument.[25] In this study, the samples containing ZnO topcoats were soaked in DMEM for 2 weeks and kept in 37°C. At the end of 2 weeks, the films were removed from the media and the media was analyzed for presence of ^{64}Zn and ^{66}Zn isotopes using a previously published method.[33]

Bacterial Adhesion Study

Bacterial adhesion study for the fabricated materials was carried out using a previously established ASTM E2180 protocol.[31] This protocol was performed with very minor modifications. The samples used for the bacterial adhesion study were CarboSil, ZnO, SNAP and SNAP-ZnO. The bacteria used for antimicrobial efficacy analyses were *S. aureus* and *P. aeruginosa*. The bacteria were grown to a mid-log phase of ~10^6-10^8 CFU ml^{-1} in LB broth at 37°C. Following this, the bacteria were then resuspended in PBS to incubate the samples. 2 ml of bacterial solution was used for each sample and kept in a shaker incubator (37°C, 200 rpm) for 24 h. After 24 h of incubation with the bacteria, samples were rinsed with DI water to remove any unattached bacteria. The samples were then homogenized for 1 min each to remove any adhered bacteria into buffer solutions. The buffer solutions, now containing bacteria from the materials, were serially diluted (up to 10^{-5}), plated on LB agar, and kept in the incubator (37°C). The colonies of bacteria were counted after 18 h of incubation of the plates. The average number of CFUs were normalized for the surface area of each sample exposed to the bacteria according to the following formula:

$$\text{Total CFUs per sample} = \frac{\text{total number of CFUs per sample} \times \text{ dilution factor } \times \text{ suspension in solution}}{\text{suspension volume plated}}$$

Cytotoxicity Analysis

The cytotoxicity test was performed on mouse fibroblast cells (3T3) using a recommended and previously published cell cytotoxicity assay.[25] The mouse fibroblast cells were cultured from a cryopreserved vial Dulbecco's Modified Eagle's Media (DMEM) containing 5% glucose, 10% Fetal bovine serum and 1% antibiotics (Penn-Strep). The culture media was changed every second day until the cell confluency was 80-90%. After this step, 100 µl of 5000 cells ml^{-1} were seeded per well of a cell culture grade 96-well plate (n=5) and kept in a humidified incubator with 5% CO_2 maintained at 37°C.

Meanwhile, leachates from the CarboSil films, SNAP-CarboSil, ZnO-CarboSil and ZnO-SNAP-CarboSil films were collected by adding 10 mg of each type of sample in 10 ml of DMEM media (n=5 for each sample type). The resulting mixture was covered in an amber vial in the incubator at 37°C for 24 hours to allow the films to leach in the DMEM medium.

After 24 hours, 10 µL of the leachates were added to each of the well-containing cells followed by incubation for 24 hours in the incubator. 10 µL of the WST-8 solution (CCK-8 kit, Sigma Aldrich) was added to the resulting mixture and incubated for 4 hours according to the manufacturer's recommendation. The NADH released by only viable fibroblast cells converted WST-8 to formazan, an orange color product that was quantified at 430 nm using a photo plate reader. The relative viability of the cells was measured with respect to CarboSil (cells exposed to CarboSil leachates) using the formula below.

$$\%\ \text{Cell Viability} = \frac{\text{Absorbance of the test samples}}{\text{Absorbance of the CarboSil samples}} \times 100$$

Statistical Analysis

All data are stated as mean ± standard deviation. The number of replicates for every experiment have been mentioned under methods used.

Results

Film Fabrication, Surface Characterization and NO Release Kinetics

Films of varying ZnO-NPs were made to test for SNAP leaching on consistent SNAP content films as mentioned on Table 1. This was done to establish the wt.% of ZnO-NP required for a longer NO-release with ideal SNAP storage. The amount of SNAP, 10 wt.%, required for sustained NO-release has already been established in previously published results.[31] To determine if ZnO-NP topcoated films helped to retain SNAP within the film, a 7-day study on films stored in PBS (pH of 7.4, 37°C) was conducted. It is ideal to have high SNAP retention within the polymer in order to ensure prolonged NO release from the material, as well as avoid adverse cytotoxic effects, if any exist. After 7 days of soaking, all film types showed a high amount of SNAP retention (Figure 2.2, Table 2.2). Minimal leaching was demonstrated in the SNAP-ZnO films with only 7.75 ± 0.51 wt.% SNAP leached after 7 days, while films containing only SNAP had the most SNAP leached (13.86 ± 3.62 wt.%).

(Note: The loading efficiency of SNAP in all the films with SNAP is estimated to be ~100% since the SNAP crystals can dissolve and blend into the polymer/THF solution and casted into the molds.)

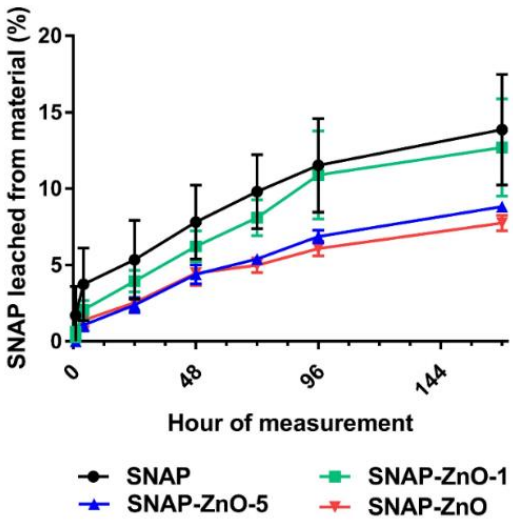

Figure 2.2: SNAP leaching profile for SNAP, SNAP-ZnO-1, SNAP-ZnO-5, and SNAP-ZnO films. SNAP leaching was tested over 7 days/168 h (n=3)

Table 2.2: Complementary table for Figure 2.2: Weight percentage of SNAP leached.

	Wt. % of SNAP Leached						
	1 hour	**4 hours**	**24 hours**	**48 hours**	**72 hours**	**96 hours**	**168 hours**
SNAP	1.70 ±1.55	3.73 ±1.94	5.34 ±2.11	7.81 ±1.98	9.81 ±1.98	11.53±2.51	13.86 ±2.96
SNAP-ZnO-1	0.45 ±0.40	2.06 ±0.50	3.94 ±0.59	6.22 ±0.83	8.10 ±0.96	10.89 ±2.35	12.70 ±2.61
SNAP-ZnO-5	0.00 ±0.00	1.06 ±0.32	2.37 ±0.41	4.39 ±0.51	5.39 ±0.26	6.86 ±0.34	8.82 ±0.26
SNAP-ZnO	0.21 ±0.30	1.38 ±0.34	2.52 ±0.30	4.47 ±0.66	4.99 ±0.39	6.08 ±0.40	7.75 ±0.41

The low water uptake property of CarboSil allows for SNAP crystal formation within the polymer matrix. Exceeding the SNAP solubility threshold allows for crystallization of the molecule, thus stabilizing the NO donor to increase longevity of NO release.[34, 35] To reach the optimum crystallization of SNAP without sacrificing mechanical properties of the polymer, 10 wt.% SNAP was used in all films, as determined from previous work.[35] It was observed that the NO flux for the SNAP-ZnO films remained in the physiological range released from the endothelium of 0.5 to 4.0 ($x10^{-10}$ mol min^{-1} cm^{-2}) for over 14 days (Figure 2.3, Table 2.3). While the SNAP samples had an initial burst (Day 0 not included in figure) in NO flux of 3.57 ± 0.814 ($x10^{-10}$ mol min^{-1} cm^{-2}), within 24 hours the flux was 0.24 ± 0.045 ($x10^{-10}$ mol min^{-1} cm^{-2}) and below 0.10 ($x10^{-10}$ mol min^{-1} cm^{-2}) by day 14. Although the average NO Flux for the SNAP-ZnO films on day 14 was 0.487 ± 0.075 ($x10^{-10}$ mol min^{-1} cm^{-2}), just below physiological levels, recent work has shown these levels still exhibit an antimicrobial effect.[36]

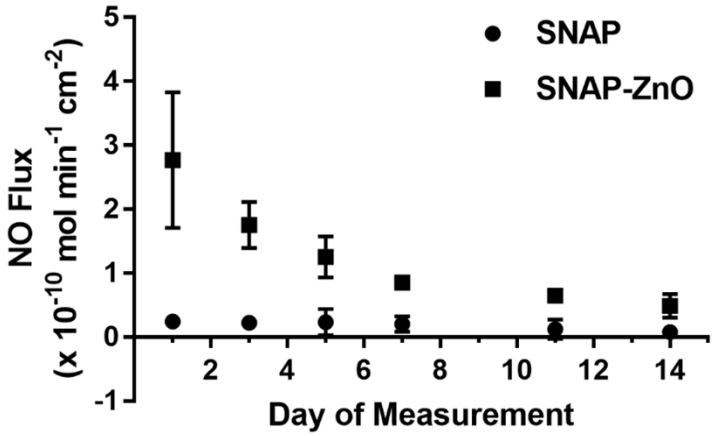

Figure 2.3: NO release profile for SNAP versus SNAP-ZnO films for 14 days (n=3)

Table 2.3: Complementary table for Release of NO ($x10^{-10}$ mol cm^{-2} min^{-1}) from SNAP films vs. SNAP-ZnO films for 14 days.

	Day 1	**Day 3**	**Day 5**	**Day 7**	**Day 11**	**Day 14**
SNAP	0.241 ±0.045	0.222 ±0.023	0.235 ±0.084	0.203 ±0.048	0.123 ±0.061	0.079 ±0.043
SNAP-ZnO	2.766 ±0.427	1.752 ±0.145	1.253 ±0.129	0.851 ±0.019	0.649 ±0.026	0.487 ±0.075

To confirm that SNAP crystals were blended, and ZnO-NPs were present and evenly distributed on the surface of the samples, fabricated films (SNAP-ZnO) were mapped by EDS and analyzed for the uniform presence of zinc and sulfur. The blending of SNAP and ZnO-NPs were found to be uniform as shown in Figure 2.4 (A and B) indicating that the fabrication method had no adverse effect on the stability of SNAP or ZnO-NPs.

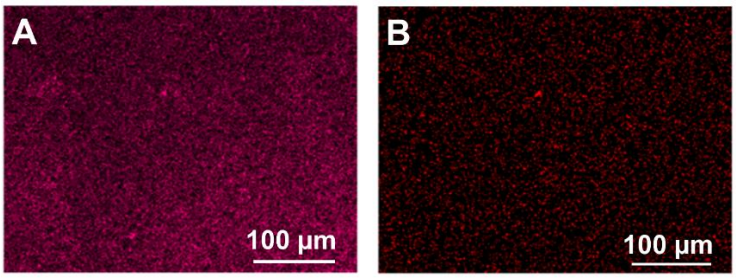

Figure 2.4: Energy dispersive X-ray spectroscopy images of the elements present in different coatings. (A) Sulfur element map for SNAP-ZnO films and (B) Zinc element map for SNAP-ZnO films

Analysis of ZnO-NP Leaching

While Zn has many beneficial effects, and is vital for numerous physiological pathways, it is important that a majority of the ZnO-NP stays within the tested polymer films to help facilitate the catalytic NO-release from the blended SNAP. To detect for any ZnO-NP diffusion, ICP-MS was performed on 1 cm^2 measured samples. Only the highest weight percent (10%) of ZnO-NPs was used for all ICP-MS studies to observe any potential leaching into the surrounding environment. After 14 days of soaking in DMEM at 37°C, ZnO films demonstrated only 1.08% of the total Zn leached into solution while SNAP-ZnO films also had a negligible 3.17% leached.

Enhanced Antimicrobial Efficacy and Low Cytotoxicity of NO-Releasing Materials Topcoated with ZnO-NP

Due to the antibacterial properties of NO, active release of NO from the donor molecule incorporated in the hydrophobic polymeric films can reduce the chances of biomedical device related infections or HAIs. The adhesion of bacteria to the NO-releasing material can further be reduced increasing the NO-release or having an initial burst release followed by the synergistic bactericidal activity of a metal ion. As seen from Figure 2.5 A, in case of *S. aureus,* there is a 78.02 ±25.03% reduction (~0.5 log) when only ZnO-NPs are applied as a topcoat on CarboSil samples. This is due to the bactericidal properties of ZnO-NPs as mentioned in the introduction. NO-releasing CarboSil (SNAP films) in comparison have a higher killing efficiency at 87.72 ±7.53% (~1 log) reduction due to even better bactericidal properties of diffusion based bacterial

cytotoxicity of NO. However, the synergistic effects are clearly seen and very prominent as there is a 99.03 ±0.50% (~2 log) reduction in case of SNAP-ZnO films. This reduction is seen to increase when ZnO-NPs are applied as topcoat to SNAP containing polymer and hence it can be concluded that ZnO-NPs and NO have synergistic bactericidal effects against *S. aureus*. It is also important to note here that in addition to the higher reduction with SNAP-ZnO materials, there was also a high reduction between ZnO vs SNAP-ZnO (95.59 ±2.29%) and SNAP vs SNAP-ZnO (92.11 ±4.10%) materials.

Similar results were observed in case of *P. aeruginosa* but with a smaller log reduction in all the bactericidal agent containing films (Figure 2.5 B). This may be attributed to the extra cell membrane that Gram negative bacteria like *P. aeruginosa* have. A 60.98 ±14.18% (~0.5 log) reduction was seen in ZnO, and a 63.76 ±14.88% reduction for SNAP materials was seen when compared to CarboSil. Although when both the bactericidal agents were combined, SNAP-ZnO materials yielded an 87.63 ±4.86% (~1 log) reduction when compared to CarboSil samples. All of these reductions were significant with a p value<0.05. This higher reduction is seen as a synergistic effect of ZnO-NPs and NO's antimicrobial activity. In addition to these reductions, there was also a high reduction between ZnO vs SNAP-ZnO (65.86 ±13.42%) and SNAP vs SNAP-ZnO (68.29 ±12.46) materials. Thus, from the antimicrobial assays used to test the synergistic combination of ZnO nanoparticles with NO donor, the hybrid materials were able to demonstrate superior infection-resistant properties that can be applied to medical device coatings (Table 2.4).

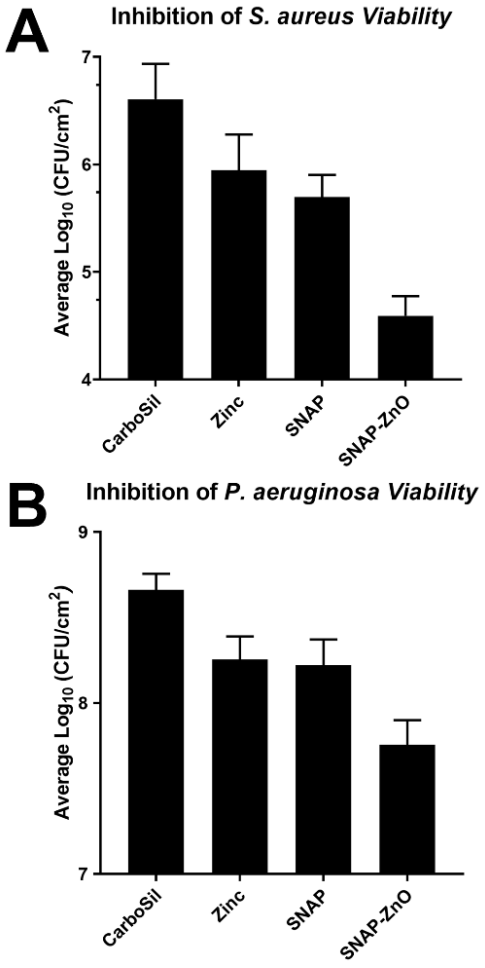

Figure 2.5: Inhibition of viable bacteria adhesion over 24-h exposure in physiological conditions. (A) Comparison in adhesion of *S. aureus* between CarboSil, ZnO, SNAP, and SNAP-ZnO films. (B) Comparison in adhesion of *P. aeruginosa* between CarboSil, ZnO, SNAP, SNAP-ZnO films (n=4 for *S. aureus*; n=3 for *P. aeruginosa*)

Table 2.4: Reduction of bacteria cm^{-2} as seen on test samples compared to CarboSil as control.

	Reduction in *S. aureus* (%)	Reduction in *P. aeruginosa* (%)
CarboSil vs. ZnO	78.02 ±25.03	60.98 ±14.18
CarboSil vs. SNAP	87.72 ±7.53	63.76 ±14.88
CarboSil vs. SNAP-ZnO	99.03 ±0.50	87.63 ±4.86
ZnO vs. SNAP-ZnO	95.59 ±2.29	65.86 ±13.42
SNAP vs. SNAP-ZnO	92.11 ±4.10	68.29 ±12.46

The WST-8 dye-based test showed that there was no significant difference in the viability when the CarboSil was compared with cells exposed to leachates from SNAP, ZnO or SNAP-ZnO materials (Figure 2.6). This means that the material does not possess any cytotoxicity toward mouse fibroblast cells. This negligible cytotoxicity was expected based from the leaching test results of Zn ions (ICP-MS results) and SNAP and serves as a proof-of-concept for the potential biocompatibility of the material.

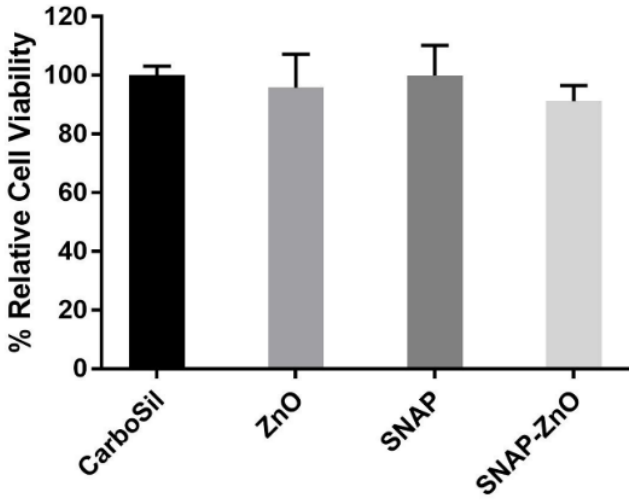

Figure 2.6: Percentage relative cell viability of mouse fibroblast cells after 24-h exposure to leachates from CarboSil, ZnO, SNAP, and SNAP-ZnO films (n=3)

Discussion

Previous work has shown SNAP-blended polymers to release NO on the low end of the physiological range.[20] This is in part due to the need for hydrophobic polymers requiring a thin top coat as a support for SNAP to prevent rapid leaching of the molecule. The hydrophobicity of these polymers delays or prevents moisture from reaching the SNAP molecule to elicit NO

release. We hypothesized that the addition of a metal ion, specifically Zn, would catalytically increase NO release from SNAP within the hydrophobic polymers without unnecessary SNAP leaching. For this study we used a biocompatible, medical grade thermoplastic urethane copolymer, CarboSil, as a support for SNAP.

This higher retention of SNAP within SNAP-ZnO may be contributed to the ZnO-NP content in the topcoat as all other variables are left consistent among the tested samples. The metal ion-blended topcoat may slow SNAP's ability to pass through the polymer layer. The catalytic effect of the ZnO-NP within the topcoat could also be facilitating a quicker degradation of the SNAP as it diffuses, resulting in the leaching of NAP instead which would be undetectable at the measured SNAP UV wavelength (340 nm). However, since NAP has been demonstrated in the past to be non-cytotoxic and is even used in heavy metal chelation therapy, the possible leaching of this would not be problematic.[37] Due to the low leaching results of SNAP from the 10wt.% of ZnO-NPs, subsequent studies (NO release measurement, EDS mapping, antibacterial efficacy, cytotoxicity) were performed with SNAP-ZnO as the proposed hybrid material demonstrated reduced loss of SNAP from the material despite having the exact same coatings as the other materials and differing only in the ZnO-NP content (10 wt.% compared to 1% and 5%).

From the low leaching characteristics of SNAP-ZnO samples, it was predicted that the samples would also have an extended NO release. As expected, the improved NO release from SNAP-ZnO films showed a promising outlook for long-term indwelling medical device applications to reduce device-associated infections. The constantly higher release of NO from the SNAP-ZnO samples confirmed them to be ideal for testing antimicrobial efficacy and cytocompatibility.

Following NO storage and release characterization, the materials were tested for distribution of the SNAP and metal ion elements. The uniform distribution was a good indication that the coating method is reliable to be used for microbial adhesion prevention on the medical device's surface.

The decomposition of all RSNOs into radical NO and disulfides is facilitated through the homolytic cleavage of the sulfur-nitroso bond which can be accelerated by the administration of certain transition metal ions. The reduction of Cu^{2+} metal ions to Cu^{+} has been thoroughly investigated in its catalytic properties with RSNOs.[38] While the exact mechanism is still being investigated, Zn has previously been reported to display a similar catalytic effect.[29] The Zn^{2+} mediated reactivity of RSNOs has a more unique proposed mechanism when compared to Cu^{+} as it keeps its ionic state consistent throughout the catalytic process. After RSNO degradation to RS^{-} + NO, residual RS^{-} molecules end up forming disulfide RSSR compounds when in an aqueous environment. Zn is able to form a complex with these residual RS^{-} ions to prevent disulfide bond formation, allowing for possible regeneration of RSH molecules after complete NO-release and subsequent renitrosation into its original RSNO form.[39] The presence of these thiols would also assist in the increased NO release of Zn incorporated SNAP films as RSH molecules have been demonstrated to have destabilizing effects to RSNOs.[40]

The minimal leaching of Zn ions from the SNAP-ZnO samples (3.17%) shows how well encapsulated the nanoparticles were within the topcoats of the synthesized CarboSil polymer films and demonstrates the potential longevity of their catalytic activity. As NO is emitted from the polymer into an aqueous environment, trace amounts of nitric acid are formed at the material interface which can increase the potential Zn solubility and account for the slightly higher

leachate result. The increase in Zn leaching from the SNAP-ZnO films could also assist in an increased antimicrobial activity.

Bacterial adhesion is a common challenge faced by medical implants. It is triggered in response to medical devices coming in contact with the fluidic biological milieu provided by the human physiology and the surgical wound provided during the insertion of the medical device. This bacterial adhesion in the first few hours of implantation can lead to infection of the site and further cause medical device failure or even death. Furthermore, *S. aureus* and *P. aeruginosa* are two of the most commonly found nosocomial pathogens. Due to the stated reasons, a bacterial adhesion study was carried out for the fabricated materials for 24 hours using *S. aureus* and *P. aeruginosa*. Another important point to note here is that both bacteria studies were done after an initial 24 hours soaking of the materials in PBS. This step allowed for initial metal-ion and SNAP leachates to be removed from the study and hence prevent any false results due to higher percentage of leachates during bacterial incubation. For both the bacteria tested, the SNAP-ZnO samples showed a greater amount of reduction in viable bacteria adhesion than any other samples. This increased antimicrobial activity was a consequence of improved NO release as well as the combined antimicrobial activity of ZnO-NPs with NO. As seen from the results, even though NO and ZnO-NPs do exhibit antimicrobial activities by themselves, they definitely work additively when combined in the SNAP-ZnO material.

While the material demonstrated controlled NO release and antibacterial efficacy, it was important to validate that the material is not toxic to the mammalian cells. In a real-life scenario, this would mean protecting the host tissue from toxic side effects during the time of application.

While the same concentration of SNAP by itself for NO-release has shown negligible cytotoxicity in the past,[41] copper nanoparticles have also assisted NO-release from SNAP and

demonstrated no toxicity towards mammalian cells.[25] However, this was the first time that similar results have been recorded with the SNAP-ZnO combination. Another advantage of such NO based strategies is that it is highly compatible with other bacteriostatic or bactericidal approaches such as zwitterions, quaternary ammonium ions, silicone oil, and diatomaceous earth particle.[31, 42-44] The non-cytotoxic nature combined with the antibacterial properties offers a potential alternative therapeutic option instead of silver nanoparticles or antibiotics which have the issue of cytotoxicity or bacterial resistance.

Conclusion

This work demonstrates the potential beneficial effects of ZnO-NPs on the catalytic release and antimicrobial effects of NO under physiological conditions. The hybrid material, SNAP-ZnO, was composed of a base film (50 mg ml^{-1} CarboSil with 10 wt.% SNAP) and a topcoat (2 dips of 25 mg ml^{-1} CarboSil solution containing 10 wt.% ZnO-NP). The 10 wt.% of ZnO-NPs in SNAP-ZnO samples was able to retain more SNAP molecules within it (7.75 wt.% loss of SNAP) when compared to samples with no (13.85 wt.%), 1 (12.697 wt.%) or 5 (8.821 wt.%) wt.% ZnO-NPs in them. EDS-mapping showed that the hybrid material, SNAP-ZnO, had a uniform distribution of ZnO-NPs and SNAP molecules in it. NO release measurements also demonstrated SNAP-ZnO's ability to maintain physiological levels of NO release for up to 14 days. Antibacterial efficacy at 99.03 ±0.50% and 87.63 ±4.86% reduction for *S. aureus* and *P. aeruginosa*, respectively, were promising results. Finally, low cytotoxicity results demonstrated by SNAP-ZnO samples establish the need to fabricate antibacterial materials that are mammalian cell friendly.

These studies represent preliminary data that can be used to design a long-term antimicrobial and biocompatible device coating that has high potential for use in different

implantable materials. In the future, more similar mammalian cell friendly metal-ions**,** such as iron or magnesium**,** that can be combined with nitric oxide donors to tune NO release for biomedical purposes can be designed for longer term use that can be tested with *in vivo* conditions.[45]

References

1. C. von Eiff, B. Jansen, W. Kohnen and K. Becker, *Drugs*, 2005, **65**, 179-214.
2. J. L. Harding and M. M. Reynolds, *Trends Biotechnol*, 2014, **32**, 140-146.
3. C. f. D. C. a. Prevention, Healthcare-Associated Infections, https://www.healthypeople.gov/2020/topics-objectives/topic/healthcare-associated-infections).
4. R. M. Donlan, *Emerging Infectious Diseases*, 2001, **7**, 277-281.
5. P. Singha, J. Locklin and H. Handa, *Acta Biomaterialia*, 2017, **50**, 20-40.
6. H. Al-Sa'doni and A. Ferro, *Clinical science (London, England : 1979)*, 2000, **98**, 507-520.
7. H. H. Al-Sa'doni, I. Y. Khan, L. Poston, I. Fisher and A. Ferro, *Nitric oxide : biology and chemistry / official journal of the Nitric Oxide Society*, 2000, **4**, 550-560.
8. B. J. Nablo, T.-Y. Chen and M. H. Schoenfisch, *Journal of the American Chemical Society*, 2001, **123**, 9712-9713.
9. E. M. Hetrick and M. H. Schoenfisch, *Biomaterials*, 2007, **28**, 1948-1956.
10. A. W. Carpenter and M. H. Schoenfisch, *Chem Soc Rev*, 2012, **41**, 3742-3752.
11. L. Yang, X. Wang, D. J. Suchyta and M. H. Schoenfisch, *Bioconjugate Chemistry*, 2017, DOI: 10.1021/acs.bioconjchem.7b00537.

12. H. Zhang, G. M. Annich, J. Miskulin, K. Stankiewicz, K. Osterholzer, S. I. Merz, R. H. Bartlett and M. E. Meyerhoff, *Journal of the American Chemical Society*, 2003, **125**, 5015-5024.

13. M. M. Reynolds, M. C. Frost and M. E. Meyerhoff, *Free Radical Biology & Medicine*, 2004, **37**, 926-936.

14. E. J. Brisbois, H. Handa, T. C. Major, R. H. Bartlett and M. E. Meyerhoff, *Biomaterials*, 2013, **34**, 6957-6966.

15. C. J. Backlund, B. V. Worley and M. H. Schoenfisch, *Acta biomaterialia*, 2016, **29**, 198-205.

16. W. Cai, J. Wu, C. Xi and M. E. Meyerhoff, *Biomaterials*, 2012, **33**, 7933-7944.

17. H. Handa, E. J. Brisbois, T. C. Major, G. M. Annich, M. E. Meyerhoff and R. H. Bartlett, 2013.

18. N. Hogg, *Annual Review of Pharmacology and Toxicology*, 2002, **42**, 585-600.

19. M. J. Goudie, P. Singha, S. P. Hopkins, E. J. Brisbois and H. Handa, *ACS Applied Materials & Interfaces*, 2019, DOI: 10.1021/acsami.8b16819.

20. M. J. Goudie, E. J. Brisbois, J. Pant, A. Thompson, J. A. Potkay and H. Handa, *International Journal of Polymeric Materials and Polymeric Biomaterials*, 2016, **65**, 769-778.

21. C. Ning, X. Wang, L. Li, Y. Zhu, M. Li, P. Yu, L. Zhou, Z. Zhou, J. Chen, G. Tan, Y. Zhang, Y. Wang and C. Mao, *Chemical research in toxicology*, 2015, **28**, 1815-1822.

22. J. Yakoob, Z. Abbas, M. W. Usman, S. Awan, S. Naz, F. Jafri, S. Hamid and W. Jafri, *Microbial Drug Resistance*, 2013, **20**, 305-309.

23. K. M. Reddy, K. Feris, J. Bell, D. G. Wingett, C. Hanley and A. Punnoose, *Applied Physics Letters*, 2007, **90**, 213902.

24. E.-K. Choi, H.-H. Lee, M.-S. Kang, B.-G. Kim, H.-S. Lim, S.-M. Kim and I.-C. Kang, *The Journal of Microbiology*, 2010, **48**, 40-43.

25. J. Pant, M. J. Goudie, S. P. Hopkins, E. J. Brisbois and H. Handa, *ACS Applied Materials & Interfaces*, 2017, **9**, 15254-15264.

26. V. Wonoputri, C. Gunawan, S. Liu, N. Barraud, L. H. Yee, M. Lim and R. Amal, *ACS Applied Materials & Interfaces*, 2015, **7**, 22148-22156.

27. V. Wonoputri, C. Gunawan, S. Liu, N. Barraud, L. H. Yee, M. Lim and R. Amal, *ACS Applied Materials & Interfaces*, 2016, **8**, 30502-30510.

28. J. L. Harding and M. M. Reynolds, *Journal of Materials Chemistry B*, 2014, **2**, 2530-2536.

29. C. W. McCarthy, R. J. Guillory, J. Goldman and M. C. Frost, *ACS applied materials & interfaces*, 2016, **8**, 10128-10135.

30. P. Singha, J. Pant, M. J. Goudie, C. D. Workman and H. Handa, *Biomaterials Science*, 2017, DOI: 10.1039/C6BM00948D.

31. Q. Liu, P. Singha, H. Handa and J. Locklin, *Langmuir*, 2017, DOI: 10.1021/acs.langmuir.7b02970.

32. K. H. Cha and M. E. Meyerhoff, *ACS Sensors*, 2017, **2**, 1262-1266.

33. H. Vanhoe, C. Vandecasteele, J. Versieck and R. Dams, *Analytical Chemistry*, 1989, **61**, 1851-1857.

34. Y. Wo, Z. Li, A. Colletta, J. Wu, C. Xi, A. J. Matzger, E. J. Brisbois, R. H. Bartlett and M. E. Meyerhoff, *Composites Part B: Engineering*, 2017.

35. Y. Wo, Z. Li, E. J. Brisbois, A. Colletta, J. Wu, T. C. Major, C. Xi, R. H. Bartlett, A. J. Matzger and M. E. Meyerhoff, *ACS applied materials & interfaces*, 2015, **7**, 22218-22227.

36. J. Sundaram, J. Pant, M. J. Goudie, S. Mani and H. Handa, *Journal of agricultural and food chemistry*, 2016, **64**, 5260-5266.

37. R. P. Kark, D. C. Poskanzer, J. D. Bullock and G. Boylen, *New England Journal of Medicine*, 1971, **285**, 10-16.

38. D. L. H. Williams, *Acc. Chem. Res.*, 1999, **32**, 869-876.

39. J. Kozhukh and S. J. Lippard, *Inorganic chemistry*, 2012, **51**, 7346-7353.

40. R. J. Singh, N. Hogg, J. Joseph and B. Kalyanaraman, *Journal of Biological Chemistry*, 1996, **271**, 18596-18603.

41. J. Pant, M. J. Goudie, S. M. Chaji, B. W. Johnson and H. Handa, *Journal of Biomedical Materials Research Part B: Applied Biomaterials*, **0**.

42. J. Pant, J. Gao, M. J. Goudie, S. P. Hopkins, J. Locklin and H. Handa, *Acta Biomaterialia*, 2017, **58**, 421-431.

43. M. J. Goudie, J. Pant and H. Handa, *Scientific Reports*, 2017, **7**, 13623.

44. B. Grommersch, J. Pant, S. P. Hopkins, M. J. Goudie and H. Handa, *ACS Applied Materials & Interfaces*, 2017, DOI: 10.1021/acsami.7b15967.

45. P. G. Wang, M. Xian, X. Tang, X. Wu, Z. Wen, T. Cai and A. J. Janczuk, *Chemical Reviews*, 2002, **102**, 1091-1134.

CHAPTER 3

ENHANCED ANTIBACTERIAL EFFICACY OF NITRIC OXIDE RELEASING THERMOPLASTIC POLYURETHANES WITH ANTIFOULING HYDROPHILIC TOPCOATS[3]

[3] Singha, P., Pant, J., Goudie, M. J., Workman, C. D., Handa, H. 2017. RSC Biomaterials Science
Reproduced by permission of The Royal Society of Chemistry

Abstract

Surface fouling is one of the leading causes of infection associated with implants, stents, catheters, and other medical devices. The surface chemistry of medical device coatings is important in controlling and/ or preventing fouling. In this study, we have shown that a combination of nitric oxide releasing hydro-phobic polymer with a hydrophilic polymer topcoat can significantly reduce protein attachment and subsequently reduce bacterial adhesion as a result of the synergistic effect. Nitric oxide (NO) is a well-known potent antibacterial agent due to its adverse reactions on microbial cell components. Owing to the surface chemistry of hydrophilic polymers, they are suitable as antifouling topcoats. In this study, four biomedical grade polymers were compared for protein adhesion and NO-release behavior: CarboSil 2080A, silicone rubber, SP60D60, and SG80A. SP60D60 was found to resist protein adsorption up to 80% when compared to the other polymers while CarboSil 2080A maintained a steady NO flux even after 24 hours ($\sim 0.50 \times 10^{-10}$ mol cm^{-2} min^{-1}) of soaking in buffer solution with a loss of less than 3% S-nitroso-N-acetylpenicillamine (SNAP), the NO donor molecule, in the leaching analysis. Therefore, CarboSil 2080A incorporated with SNAP and top-coated with SP60D60 was tested for antibacterial efficacy after exposure to fibrinogen, an abundantly found protein in blood. The NO-releasing CarboSil 2080A with the SP60D60 top-coated polymer showed a 96% reduction in Staphylococcus aureus viable cell count compared to the control samples. Hence, the study demonstrated that a hydrophilic polymer topcoat, when applied to a polymer with sustained NO release from an underlying SNAP incorporated hydrophobic polymer, can reduce bacterial adhesion and be used as a highly efficient antifouling, antibacterial polymer for bio-medical applications.

Introduction

Fouling caused by proteins and bacteria is a very common phenomenon found on interfaces of biomaterials of medical devices and biological environments of the human body.[1] According to the Centers for Disease Control and Prevention, fouling is a major problem that causes nosocomial or hospital-associated infections (HAIs) and has led to the increase in medical costs (overall annual direct medical costs of HAIs in U.S. hospitals ranges from $28.4 to $33.8 billion).[2] Medical implants and devices like biosensors, drug carriers, soft contact lenses, vascular stents, and urological devices upon contact with the biological milieu can cause subsequent settling of non-specific biomacromolecules on the foreign surfaces [3] and trigger a cascade of events that can bring about device failure. Biomacromolecules like proteins and bacteria settle down on the surface of these medical devices and start forming a layer of extrapolymeric substance (EPS) which is followed by settling of pathogens like bacteria and fungi on these protein layers.[4, 5] These layers can develop into large films of a mixture of EPS and bacteria called biofilms. Biofilms are tough to get rid of due to their stable aggregation of bacteria covered with a film of proteins and can thus block pathways for medical devices and cause device failure. This stage of device contamination is infection and may lead to sepsis and eventually cause patient death. In the recent times, significant research efforts have been directed towards finding efficient antifouling polymers combined with antibacterial properties in the medical industry to combat the problem of biofilms.[6-11]

Some of the methods that have been used for antifouling mechanisms of polymers are steric repulsion,[12, 13] electrostatic repulsion,[14, 15] and hydrophilicity.[15-17] While steric and electrostatic repulsion are reliable methods for antifouling, both involve major processing changes that is possible in lab scale but not practical for industrial applications. Increasing

hydrophilicity of a material for antifouling mechanism is advantageous because most proteins that contaminate surfaces are hydrophobic in nature and the hydration layer formed on the hydrophilic polymer keeps proteins from adhering to the coating surface of the medical device.[18, 19] Hydrophilic polymers tend to be smooth and a water layer can easily form on these medical device coatings as they are kept in contact with bodily fluids.[20] This hydration layer helps in repulsion of non-specific proteins and acts as an antifouling mechanism.[19] Roughness of surfaces also play a critical role in adhesion of proteins.[21, 22] It has been found to be an important factor at the nanometer scale for both fibrinogen and bovine serum albumin attachment.[21] Increasing random roughness increases the adhesion of proteins to surfaces of biomaterials. Therefore in comparison with smoother polymers that do not allow adherence of proteins, rough polymers tend to act as support for proteins and pathogens to attach to and hence are not considered to be antifouling in nature.[23]

Antimicrobial polymers can be broadly classified into three types according to their general working principles: polymeric biocides, biocidal polymers, and biocide-releasing polymers.[24] Polymeric biocides have repeating units of biocides and in case of biocidal polymers, the whole polymer acts like one antimicrobial agent so no repeating units of biocidal groups are required. Biocide-releasing polymers carry the biocidal agents and release them into the microbes. While passive approaches like polymeric biocides and biocidal polymers are very closely related where the microbe has to come in contact with the polymer to be acted on, the dynamic action of biocide releasing polymers to act from a distance gives them an advantage over the other two classifications. This means that the microbe does not have to be in contact with the polymer to be killed. Another advantage of biocide releasing polymers is that since they discharge antimicrobial agents incorporated within them, the concentration of these biocides can

be controlled according to the applications. Biocide releasing polymers also do not let dead microbes bind to the polymers themselves and hence do not allow for accumulation of dead microbes. These advantages of biocide releasing polymers have led to intensive research on antimicrobial agents that can be incorporated within them.

Some commonly studied antimicrobial agents are silver,[25-29] antimicrobial peptides,[30-34] and nitric oxide (NO).[35-37] While silver has been found to be an effective antimicrobial agent, it has also demonstrated concerns for cytotoxicity.[38, 39] Antimicrobial peptides are also being studied in great detail but due to the complexity of their interactions,[40] they are not a popular class of practically useful antimicrobial agents.

Besides being an endothelium derived relaxing factor which functions as a vasodilator, NO is a well-known antibacterial agent and it has been tested in various polymers along with its production from different sources/donors.[35, 41-61] It is a free radical that reacts with superoxides and oxygen to form peroxynitrite and dinitrogen trioxide, respectively.[42, 43, 62] Nitric oxide's mechanisms of action against bacteria include nitrosation of amines and thiols in the extracellular matrix, lipid peroxidation and tyrosine nitration in the cell wall, and DNA cleavage in the cellular matrix.[63] It's antibacterial activity has been found to be successful in various hospital associated infection pathogens such as *Pseudomonas aeruginosa*,[64, 65] *Staphylococcus aureus*,[45, 46, 65] *Escherichia coli*,[45, 46, 56, 65-67] *Staphylococcus epidermidis* [46], and *Acinetobacter baumannii*.[35, 68]

However, even though the antibacterial effects of NO have been studied without any other aids, it's synergistic effects when combined with an antifouling polymer has not been extensively studied. This is important to study because despite its antibacterial nature, NO by itself cannot prevent the adsorption of proteins. Study of NO releasing materials with the

combination of antifouling materials would be essential to eliminate any fouling from proteins that takes place when a medical device first comes in contact with bodily fluids and consequently facilitates bacterial adhesion.

Herein, we combine a hydrophilic antifouling polymer topcoat (SP60D60) on a sustained NO-releasing low water uptake polymer (CarboSil 2080A). Initially, four polymers were chosen to test the different parameters required for the desirable antifouling and antibacterial effects. CarboSil 2080A and Dow Corning® RTV 3140 Silicone Rubber (RTV) were the hydrophobic polymers while SP60D60 and SG80A were the comparatively hydrophilic polymers tested. CarboSil 2080A is a thermoplastic urethane copolymer with a mixed soft segment of poly (dimethyl siloxane) and hydroxyl-terminated polycarbonate and a hard segment of an aromatic diisocyanate.[69] RTV is a coating material with a chemical composition of silicone elastomer. SP60D60 is a Tecophilic® solution grade thermoplastic polyurethane resin which is commonly used as a biomedical device coating polymer. SG80A is a Tecoflex® solution processible grade thermoplastic polyurethane resin which, like SP60D60, is also commonly used in the medical industry for coating purposes.

The four polymers were tested for their wetting properties by measurement of static contact angles, water uptake, and surface roughness. Once the wetting nature of the polymers was established, they were tested for their antifouling nature. Protein adhesion test was performed using spectroscopic ellipsometric measurements. Least amount of protein was found attached to SP60D60's surface which was also supported by its hydrophilic and smooth surface and hence it was chosen as the topcoat material. Following this, NO-release behavior for the polymers were determined with *S*-nitroso-*N*-acetylpenicillamine (SNAP) leaching study and nitric oxide release analysis. CarboSil 2080A and RTV both displayed a minimal loss of SNAP

(<5% and <7% of total SNAP present in the sample, respectively) during the leaching analysis and hence were chosen for further NO release measurements. Finally, antibacterial efficacy test with gram positive bacteria *Staphylococcus aureus* was performed to analyze if the hydrophilic coated polymers were more efficient than the control. The increase in killing efficiency of the test samples when compared to the hydrophobic polymer coated controls validated that a SNAP-incorporated CarboSil 2080A with a topcoat of SP60D60 showed the highest reduction in microbial viability.

Materials and methods

Materials

N-acetyl-*D*-penicillamine (NAP), sodium nitrite, concentrated sulfuric acid (conc. H_2SO_4), tetrahydrofuran (THF), sodium phosphate monobasic (NaH_2PO_4), sodium phosphate dibasic (Na_2HPO_4), potassium chloride, sodium chloride, fibrinogen from bovine plasma, and ethylenediamine tetraacetic acid (EDTA) were obtained from Sigma Aldrich (St. Louis, MO). Luria Agar (LA), Miller and Luria broth (LB), Lennox were purchased from Fischer BioReagents (Fair Lawn, NJ). Concentrated hydrochloric acid (conc. HCl), sodium hydroxide (NaOH), and methanol were purchased from Fisher-Scientific (Hampton, NH). Potassium phosphate monobasic (KH_2PO_4) was purchased from BDH Chemicals - VWR International (West Chester, PA). Tecophilic SP-60D-60 and Tecoflex SG-80A were products of Lubrizol Advanced Materials Inc. (Cleveland, OH). Dow Corning RTV 3140 Silicone Rubber (SR) was purchased from Ellsworth Adhesives (Germantown, WI). CarboSil™ 2080A was obtained from DSM Biomedical Inc. (Berkeley, CA). Milli-Q filter was used to obtain de-ionized water for the aqueous solution preparations. *Staphylococcus aureus* (ATCC 5538, *S. aureus*) was used for all bacterial experiments.

Synthesis of S-nitroso-N-acetylpenicillamine (SNAP)

S-nitroso-*N*-acetylpenicillamine was synthesized using methods previously reported with a few modifications.[44, 70] 1M HCl and 1M H_2SO_4 was added to an equimolar amount of NAP, methanol and sodium nitrite solution containing DI water. This reaction was stirred for 15 minutes and then cooled in an ice bath for 4 hours. After evaporation of the reaction mixture, precipitated green crystals of SNAP were vacuum filtered, collected and allowed to air dry in dark conditions. Dried crystals of SNAP were used for all experiments.

Preparation of SNAP-incorporated Polymer Films

Polymers containing 10 wt% SNAP were prepared by solvent evaporation method. The casting solutions were prepared by dissolving 210 mg of the respective polymer (CarboSil 2080A, RTV, SP60D60 or SG80A) in 3 mL of THF. The polymers were allowed to dissolve before the addition of 23.1 mg of SNAP for a final concentration of 10 wt% of SNAP. This mixture was protected from light and stirred until the SNAP crystals dissolved completely. The polymer solutions were then poured into Teflon molds (d = 2.5 cm) and allowed to dry overnight in fume hood. The dried films were then cut into small disks (d = 0.7 cm) and dip coated with a topcoat solution of the polymer without SNAP (40 mg/mL of polymer concentration in THF). The small disks were dried overnight and then dried under vacuum for an additional 24 hours. This was done to remove any residual THF which can hamper the following studies. Weight of each small disk was measured before topcoat. The prepared disks were kept in the freezer (-18°C) in the dark to retain its NO releasing properties and prevent leaching of SNAP. These SNAP-incorporated films were used for NO-release, SNAP leaching and bacterial adhesion studies.

Preparation of Thin Polymer Films on Silicon wafers

Thin polymer films on silicon wafers were deposited by spin coating the polymer solution using a CHEMAT Technology KW-4A spin coater. Films were spin coated at 2500 rpm for 30 seconds, yielding highly uniform pinhole free layers with a surface thickness of 70-100 nm. These thin films were used for studying protein adhesion measurement (section *2.5.3.*) using a M-2000 spectroscopic ellipsometer (J.A. Woollam Co., Inc.).

Characterization of Topcoat Material with Least Protein Adhesion

Static Contact Angle and Water Uptake Measurement

Static contact angle for the four chosen biomedical grade polymers (two hydrophilic- SP60D60 and SG80A, and two hydrophobic- CarboSil 2080A and RTV, comparatively) were measured using a Krüss DSA100 Drop Shape Analyzer (sessile drop method with deionized water). Spin coated polymers on silicon wafers were used for the measurement.

For water uptake measurement, polymer films prepared with the solvent evaporation method were weighed and soaked in water overnight. Three replicates were used for each measurement. Their mass was checked the next day to measure the water uptake for the polymers.

Surface Roughness Measurement

Surface roughness measurement to check for consistency with protein adhesion study was measured using PeakForce QNM (Bruker Multimode AFM) over a 10 μm^2 region. AFM imaging was done on polymer films dried on silicon wafers using solvent evaporation technique. Three images and roughness average measurements (R_a in nm) were collected for each polymer to confirm the measurements.

Protein Adhesion Study

The thicknesses of spin coated films (prepared according to section *2.4*.) were measured using a M-2000 spectroscopic ellipsometer (J.A. Woollam Co., Inc.) with a white light source at three angles of incidence (65, 70, and 75°) to the silicon wafer normal. Three replicates were used for each measurement. After thickness of each film was measured, a non-saline phosphate buffer solution was prepared from 1 M sodium phosphate dibasic and 1 M potassium phosphate monobasic. The solution was adjusted to a pH of 7.41 at room temperature (25°C). Samples were kept in the non-saline phosphate buffer for 30 minutes at 37°C. A solution of fibrinogen from bovine plasma and non-saline phosphate buffer was prepared to achieve a concentration of 1mg mL^{-1} once added to the non-saline phosphate buffer the samples were first placed in. After the protein solution was added to the samples, they were allowed to incubate at 37°C for 90 minutes. After incubation each sample was washed with 5mL of non-saline PBS five consecutive times followed by 5mL of distilled water five consecutive times. The thickness of the wafers before and after submersion in the protein solution was measured by spectroscopic ellipsometry. Care was taken to measure the thickness on the same area of the films as measured before to avoid any inconsistency in data collection.

Characterization of SNAP-incorporated films for optimized NO-releasing polymer

SNAP leaching Study

The weight percentage of SNAP leached out from the polymers were measured by recording the absorbance of buffer solutions in time intervals of 0.5 h, 1 h, 4 h, and 24 h at 340 nm. Three sample for each type of film was prepared and weighed before topcoating to determine the initial amount of SNAP in each film. These films were then soaked in PBS (with EDTA) at 37°C. A UV-vis spectrophotometer (Thermoscientific Genesys 10S UV-Vis) was used

to measure the absorbance of the buffer solutions in the above-mentioned time intervals. Absorbance was measured at an optical density of 340 nm which is the maxima in the UV-Vis absorbance spectra for SNAP. The calibration graph of SNAP in PBS (with EDTA) was used to interpolate the absorbance measurements recorded from the study and convert them to concentrations of SNAP in the measured sample. This concentration was converted to weight % of SNAP in the buffer using the initial amount of SNAP present in each sample used. Care was taken to make sure that buffer solution amount for each sample was maintained at the same amount throughout the experiment to avoid any inconsistent readings and three replicates were used for each measurement.

NO-Release Measurements

S-nitroso-*N*-acetylpenicillamine present in the samples releases NO under physiological conditions (Figure 3.1**)** and this was measured and recorded for the study. Real time NO-release from the polymer films was measured using Sievers chemiluminescence NO analyzers® (NOA 280i, GE Analytical, Boulder, CO, USA). The sample holder of the NOA was shielded from light and injected with 4 mL of PBS (containing EDTA). This buffer solution was warmed up to 37°C by a water jacket placed around the sample holder. Once PBS warms up and a baseline of NO flux is established for the sample (prepared according to section *2.3.*), the sample is then placed in the sample holder. Nitric oxide released by the sample in the sample holder was swept and purged by a continuous supply of high purity nitrogen maintained at a constant flowrate of 200 mL min^{-1} through the sweep and bubble flows. At the same time, oxygen produces the ozone required for the reaction that would take place in the reaction chamber. The NO released by the sample is pushed towards the chemiluminescence detection chamber. The voltage signal produced is converted to concentration and displayed on the analyzer's screen. Using the raw

data in ppb form and NOA constant (mol ppb^{-1} s^{-1}), the data in ppb is normalized and converted to NO flux units (x 10^{-10} mol cm^{-2} min^{-1}) according to the surface area of the sample used for analysis. Data is collected in the time intervals mentioned and samples are stored in a PBS (with EDTA) solution at 37°C in dark conditions. The PBS is replaced daily to avoid any accumulation of NO released during the storage time.

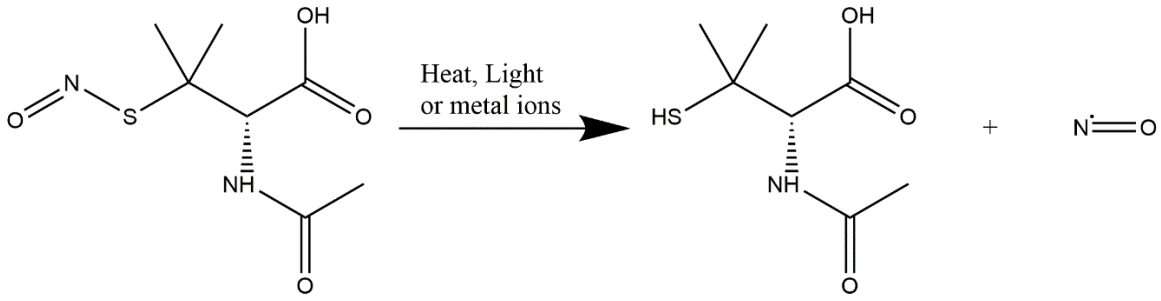

Figure 3.1: Scheme showing release of nitric oxide from *S*-nitroso-*N*-acetylpenicillamine on exposure to heat, light and/or metal ions.

The samples were always submerged in the buffer solution through the NO-release flux recording. The instrument operating parameters were a cell pressure of 7.4 Torr, a supply pressure of 5.9 psig and a temperature of − 12 °C. Three replicates were used for each measurement.

Top Coat Stability Study

Static contact angles were measured to make sure that the antifouling hydrophilic polymer, SP60D60, would not delaminate from the hydrophobic polymer, CarboSil 2080A, due to exposure to physiological conditions including soaking in PBS and temperature of 37°C. Spin-coated silicon wafers with CarboSil 2080A and a topcoat of SP60D60 were kept in PBS solution at 37°C. Static contact angle was measured using a Krüss DSA100 Drop Shape Analyzer before

and after 24 hours of incubation in the PBS solutions. This environment was used to mimic the physiological environment used for protein adhesion and NO-release study.

In vitro Analysis of Inhibition of Bacterial Adhesion on Polymer Surface

In this study section, the combined effect of SP60D60 coat on CarboSil 2080A base in terms of bacteria adhesion post protein (fibrinogen from bovine plasma) exposure was assessed using a modified method based on the American Society for Testing and Materials E2180 test protocol. This protocol is effective in testing antimicrobial efficacy of hydrophobic polymers. The multidrug resistant Gram-positive *S. aureus* bacteria which is among the most common cause of hospital acquired infections (HAIs) was used as the model organism to test the efficacy of SP60D60 coating in preventing bacteria adhesion.

Bacterial Culture Preparation

Luria Broth (LB) medium was prepared according to the manufacturer's instructions. This broth was sterilized in an autoclave prior to using it for the study. A bacterial suspension was cultured in LB medium for 14 hours at 37°C and a horizontal rotating speed of 150 rpm in shaker incubator. After 14 hours of culture, the optical density (O.D.) of the culture was measured at a wavelength of 600 nm ($O.D._{600}$) using a UV-vis spectrophotometer (Thermoscientific Genesys 10S UV-Vis) to ensure that the bacteria are in actively dividing phase. The bacteria culture was then centrifuged at 3500 rpm for 7.5 mins and the supernatant was discarded. The bacterial cells were washed with fresh sterile phosphate buffer saline (PBS)-pH 7.4, centrifuged at 3500 rpm for 7.5 mins. The supernatant was discarded and fresh PBS was added to resuspend the bacteria. The $O.D._{600}$ of the cell suspension in PBS was measured using PBS as blank and adjusted to the CFU in the range of 10^6-10^8. In order to verify the consistency of concentration of viable cells between experiments, serial dilutions of *S. aureus* bacteria were

prepared and plated petri dishes containing autoclaved LB agar. LB agar was prepared according manufacturer's instructions.

Bactericidal Activity Analysis

CarboSil 2080A base with CarboSil 2080A topcoat (CarboSil 2080A/CarboSil 2080A) (n=3) was used as the control to compare the difference in number of viable bacteria on CarboSil 2080A base with SP60D60 topcoat (SP60D60/CarboSil 2080A) and 10 wt.% SNAP films with SP60D60 top coat (SP60D60/SNAP) (n=3). These films were exposed to 1 mg mL^{-1} of fibrinogen from bovine plasma for 1 hour in the method as described in section *2.5.3*. Post 1h of protein exposure, the films were exposed to bacterial cells (10^6-10^8 CFU mL^{-1}) at 37°C for 3 hours at a speed of 200 rpm in a shaker incubator. After 3 hours, films were rinsed with sterile PBS to remove any loosely bound bacteria from the film surface and transferred to fresh PBS. The films were homogenized for 45 seconds, vortexed for 20 seconds and *S. aureus* was plated in the solid LB agar medium after preparing serial dilutions in the range of 10^{-1}-10^{-5}. The LB agar plates with the plated bacteria culture were incubated at 37°C for 20 hours. After 20 hours, the CFUs were counted considering the dilution factor and the number of viable bacteria on SP60D60/SNAP films were compared to the control films. Three replicates were used.

Statistical analysis of data

All data are expressed as mean ± standard deviation. The results between the control and test films were analyzed by a comparison of means using Student's t-test. Values of p were obtained for the data analyzed to show significance of results.

Results and Discussion

Characterization of Polymers for an Antifouling Topcoat

The four polymers chosen for this study were at first tested for their wetting properties. These preliminary data would help in predicting their hydrophilic nature and subsequently antifouling properties. At first, static contact angle for the spin coated films was measured. The static contact angle for SP60D60 was the lowest (51.10 ± 2.21°) among the polymers while CarboSil 2080A and RTV both displayed high contact angles (Table 3.1). This demonstrated that SP60D60 was the most hydrophilic polymer among the four polymers selected for the study. Following this, the results of water uptake study supported the contact angles measurements as predicted. Water uptake was the highest for SP60D60 (57.55 ± 1.80 %) (Table 3.2) and the least for RTV (0.47 ± 0.25 %).

Table 3.1: Static contact angle of the polymers used in the study by a Krüss DSA100 Drop Shape Analyzer. Data represents mean ± SD (n=3).

Polymer	**Static Contact Angle (°)**
CarboSil	104.62 ± 0.08
RTV	111.40 ± 0.30
SP60D60	51.10 ± 2.21
SG80A	93.27 ± 0.66

Table 3.2: Water uptake of the polymers used in the study measured in weight%. Data represent mean ± SD (n = 3)

Polymer	**Water Uptake (wt. %)**
CarboSil	0.83 ± 0.27
RTV	0.47 ± 0.25
SP60D60	57.55 ± 1.80
SG80A	3.37 ± 1.89

The four polymers were further studied for their surface roughness (roughness average) by using atomic force microscopy. A 10 μm^2 scan was taken for each substrate and as shown in Figure 3.2, the difference in surface roughness was clearly visible. The hydrophobic polymers, (CarboSil 2080A=0.873 ± 0.048 nm and RTV=2.257 ± 0.458 nm) exhibited higher surface roughness while the hydrophilic polymers (SP60D60=0.360 ± 0.099 nm and SG80A=0.362 ± 0.003 nm) were both smoother. It is understood that this smooth surface of the hydrophilic surface helps in retaining the hydration layer above the polymer and creates a slippery surface on which adhesion by proteins and bacteria is significantly reduced. As previously mentioned, the random roughness of the hydrophobic polymers would also help in protein attachment instead of repulsion. Random roughness increases the amount of surface area available for attachment and hence can increase the amount of adsorbed protein. Random roughness can also increase van der Waals force and electrostatic force, thereby increasing the adsorption of proteins on rough surfaces.[21] Therefore, from the results of the wetting properties and surface roughness analysis, the hydrophilic polymers were expected to perform better than the hydrophobic polymers on testing for repulsion of proteins from the polymer surface.

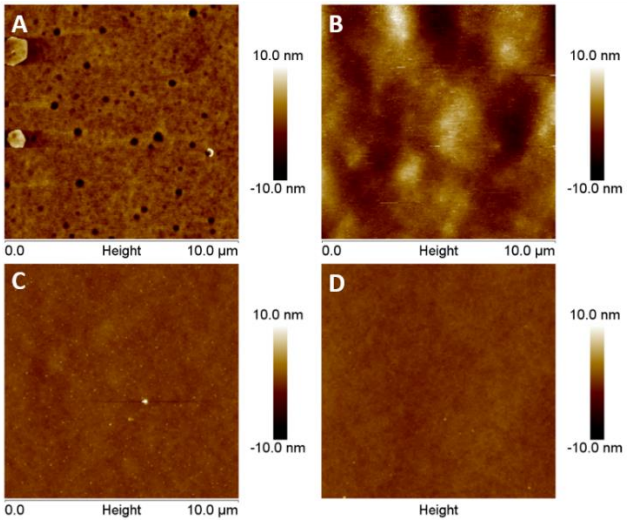

Figure 3.2: AFM topography images of the four polymers used in the study to compare surface roughness between the hydrophobic and hydrophilic polymers. The surface roughness (nm) for the polymers were: A) CarboSil = 0.873 ± 0.048 B) RTV = 2.257 ± 0.458 C) SP60D60 = 0.360 ± 0.099 D) SG80A = 0.362 ± 0.003. Data represents mean ± SD. (n=3)

Protein adhesion test for an Antifouling Topcoat

For the protein adhesion test, all four polymers were soaked in a buffer solution of fibrinogen protein (concentration of 1mg/mL) for 90 minutes because the bulk of protein adhesion to medical device surfaces typically occurs within the first few minutes of exposure to physiological fluids.[71] The samples were incubated in the fibrinogen solution at 37°C to mimic physiological conditions.

Fibrinogen (340 kDA) is an anisotropic protein and has shown to increase bacterial adhesion.[11, 72-76] It is an adhesive protein that is known to replace proteins like albumin on the surface of materials (Vroman effect) due to its higher surface affinity.[72] Fibrinogen molecules act as extracellular matrix (ECM) for bacteria such as *S. aureus* and the interaction between them has been studied extensively.[77] The receptors of ECM molecules bind to adhesins present on bacteria and trigger complex signal transduction cascades in the bacterial cell that can provide impetus to bacterial invasion. In the case of fibrinogen and *S. aureus*, the fibrinogen binding proteins present on the bacterial cells are called clumping factors A and B.[78] The favorable binding interactions between proteins like fibrinogen and bacteria like *S. aureus* make it an important aspect to control while fabricating implants and medical devices since consequences like biofilm growth can cause device failure.

Any unattached proteins were removed from the polymer surfaces by rinsing the surfaces with non-saline buffer and DI water. The data obtained in Figure 3.3 shows the change in the thickness for the respective polymers. The nanometer change in thickness of the films were measured using a spectroscopic ellipsometer. Spectroscopic ellipsometry can easily detect changes in the nanometer scale. As studied using electron microscopy and atomic force microscopy, fibrinogen is a highly elongated and anisotropic protein which has dimensions of 5-6.5 nm in diameter and 47.5 nm in length.[79, 80] Therefore, in the ellipsometric measurements, any change above 5 nm would be considered adsorption of the fibrinogen protein.

From the data, we can infer that protein adhesion was confirmed to be non-existent ($p = 0.004$) on SP60D60 (2.24 ± 0.68 nm) while the other polymers (CarboSil 2080A = 6.63 ± 0.78 nm, RTV = 5.96 ± 1.66 nm and SG80A = 6.14 ± 1.47 nm) did show a monolayer of fibrinogen adsorption on the surfaces. SP60D60 shows a high resistance to protein adsorption on its surface due to its surface properties. It is hydrophilic in nature which enables it to form a hydration layer with the surrounding environment. This hydration layer in turn protects it from formation of a protein layer on it. The protein molecules are unable to bind to the surface because of the presence of the hydration layer. However, the small increase in thickness observed on SP60D60 can be due to two reasons. It can indicate slight swelling of the SP60D60 surface due to the formation of a hydration layer. It can also indicate the presence of particles on its surface from the environment as spectroscopic ellipsometric measurements are highly sensitive and even despite of avoiding any contact with dust particles, other accidentally settled particles can cause this increase in thickness of only 2.24 nm. Thus, from the mentioned results obtained for characterization of antifouling topcoat polymer, SP60D60 was chosen to be topcoated to the optimal NO-releasing polymer.

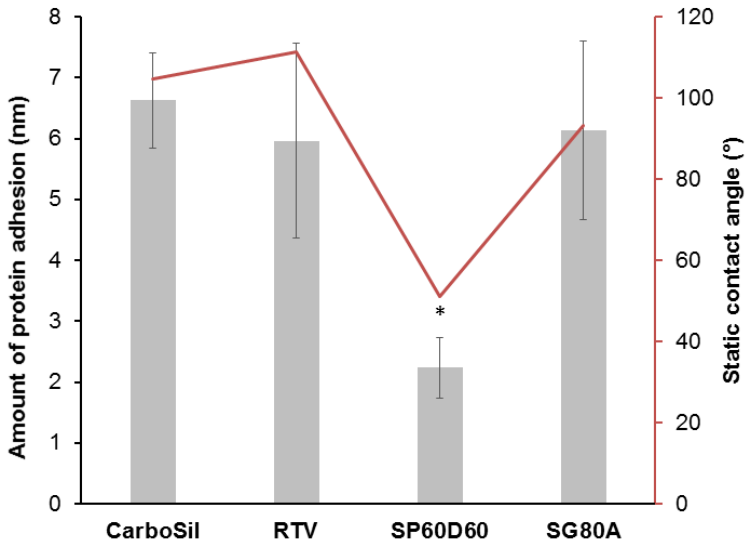

Figure 3.3: Graph shows relationship between wetting characteristic and protein adhesion of the surface. It shows thickness of protein layer attached to the polymer after exposure to 1 mg mL^{-1} of fibrinogen from bovine serum for 90 minutes. Static contact angle represents wetting characteristic of the material with no protein on it. Data represents mean ± SD (n=3) ($p<0.004$)

Characterization of Polymers for Optimized NO-release

After selecting SP60D60 for the topcoat, the four commercial biomedical grade polymers were tested for incorporation of SNAP to choose the optimal NO-releasing polymer. SNAP leaching study was performed at first to determine the polymers that retain significant amount of SNAP in them after 24 hours of soaking in PBS (Figure 3.4). High amount of SNAP retention in the polymers ensures sustained release of NO from the polymers and minimizes the risks (if any) associated with SNAP leaching. After 4 hours of storing the higher water uptake polymer, SP60D60, in the buffer solution at 37°C, a loss of 84.55±1.83 % was recorded. With this initial high rate of leaching from the polymer it was expected that the samples would leach a significant amount of SNAP within 24 h. Overnight storage of the same films of SP60D60 showed a loss of

99.00±0.88 % of SNAP. This was in contrast to the SNAP leaching behavior of lower water uptake polymers, CarboSil 2080A, RTV, and SG80A. At the end of 4 hours, all three had a very low leaching of 2.54±0.18 %, 4.70±1.01 % and 7.25±0.20 % for CarboSil 2080A, RTV, and SG80A, respectively. As expected, these polymers also displayed a minimal leaching of 4.75±0.18 % (CarboSil 2080A),6.96±1.01 % (RTV) and 11.26±0.07 % (SG80A) at the end of 24 h of being soaked in PBS at 37°C. The behavior of high leaching of SNAP from SP60D60 is expected as it is a hydrophilic polymer and hence absorbs water while releasing SNAP molecules from within. However, comparatively hydrophobic polymers, SG80A, CarboSil 2080A, and RTV, leached out <10% of total SNAP content. This characteristic of hydrophobic polymers makes them desirable for incorporating NO donors to maintain a controlled release of NO for a longer period of time.

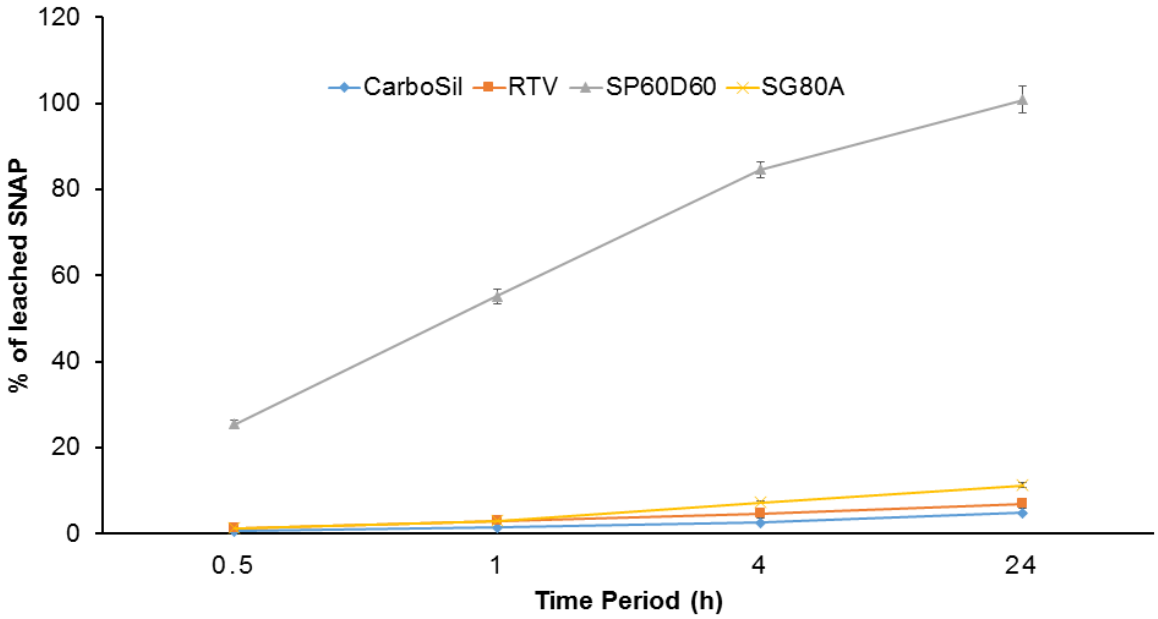

Figure 3.4: SNAP content in PBS buffer as a result of leaching activity in the polymer. Calculated as a percentage of SNAP leached into the PBS buffer from the polymer. Data represents mean ± SD (n=3).

The desirable characteristics of CarboSil 2080A and RTV to retain SNAP within them for with minimal leaching made them ideal polymers to test for NO release. In the first hour, CarboSil 2080A displayed an NO flux of 12.42±3.20 (x 10^{-10} mol cm^{-2} min^{-1}) and RTV displayed 5.34±0.91 (x 10^{-10} mol cm^{-2} min^{-1}). This trend of higher NO flux from CarboSil 2080A compared to RTV is seen through the 24-hour study (**Figure 3.5**). This tendency of higher release of NO from CarboSil 2080A despite lower leaching of SNAP is advantageous because it means the material properties of CarboSil 2080A allow it to release NO without leaching of SNAP. This helped in determining CarboSil 2080A as the polymer for optimal release of NO for this study. This would enable us to carry out further research on the SNAP-incorporated CarboSil 2080A owing to its remoldable nature, high recyclability, chemical resistance, and aesthetic finish.

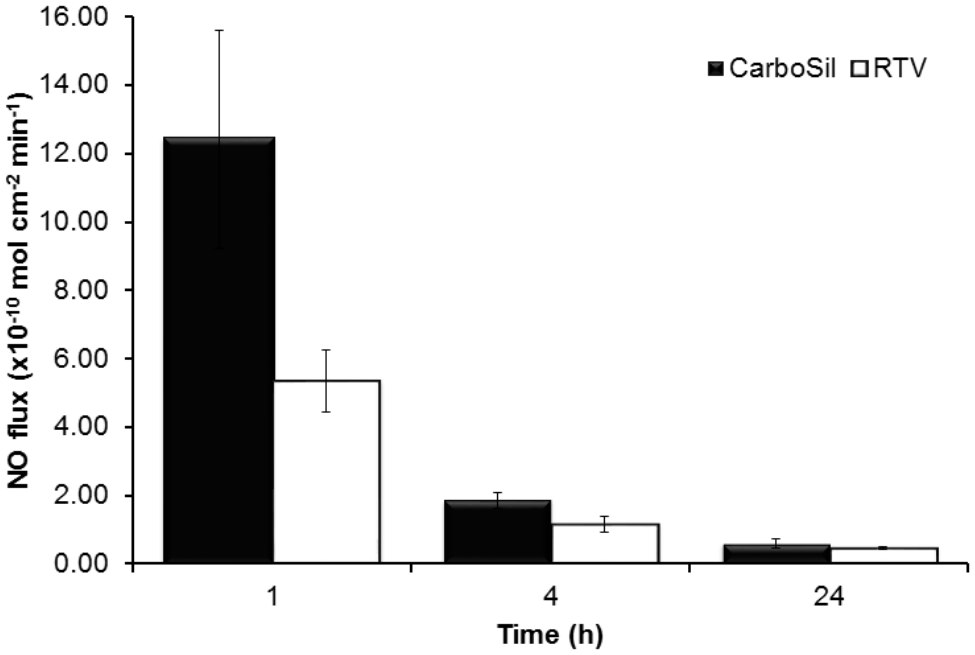

Figure 3.5: NO-release from two hydrophobic (CarboSil and RTV) under physiological conditions (soaked in PBS buffer at 37°C in dark condition). Data represents mean ± SD (n=3)

Antibacterial Efficacy of SNAP-incorporated Polymer with Antifouling Topcoat

Coating of a hydrophobic polymer with a hydrophilic polymer is sometimes not possible due to the high solubility of the hydrophilic polymer in water. This high solubility can cause delamination of the hydrophilic polymer from the hydrophobic surface that it is coated on. To make sure that the polymers used in the study would complement each other and do not get delaminated, the film of CarboSil 2080A topcoated with SP60D60 was soaked in PBS at 37°C for 24 hours. Contact angle was checked before and after soaking in PBS. Three replicates were checked at three different spots on the samples and found to maintain their static contact angles ~50°. This is the contact angle for SP60D60 and hence it was confirmed that the hydrophilic SP60D60 would not delaminate from the hydrophobic CarboSil 2080A.

Bacteria adhesion, which often results in biofilm formation on the polymer surface, is a very common problem in moist and humid environment, which is found in implanted devices. The basic nutrients important for colony formation may be resourced from the polymer material itself, the fluid's proteins that adhere to the polymer post-implant or a variety of contaminants that end up on the surface of the material. *S. aureus* is a major cause of infections associated with wounds, indwelling catheters, and cardiovascular and orthopedic implant devices.[77, 81, 82]

Owing to the antibacterial properties of NO, active release of NO from the donor molecule incorporated in the hydrophobic polymeric films can reduce the chances of biomedical device related infections or hospital-associated infections. The binding of bacteria to the polymer surface (base) can further be reduced by layering it with a comparatively hydrophilic polymer as the top coat. This hydrophilic layer is antifouling in nature and hence prevents the attachment of non-specific contaminants like proteins and bacteria on the material's surface. In comparison to CarboSil 2080A (base polymer), SP60D60 (topcoat polymer) is less hydrophobic and hence can

form a hydration layer on it. While the hydrophobic nature and low water uptake of CarboSil 2080A provides sustained release of NO, the formation of hydration layer on SP60D60 is expected to prevent protein attachment (as mentioned in the results from section 3.2) and also reduce bacterial adhesion on the material's surface directly and indirectly (by repulsion of proteins).

Therefore, all samples tested were first exposed to 1 mg/ml of fibrinogen protein for 90 minutes (as done in section 2.5.3) and then exposed to the bacterial solution. The polymers used in this study were exposed to 10^8 CFU mL^{-1} of *S. aureus* for three hours. After the three-hour exposure to the bacteria, the SP60D60/CarboSil 2080A hybrid films (first set of test films) with no SNAP showed 78.95 % reduction in viable *S. aureus* cells when compared to CarboSil 2080A/CarboSil 2080A (control). This reduction is significant and therefore test with SNAP-incorporated material was done to demonstrate the increase in significant reduction. The second set of test films (10 wt. % SNAP in SP60D60/CarboSil 2080A) generated an NO flux of 1.89 ± 0.64 (x 10^{-10} mol cm^{-2} min^{-1}) (Figure 3.6), reducing the bacterial growth on the material's surface by 95.83 % ($p < 0.05$) and 80.20 % ($p < 0.05$), when compared to CarboSil 2080A/CarboSil 2080A (control) and SP60D60/CarboSil 2080A films, respectively (Figure 3.7). This reduction in number of viable bacteria attached to the second set of test films is significant compared to both control and first set of test films. These results are consistent with the theoretical expectations underlying the surface chemistry of SP60D60 and bactericidal properties of NO. To summarize, the combined effect of the tunable NO-release kinetics from CarboSil 2080A's surface and prevention of protein and/or bacterial adhesion due to SP60D60's surface chemistry can help reduce undesired clinical consequences post-implantation of a medical device.

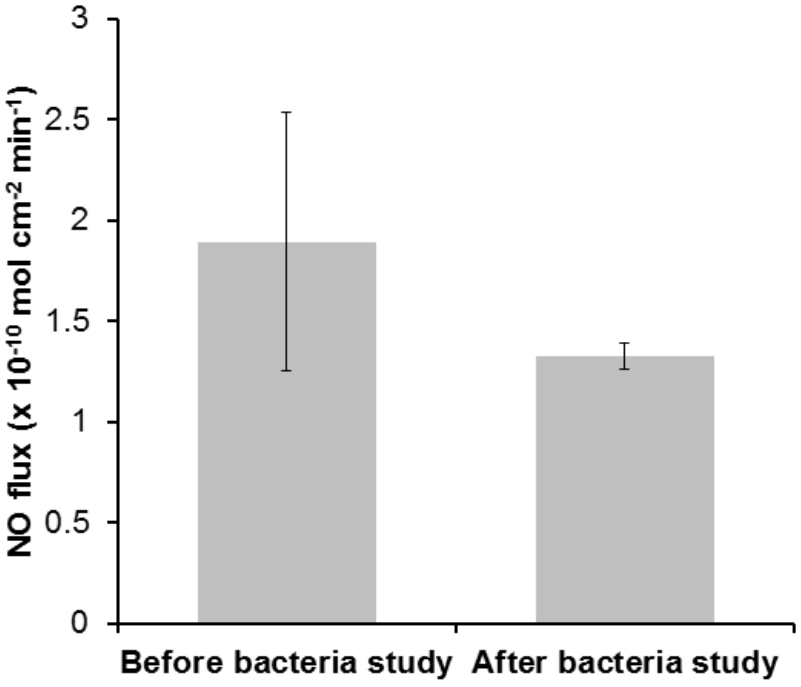

Figure 3.6: NO flux data before and after the bacterial study. NO flux was 1.89 (x 10^{-10} mol cm^{-2} min^{-1}) and 1.33 (x 10^{-10} mol cm^{-2} min^{-1}) before and after the bacterial incubation respectively. Data represents mean ± SD (n=3).

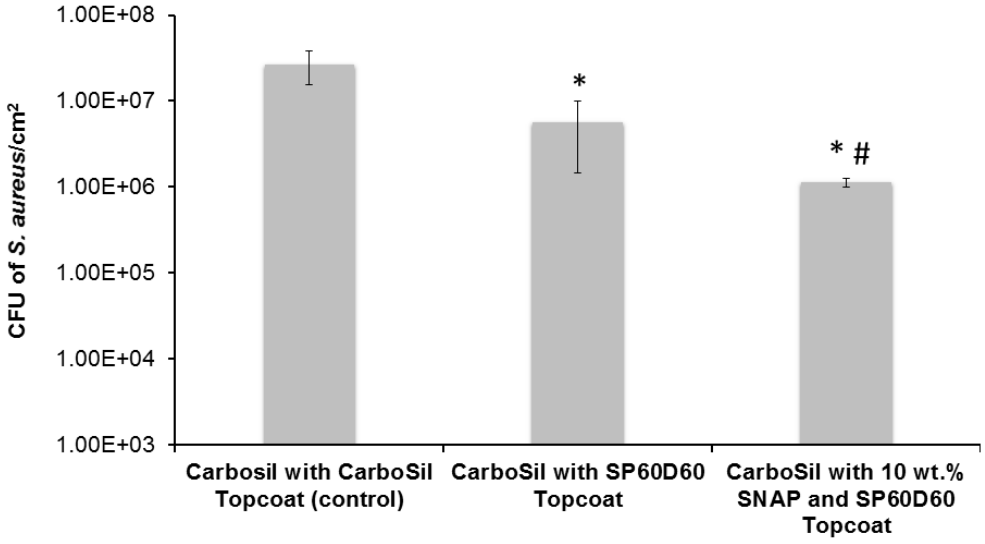

Figure 3.7: Bacterial adhesion data showing the CFU of *S. aureus* per cm^{-2} after 3 hours of incubation in the post-protein adhesion treated (1 hour) polymer material. A reduction of 78.95%

in viable bacteria is seen on first set of test films (CarboSil topcoated with SP60D60) when compared to control films (CarboSil with CarboSil topcoat) (indicated by *). A reduction of 80.20% is seen on second set of test films when compared to the first set of test films (CarboSil with SP60D60 topcoat and no SNAP) (indicated by #). A reduction of 95.83% in viable bacteria is seen on second set of test films (CarboSil with 10 wt. % SNAP topcoated with SP60D60) when compared to control films (CarboSil with CarboSil topcoat) (indicated by *). Data represents mean ± SD (n=3). * = $p \leq 0.05$ for * and *#.

Conclusion

In this study we were able to design an efficient antifouling hydrophilic biomedical grade coating for NO releasing hydrophobic polymers which had significant reduction in protein adhesion and microbial growth. This approach was supported by the rigorous testing of the materials in a protein solution found commonly in physiological conditions and analysis of a sustained release of nitric oxide over a period of 24 hours. This study was able to prove two important points: 1) non-NO releasing hydrophobic polymer with a hydrophilic topcoat can reduce bacterial adhesion when compared to hydrophobic polymer topcoats 2) SNAP incorporated in hydrophobic polymer and topcoated with a hydrophilic polymer could significantly reduce microbial growth of a commonly found pathogenic bacteria (*S. aureus*) compared to polymers with no SNAP. The conclusion supports the theoretical explanation that hydrophilic antifouling polymers can further reduce microbial growth and surface roughness is a very important aspect of surface chemistry while considering it. Therefore, hydrophilic polymers can be a useful strategy of coatings for nitric oxide and other biocide releasing materials which

can consequently reduce microbial adhesions while keeping a controlled release of antibacterial agents.

References

1. J. L. Harding and M. M. Reynolds, *Trends Biotechnol*, 2014, **32**, 140-146.
2. R. Douglas Scott II, *The Direct Medical costs of Healthcare-Associated Infections in U.S. Hospitals and the Benefits of Prevention*, Centers for Disease Control and Prevention, 2009.
3. J. L. Dalsin and P. B. Messersmith, *Materials Today*, 2005, **8**, 38-46.
4. R. M. Donlan, *Emerging Infectious Diseases*, 2001, **7**, 277-281.
5. R. M. Donlan and J. W. Costerton, *Clinical Microbiology Reviews*, 2002, **15**, 167-193.
6. I. Banerjee, R. C. Pangule and R. S. Kane, *Advanced Materials*, 2011, **23**, 690-718.
7. S. Q. Liu, C. Yang, Y. Huang, X. Ding, Y. Li, W. M. Fan, J. L. Hedrick and Y.-Y. Yang, *Advanced Materials*, 2012, **24**, 6484-6489.
8. J. Zhang, Z. Xu, W. Mai, C. Min, B. Zhou, M. Shan, Y. Li, C. Yang, Z. Wang and X. Qian, *Journal of Materials Chemistry A*, 2013, **1**, 3101-3111.
9. C. Xu, X. Hu, J. Wang, Y. M. Zhang, X. J. Liu, B. B. Xie, C. Yao, Y. Li and X. S. Li, *ACS Appl Mater Interfaces*, 2015, **7**, 17337-17345.
10. B. Mizrahi, X. Khoo, H. H. Chiang, K. J. Sher, R. G. Feldman, J.-J. Lee, S. Irusta and D. S. Kohane, *Langmuir*, 2013, **29**, 10087-10094.
11. H. Zhang and M. Chiao, *Journal of Medical and Biological Engineering*, 2015, **35**, 143-155.
12. S. Kang, A. Asatekin, A. M. Mayes and M. Elimelech, *Journal of Membrane Science*, 2007, **296**, 42-50.

13. B. Dong, H. Jiang, S. Manolache, A. C. L. Wong and F. S. Denes, *Langmuir*, 2007, **23**, 7306-7313.

14. M. Muller, T. Rieser, K. Lunkwitz and J. Meier-Haack, *Macromolecular Rapid Communications*, 1999.

15. G.-d. Kang and Y.-m. Cao, *Water research*, 2012, **46**, 584-600.

16. J. Tsibouklis, M. Stone, A. A. Thorpe, P. Graham, V. Peters, R. Heerlien, J. R. Smith, K. L. Green and T. G. Nevell, *Biomaterials*, 1999, **20**, 1229-1235.

17. M. E. Callow and R. L. Fletcher, *International Biodeterioration & Biodegradation*, 1994, **34**, 333-348.

18. D. Rana and T. Matsuura, *Chem. Rev*, 2010, **110**, 2448–2471.

19. S. Chen, L. Li, C. Zhao and J. Zheng, *Polymer*, 2010, **51**, 5283-5293.

20. J. S. Louie, I. Pinnau, I. Ciobanu, K. P. Ishida, A. Ng and M. Reinhard, *Journal of Membrane Science*, 2006, **280**, 762-770.

21. K. Rechendorff, M. B. Hovgaard, M. Foss, V. P. Zhdanov and F. Besenbacher, *Langmuir*, 2006, **22**, 10885-10888.

22. T. Akkas, C. Citak, A. Sirkecioglu and F. S. Güner, *Polymer International*, 2013, **62**, 1202-1209.

23. Q. An, F. Li, Y. Ji and H. Chen, *Journal of Membrane Science*, 2011, **367**, 158-165.

24. F. Siedenbiedel and J. C. Tiller, *Polymers*, 2012, **4**, 46-71.

25. J. R. Johnson, P. L. Roberts, R. J. Olsen, K. A. Moyer and W. E. Stamm, *Journal of Infectious Diseases*, 1990, **162**, 1145-1150.

26. J. M. Schierholz, L. J. Lucas, A. Rump and G. Pulverer, *Journal of Hospital Infection*, 1998, **40**, 257-262.

27. M. E. Rupp, T. Fitzgerald, N. Marion, V. Helget, S. Puumala, J. R. Anderson and P. D. Fey, *American Journal of Infection Control*, 2004, **32**, 445-450.

28. R. Kumar and H. Münstedt, *Biomaterials*, 2005, **26**, 2081-2088.

29. R. Pickard, T. Lam, G. Maclennan, K. Starr, M. Kilonzo, G. McPherson, K. Gillies, A. McDonald, K. Walton, B. Buckley, C. Glazener, C. Boachie, J. Burr, J. Norrie, L. Vale, A. Grant and J. N'Dow, *Health Technol Assess*, 2012, **16**, 1-197.

30. R. L. Gallo and K. M. Huttner, *J Investig Dermatol*, 1998, **111**, 739-743.

31. K. M. Huttner and C. L. Bevins, *Pediatr Res*, 1999, **45**, 785-794.

32. Y. Shai, *Peptide Science*, 2002, **66**, 236-248.

33. S. K. Straus and R. E. W. Hancock, *Biochimica et Biophysica Acta (BBA) - Biomembranes*, 2006, **1758**, 1215-1223.

34. A. K. Marr, W. J. Gooderham and R. E. W. Hancock, *Current Opinion in Pharmacology*, 2006, **6**, 468-472.

35. E. J. Brisbois, J. Bayliss, J. Wu, T. C. Major, C. Xi, S. C. Wang, R. H. Bartlett, H. Handa and M. E. Meyerhoff, *Acta Biomaterialia*, 2014, **10**, 4136-4142.

36. A. Lutzke, B. H. Neufeld, M. J. Neufeld and M. M. Reynolds, *Journal of Materials Chemistry B*, 2016, **4**, 1987-1998.

37. C. Deppisch, G. Herrmann, U. Graepler-Mainka, H. Wirtz, S. Heyder, C. Engel, M. Marschal, C. C. Miller and J. Riethmüller, *Infection*, 2016, DOI: 10.1007/s15010-016-0879-x, 1-8.

38. T. Zhang, L. Wang, Q. Chen and C. Chen, *Yonsei Medical Journal*, 2014, **55**, 283-291.

39. R. de Lima, A. B. Seabra and N. Duran, *Journal of applied toxicology : JAT*, 2012, **32**, 867-879.

40. K. A. Brogden, *Nat Rev Micro*, 2005, **3**, 238-250.

41. K. A. Amoako, H. S. Sundaram, A. Suhaib, S. Jiang and K. E. Cook, *Advanced Materials Interfaces*, 2016, DOI: 10.1002/admi.201500646, n/a-n/a.

42. C. J. Backlund, B. V. Worley and M. H. Schoenfisch, *Acta biomaterialia*, 2016, **29**, 198-205.

43. E. J. Brisbois, R. P. Davis, A. M. Jones, T. C. Major, R. H. Bartlett, M. E. Meyerhoff and H. Handa, *J Mater Chem B Mater Biol Med*, 2015, **3**, 1639-1645.

44. E. J. Brisbois, H. Handa, T. C. Major, R. H. Bartlett and M. E. Meyerhoff, *Biomaterials*, 2013, **34**, 6957-6966.

45. W. Cai, J. Wu, C. Xi and M. E. Meyerhoff, *Biomaterials*, 2012, **33**, 7933-7944.

46. G. W. Charville, E. M. Hetrick, C. B. Geer and M. H. Schoenfisch, *Biomaterials*, 2008, **29**, 4039-4044.

47. F. C. Fang, *Nitric oxide : biology and chemistry / official journal of the Nitric Oxide Society*, 2012, **27, Supplement**, S10.

48. M. C. Frost, M. M. Reynolds and M. E. Meyerhoff, *Biomaterials*, 2005, **26**, 1685-1693.

49. S. Gupta, K. A. Amoako, A. Suhaib and K. E. Cook, *Advanced Materials Interfaces*, 2014, **1**.

50. H. Handa, E. J. Brisbois, T. C. Major, L. Refahiyat, K. A. Amoako, G. M. Annich, R. H. Bartlett and M. E. Meyerhoff, *Journal of Materials Chemistry B*, 2013, **1**, 3578-3587.

51. H. Handa, T. C. Major, E. J. Brisbois, K. A. Amoako, M. E. Meyerhoff and R. H. Bartlett, *Journal of Materials Chemistry B*, 2014, **2**, 1059-1067.

52. J. L. Harding and M. M. Reynolds, *Journal of Materials Chemistry B*, 2014, **2**, 2530-2536.

53. E. M. Hetrick and M. H. Schoenfisch, *Chemical Society Reviews*, 2006, **35**, 780-789.

54. B. J. Privett, A. D. Broadnax, S. J. Bauman, D. A. Riccio and M. H. Schoenfisch, *Nitric oxide : biology and chemistry / official journal of the Nitric Oxide Society*, 2012, **26**, 169-173.

55. G. Regev-Shoshani, M. Ko, A. Crowe and Y. Av-Gay, *Urology*, 2011, **78**, 334-339.

56. G. Regev-Shoshani, M. Ko, C. Miller and Y. Av-Gay, *Antimicrobial Agents and Chemotherapy*, 2010, **54**, 273-279.

57. M. M. Reynolds, M. C. Frost and M. E. Meyerhoff, *Free Radical Biology & Medicine*, 2004, **37**, 926-936.

58. P. Taladriz-Blanco, V. Pastoriza-Santos, J. Pérez-Juste and P. Hervés, *Langmuir*, 2013, **29**, 8061-8069.

59. Y. Wo, Z. Li, E. J. Brisbois, A. Colletta, J. Wu, T. C. Major, C. Xi, R. H. Bartlett, A. J. Matzger and M. E. Meyerhoff, *ACS Applied Materials & Interfaces*, 2015, **7**, 22218-22227.

60. B. Wu, B. Gerlitz, B. W. Grinnell and M. E. Meyerhoff, *Biomaterials*, 2007, **28**, 4047–4055.

61. M. J. Goudie, E. J. Brisbois, J. Pant, A. Thompson, J. A. Potkay and H. Handa, *International Journal of Polymeric Materials and Polymeric Biomaterials*, 2016, **65**, 769-778.

62. E. J. Brisbois, T. C. Major, M. J. Goudie, R. H. Bartlett, M. E. Meyerhoff and H. Handa, *Acta biomaterialia*, 2016, **37**, 111-119.

63. F. C. Fang, *Journal of Clinical Investigation*, 1997, **99**, 2818-2825.

64. E. M. Hetrick and M. H. Schoenfisch, *Biomaterials*, 2007, **28**, 1948-1956.

65. A. F. Engelsman, B. P. Krom, H. J. Busscher, G. M. van Dam, R. J. Ploeg and H. C. van der Mei, *Acta Biomaterialia*, 2009, **5**, 1905-1910.

66. S. Carlsson, E. Weitzberg, P. Wiklund and J. O. Lundberg, *Antimicrobial Agents and Chemotherapy*, 2005, **49**, 2352-2355.

67. G. Regev-Shoshani, M. Ko, A. Crowe and Y. Av-Gay, *Urology*, 2011, **78**, 334-339.

68. M. R. Mihu, U. Sandkovsky, G. Han, J. M. Friedman, J. D. Nosanchuk and L. R. Martinez, *Virulence*, 2010, **1**, 62-67.

69. J. Yu, E. Brisbois, H. Handa, G. Annich, M. Meyerhoff, R. Bartlett and T. Major, *Journal of Materials Chemistry B*, 2016, **4**, 2264-2272.

70. I. Chipinda and R. H. Simoyi, *The Journal of Physical Chemistry B*, 2006, **110**, 5052-5061.

71. A. R. Statz, A. E. Barron and P. B. Messersmith, *Soft Matter*, 2008, **4**, 131-139.

72. M. Martins, D. Wang, J. Ji, L. Feng and M. Barbosa, *Biomaterials*, 2003, **24**, 2067-2076.

73. M. Shen, Y. V. Pan, M. S. Wagner, K. D. Hauch, D. G. Castner, B. D. Ratner and T. A. Horbett, *Journal of biomaterials science. Polymer edition*, 2001, **12**, 961-978.

74. P. B. Messersmith and M. Textor, *Nature nanotechnology*, 2007, **2**, 138-139.

75. M. Salim, G. Mishra, G. J. S. Fowler, B. O'Sullivan, P. C. Wright and S. L. McArthur, *Lab on a Chip*, 2007, **7**, 523-525.

76. Z. Zhang, S. Chen, Y. Chang and S. Jiang, *The Journal of Physical Chemistry B*, 2006, **110**, 10799-10804.

77. T. Boland, R. A. Latour and F. J. Stutzenberger, in *Handbook of Bacterial Adhesion*, Springer, 2000, pp. 29-41.

78. D. Ní Eidhin, S. Perkins, P. Francois, P. Vaudaux, M. Höök and T. J. Foster, *Molecular Microbiology*, 1998, **30**, 245-257.

79. S.-Y. Jung, S.-M. Lim, F. Albertorio, G. Kim, M. C. Gurau, R. D. Yang, M. A. Holden and P. S. Cremer, *Journal of the American Chemical Society*, 2003, **125**, 12782-12786.

80. A. Toscano and M. M. Santore, *Langmuir*, 2006, **22**, 2588-2597.

81. N. Safdar and D. G. Maki, *Annals of Internal Medicine*, 2002, **136**, 834-844.

82. S. Y. Tong, J. S. Davis, E. Eichenberger, T. L. Holland and V. G. Fowler, *Clinical microbiology reviews*, 2015, **28**, 603-661.

CHAPTER 4

ACTIVE RELEASE OF AN ANTIMICROBIAL AND ANTIPLATELET AGENT FROM A NON-FOULING SURFACE MODIFICATION[4]

[4] Goudie, M.G., Singha, P., Hopkins, S.P., Brisbois, E.J., Handa, H. 2019. *ACS Applied Materials & Interfaces.* Reprinted with permission of the publisher.

Abstract

Two major challenges faced by medical devices are thrombus formation and infection. In this work, surface tethered nitric oxide (NO) releasing molecules are presented as a solution to combat infection and thrombosis. These materials possess a robust NO release capacity lasting ca. 1 month while simultaneously improving the non-fouling nature of the material by preventing platelet, protein, and/or bacteria adhesion. Nitric oxide's potent bactericidal function has been implemented by a facile surface covalent attachment method to fabricate a triple action surface - **s**urface **im**mobilized ***S***-nitroso-*N*-acetylpenicillamine (SIM-S). Comparison of NO loading amongst the various branching configurations is shown through the NO release kinetics over time and the cumulative NO release. Biological characterization is performed using *in vitro* fibrinogen and *Staphylococcus aureus* assays. The material with the highest NO release, SIM-S2, is also able to reduce protein adhesion by 65.8 ± 8.9% when compared to unmodified silicone. SIM-S2 demonstrates a 99.99% (i.e. ~4 log) reduction for *Staphylococcus aureus* over 24 h. The various functionalized surfaces significantly reduce platelet adhesion *in vitro*, for both NO releasing and non-NO releasing surfaces (up to 89.1 ± 0.9%), demonstrating the non-fouling nature of the surface immobilized functionalities. The ability of the SIM-S surfaces to retain antifouling properties despite gradual depletion of the bactericidal source, NO, demonstrates its potential use in long term medical implants.

Introduction

Fouling of materials used in medical devices leads to increased risk of infection and device failure, and is the result of the adherence of proteins, bacteria, or thrombus formation. These complications can lead to large increases in healthcare costs and mortality.[1, 2] While systemic heparin is often administered to aid in the prevention of thrombus formation, its

prolonged use can result in morbidity and mortality while providing no activity to prevent infection.[3] In addition to this, the increasing use of antibiotics has led to the development of resistant strains of bacteria, which can be attributed to the high dosages required to be effective against established biofilms.[4] The degree of bacteria or platelet adhesion is highly influenced by the ability to prevent protein adhesion to the materials surface.[5-7] A number of strategies have been used to develop adhesion resistant materials,[8] such as increasing the hydrophilicity,[5, 9] super hydrophobic or patterned surfaces,[10-13] liquid-infused materials,[14-16] or grafting of polymer brushes.[17-24] While these materials are suitable for decreasing the adhesion of protein and bacteria through "passive" mechanisms, they provide no "active" mechanism to prevent platelet activation and adhesion or any bactericidal activity towards bacteria that have adhered, which ultimately leads to proliferation and biofilm formation.

Nitric oxide (NO) is an endogenous, gaseous, free radical that is produced naturally by macrophages and by endothelial cells lining the vascular walls, and is involved in various biological processes, such as preventing platelet activation and adhesion, while also being a potent, broad spectrum bactericidal agent.[25] To take advantage of these properties, NO donors (e.g. S-nitrosothiols or diazeniumdiolates) have been developed to allow for the storage and localized delivery of NO, and are particularly advantageous for polymeric materials typically used for medical devices, such as polyurethanes, silicones, or polyvinyl chloride.[26, 27] The addition of these donors at various levels also provides a simple method for controlling the level of NO that is delivered from the materials.[28] Materials releasing NO have been shown to significantly reduce thrombus formation in both extracorporeal circuits and vascular catheter models, and have been shown to provide significant reductions in viable bacteria during long term catheterization.[2, 29, 30]

In this work, a novel method to prepare a material surface with the ability to not only offer an improved steric ability to prevent platelet and protein adhesion through a passive mechanism, but also utilize the active biocidal mechanism of NO. In addition to combining these mechanisms, the antifouling capability of the material is retained after the entire NO payload has been released from the surface, making it attractive for long-term applications. Specifically, this is achieved by the immobilization of the NO donor precursor *N*-acetyl-D-penicillamine (NAP) to various amine functionalized silicone surfaces (Figure 4.1 A).

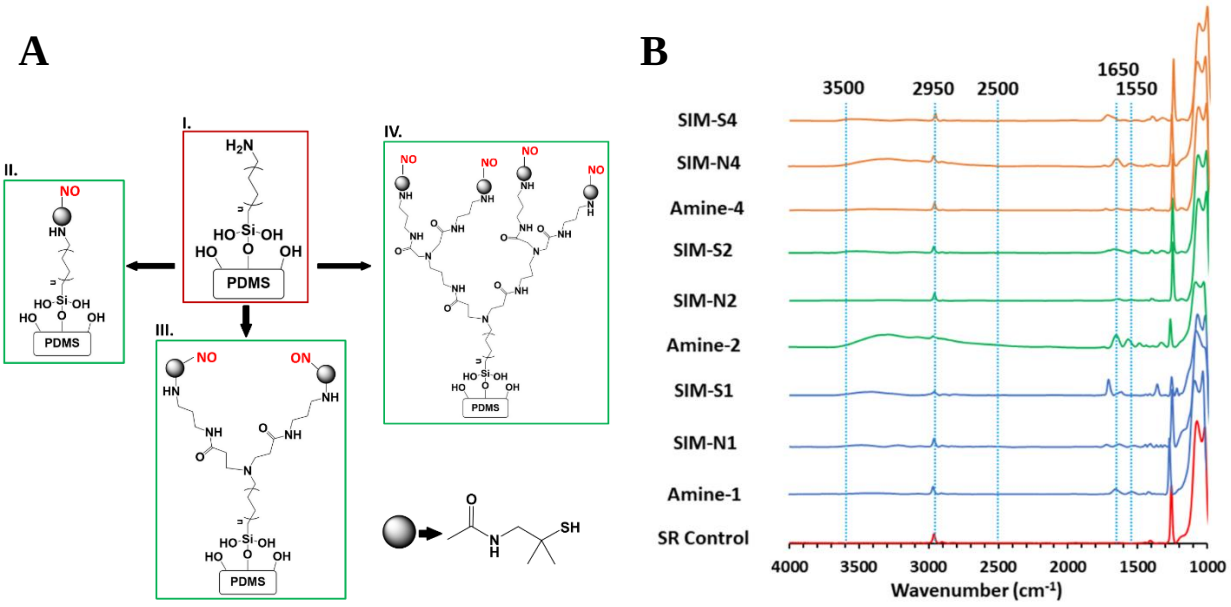

Figure 4.1: A) Preparation of surface immobilized *S*-nitroso-*N*-acetyl-d-penicillamine (II. SIM-S1, III. SIM-S2, IV. SIM-S4) Structure I is a product of functionalization of PDMS surface with hydroxyl groups by submerging it in 50:50 ratio of 13 N HCl:30 wt.% H_2O_2 in H_2O and treatment with APTMES for amine functionalization. Structure II is a product of nitrosation of thiol groups with tert-butyl nitrite. Structure III and IV are synthesized after branching of primary amine via reaction with methyl acrylate and amine functionalization of branched site using ethylene diamine. B) FTIR spectra for different samples. Amine-1, Amine-2 and Amine-4

correspond to amine functionalized surfaces with unbranched and branched surfaces. 3500-2500 represents unreacted –COOH groups present after amine-functionalization for SIM-N4 and Amine-2. 2950 represents alkyl groups present in abundance in SR and aminated surfaces of SR. Double peaks of 1650,1550 represent primary amine groups in Amine-1, Amine-2 and Amine-4. 1650 represents saturated amide groups in SIM-N1, SIM-N2, SIM-N4, SIM-S1, SIM-S2 and SIM-S4. 1550 in SIM-S2 represents nitroso group of the NO-donor attached.

Materials and Methods

Materials

N-Acetyl-*D*-penicillamine (NAP), sodium chloride, potassium chloride, sodium phosphate dibasic, potassium phosphate monobasic, phosphate buffered saline (PBS, pH 7.4 at 25°C), ethylenediaminetetraacetic acid (EDTA), tetrahydrofuran (THF), tert-butyl nitrite, and sulfuric acid were purchased from Sigma-Aldrich (St. Louis, MO). Aminopropyl trimethoxy silane (APTMES) was purchased from Gelest. All silicone substrates were fabricated with polydimethylsiloxane Sylgard 184 (Dow Corning). Methanol, hydrochloric acid, and sulfuric acid were obtained from Fisher Scientific (Pittsburgh, PA). Trypsin-EDTA and Dulbecco's modification of Eagle's medium (DMEM) were obtained from Corning (Manassas, VA 20109). The bacterial *Staphylococcus aureus* (ATCC 5538) strain was obtained from American Type Culture Collection (ATCC). Luria Agar (LA), Miller and Luria broth (LB), Lennox were purchased from Fischer BioReagents (Fair Lawn, NJ). All aqueous solutions were prepared with 18.2 MΩ deionized water using a Milli-Q filter (Millipore Corp., Billerica, MA).

Synthesis of SIM material

Silicone films were first fabricated by mixing Sylgard 184 base to curing agent (ratio of 10:1). The solution was cast into Teflon molds and placed under vacuum for degassing. The casted solution was then placed in an oven (80°C, 90 min) for curing. To create a hydroxyl group functionalized surface, the silicone films were submerged in a mixture of 13 N HCl : 30 wt.% H_2O_2 (50:50) in H_2O under mild agitation (15 min). The surfaces were then rinsed with DI H_2O and dried under vacuum. The amine functionalization was then achieved by submerging the hydroxyl-functionalized surfaces in 5 wt.% APTMES in extra dry acetone for 2 h. Films were then rinsed with extra dry acetone to remove any non-covalently attached silane from the surface, and vacuum dried for 24 h. Branching of the immobilized moieties was achieved through incubation of the amine functionalized surface in 2:1 (v/v) methanol:methyl acrylate (24 h) followed by 2:1 (v/v) methanol: ethylenediamine (24h) as shown in Figure 4.1 A. Samples were rinsed twice with methanol (20 mL) between incubating solutions. Amine-functionalized surfaces were then submerged in 10 mg mL^{-1} NAP-thiolactone in toluene for 24 h, allowing for the ring opening reaction of thiolactone to bind to free amines.[31, 32] The samples were then air-dried for 5 h to completely remove any residual solvent. Nitrosation of the immobilized NAP was achieved by incubation in neat tert-Butyl nitrite for 2 h. The resultant SIMS samples were stored at -20°C for further experiments. (Details in Appendix 1)

Contact angle and FTIR analysis

Surface properties and proof of attachment of nitric oxide donors to silicone surfaces was analyzed using contact angle measurements and FTIR. Static contact angle was measured using a DSA 100 drop shape analysis system (KRÜSS) with a computer-controlled liquid dispensing system (Krüss). A 3 µL droplet of water was placed on various silicone films, and the average of

left and right contact angles were measured via the Krüss software. Infrared spectroscopy studies of the samples were done using a Thermo-Nicolet model 6700 spectrometer with a grazing angle attenuated total reflectance accessory at 64 scans with a 6 cm^{-1} resolution.

Nitric Oxide Release Characteristics

Nitric oxide release from the films containing SNAP was measured using a Sievers Chemiluminescence Nitric Oxide Analyzer (NOA) 280i (Boulder, CO). The Sievers chemiluminescence Nitric Oxide analyzer is considered as the gold standard for detecting nitric oxide and is widely used due to its ability to limit interfering species, such as nitrates and nitrites, as they are not transferred from the sample vessel to the reaction cell. Films were then placed in the sample vessel immersed in PBS (pH 7.4, 37°C) containing 100 µM EDTA. Nitric oxide was continuously purged from the buffer and swept from the headspace using nitrogen sweep gas and bubbler into the chemiluminescence detection chamber.

Samples were analyzed for NO release and stored in the same conditions as found physiologically for medical implants/devices (shielded from light and at 37°C). For each measurement, NO release was allowed to plateau so that burst effect of NO release was not included in the average flux for each time point measurement (approximately 0.5 h for each measurement). The detection limit of the NOA for measurement of gas-phase NO is ~0.5 part per billion by volume (~1 picomole).

Thiol quantification by Ellman's assay

The covalent attachment of NAP-thiolactone can be directly related to the amount of free sulfhydryl groups on the surface of the PDMS. Measurement of these functional groups was done using Ellman's assay, which reacts 5,5'-dithio-bis-(2-nitrobenzoic acid) (DTNB) with free sulfhydryl groups to form conjugated disulfide and 2-nitro-5-thiobenzoic acid (TNB). While in

solution, TNB's extinction coefficient has been recorded to be 14,150 M^{-1} at 412 nm. Surface functionalized films were first cut to a recorded surface area before being placed in a solution containing 50 µL of DNTB stock solution (50 mM sodium acetate and 2 mM DTNB in DI water), 100 µL of PBS, and 850 µL of DI water. The samples were then thoroughly mixed and allowed to incubate at room temperature for 5 minutes. Optical absorbance was then recorded at 412 nm using a UV-Vis spectrophotometer. A standard calibration curve using acetyl cysteine was made to correlate thiol concentration with absorbance.

Protein Repulsion Quantification

Levels of protein adhesion were quantified for the various materials using a modified version of a previously reported method.[7] FITC-human fibrinogen (13 mg/mL, Molecular Innovations) was diluted to achieve 2 mg mL^{-1} in PBS (pH 7.4). Silicone disks were incubated at 37°C for 30 min in a 96-well plate, followed by the addition of the stock protein solution to achieve a concentration of 2 mg mL^{-1}.[7] Following 2h of incubation, infinite dilution of the well contents was carried out to wash away the bulk and any loosely bound protein from the materials. The fluorescence of each well (n=8) was then measured using a 96-well plate reader (Biotek Cytation 5), and the amount of protein adsorbed was determined via a calibration curve. The excitation and emission wavelength for FITC are 495 and 519 nm.

Bacterial Adhesion Assay

The ability of the samples to inhibit growth and promote killing of the adhered bacteria on the polymer surface was tested following guidelines based on American Society for Testing and Materials E2180 protocol with the commonly found nosocomial pathogen, Gram-positive *S. aureus* (ATCC 6538). A single colony of bacteria was isolated from a previously cultured LB-agar plate and incubated in LB Broth (37°C,150 rpm, 14-16h). The optical density of the culture

was measured at a wavelength of 600 nm using a UV-vis spectrophotometer (Thermoscientific Genesys 10S UV-Vis) to ensure the presence of ~10^8 CFU mL^{-1}. The overnight culture was then centrifuged at 2500 rpm for 7 min to obtain the bacterial pellet. The bacterial pellet obtained was resuspended in sterile PBS. The polymer samples (SR control, SIM-N1, SIM-S1, SIM-N2 and SIM-S2) were then incubated in the bacterial suspension (37°C, 24h, 140 rpm). After incubation, samples were removed from the bacterial suspension and rinsed with sterile PBS to remove any unbound bacteria. They were then sonicated for 1 min each using an Omni Tip homogenizer for 1 min to collect adhered bacteria in sterile PBS. To ensure proper homogenization of the collected bacteria, the samples were vortexed for 45s each. The solutions were serially diluted, plated on LB agar medium and incubated at 37°C. After 24h, the total CFUs for serially diluted and plated bacterial solutions were counted.

A second antimicrobial test was done, in addition to the one mentioned in the main paper, to prove the robustness of the NO-releasing materials when compared to antifouling materials. In this method, all steps were followed according to the process mentioned in the main paper except for the addition of an extra 24h of incubation in fibrinogen (2 mg/ml) from human serum. This incubation step was added before the bacterial incubation step due to the sequence of exposure seen in physiological conditions. The results are shown on Appendix 2.[33]

The efficiency of the sample to inhibit bacterial attachment was calculated according to the following formula:

$$Bacteria\ inhibition\ (\%) = \frac{(CFU\ cm^{-2}\ on\ control\ sample - CFU\ cm^{-2}\ on\ test\ sample\ )}{(CFU\ cm^{-2}\ on\ control\ sample)} \times 100$$

Platelet Adhesion Assay

Freshly drawn citrated (3.8%, 9:1 citrate: whole blood) porcine blood was purchased from Lampire Biologicals. The anticoagulated blood was centrifuged (1100 rpm, 12 min) using the Eppendorf Centrifuge 5702. The platelet rich plasma (PRP) portion was collected carefully with a pipet as to not disturb the buffy coat. The remaining samples were then centrifuged (4000 rpm, 20 min) to retrieve platelet poor plasma (PPP). Total platelet counts in both PRP and PPP fractions were determined using a hemocytometer (Fisher). The PRP and PPP were combined in a ratio to give a final platelet concentration ca. 2×10^8 mL^{-1}. Calcium chloride ($CaCl_2$) was added to the final platelet solution to achieve a final concentration of 2.5 mM.[7] Disks of each respective surface were placed in a 5 mL blood tube. Approximately 4 mL of the calcified PRP was added to each tube and incubated (37°C, 90 min) with mild rocking (25 rpm). Following the incubation, the tubes were infinitely diluted with normal saline. The degree of platelet adhesion was determined using the lactate dehydrogenase (LDH) released when the adherent platelets were lysed with a Triton-PBS buffer using a Roche Cytotoxicity Detection Kit (LDH). The silicone disks were then incubated in 1 mL of Triton-PBS buffer. After 25 min, 100 μL of the buffer was transferred to a 96-well plate and combined with 100μL of the LDH reagent buffer per the supplier specifications. The absorbance of each well (duplicates of n=6,492 nm and 690 nm) was further duplicated) was then measured using a 96-well plate reader (Biotek Cytation 5), and the number of platelets adhered was determined using the calibration curve.

Results and Discussion

Functionalization and characterization of silicone surfaces for non-fouling coatings with active release of NO

A detailed schematic of the reactions used for branching of the initial alkyl-amine spacer is included in Appendix 1. Briefly, the increasing grafting density of free amines was done through branching free amines using sequential reactions of 1:2 methyl acrylate: methanol and 1:2 ethylene diamine:methanol for 24 h. The surfaces were then incubated for 24 h in 10 mg/mL NAP-thiolactone (dissolved in toluene). Following immobilization, the free thiols of the grafted donor are nitrosated to its NO-rich form *S*-nitroso-*N*-acetyl-D-penicillamine (SNAP) using tert-butyl nitrite. To ensure covalent bonding of the surface modifications, FTIR measurements were carried out (Figure 4.1 B). Since nitrogen atoms overlap in terms of FTIR peaks, appearance and disappearance of amide and primary amines were observed as the reaction steps were completed. This was followed by measurement of water contact angle (Table 4.1) to evaluate any significant differences in hydrophilicity of the functionalized surface. It is interesting to note here that hydrophilicity of the surfaces increased with increased NO-release (will be discussed in the next section). This could be attributed to lower availability of amine functionalized surfaces as the reaction is more complete.

Table 4.1: Contact angle measurements compared between all NAP-thiolactone and nitroso group functionalized surfaces.

Material	Static Water Contact Angle (°)
SR	106.77 ± 3.36
SIM-N1	94.36 ± 3.36
SIM-S1	101.56 ± 4.48
SIM-N2	64.95 ± 11.87
SIM-S2	53.78 ± 5.23
SIM-N4	93.09 ± 2.91
SIM-S4	90.90 ± 7.97

As seen in the design strategy, the NO-load and release capacity of the materials was varied by branching of the initial alkyl spacer to increase the number of free amines. This variation in NO-load and release capacity was measured by using a chemiluminescence nitric oxide analyzer (NOA). The NOA is the gold standard for measurement of NO flux from materials and is a very efficient and sensitive instrument which can analyze NO release down to $1/10^{th}$ of ppb.[34] Samples are analyzed for NO release by shielding them from light and incubated in a phosphate buffered saline at 37 °C. These parameters mimic the physiological conditions of indwelling medical devices and have been used as a guideline in previous research.[5, 35, 36] One of the theoretical expectations was to see increasing NO-load and release measurements with an increase in branching. However, as seen in Figure 4.2, NO release measurements were significantly higher for SIM-S2 (cumulative release: 4. 34 ± 0.04 μmol cm^{-2}) when compared to SIM-S4 (cumulative release: 2.33 ± 0.03 μmol cm^{-2}) over the 25-d period. Tabulated values for instantaneous and cumulative NO release are in Appendix 3 and 4, respectively, and were comparable to total free thiol content as measured via Ellman's assay (Appendix 5).[37] There could be two possible explanations for this: steric hindrance in the case of higher branching and hence NAP thiolactone was not able to completely bind to the amine groups, and/or more branching increases the probability of chain interactions within the polymer during reactions with ethylene diamine, decreasing the total free amines available for binding with NAP thiolactone. Therefore, the conclusion from this study was that increased branching does not necessarily increase the total NO-load or release. Further, this enables the designed surface to release NO up to 25 d at effective flux levels (ability to reduce platelet activation and bacterial adhesion significantly).[5, 35, 36] This increasing branching method is a novel technique to increase

NO release characteristics much like the function of metal ions when added to NO releasing polymers.[38] However, this material proves to be more advantageous as it also imparts antifouling characteristics to the material as seen in the following studies conducted. To ensure NO release was only from the surface functionalization and not from the bulk material due to possible swelling of the diamine group during the reaction period, control measurements were done on samples using the same reaction scheme without immobilization of the aminosilane. The results are not shown in figures or tables since no NO release was observed without the immobilization of the aminosilane. This proved that the aminosilanes immobilization was a necessary step for NO release and that NO release was not due to any swelling of the material from the solvents/reactions used for immobilization of the NO donor.

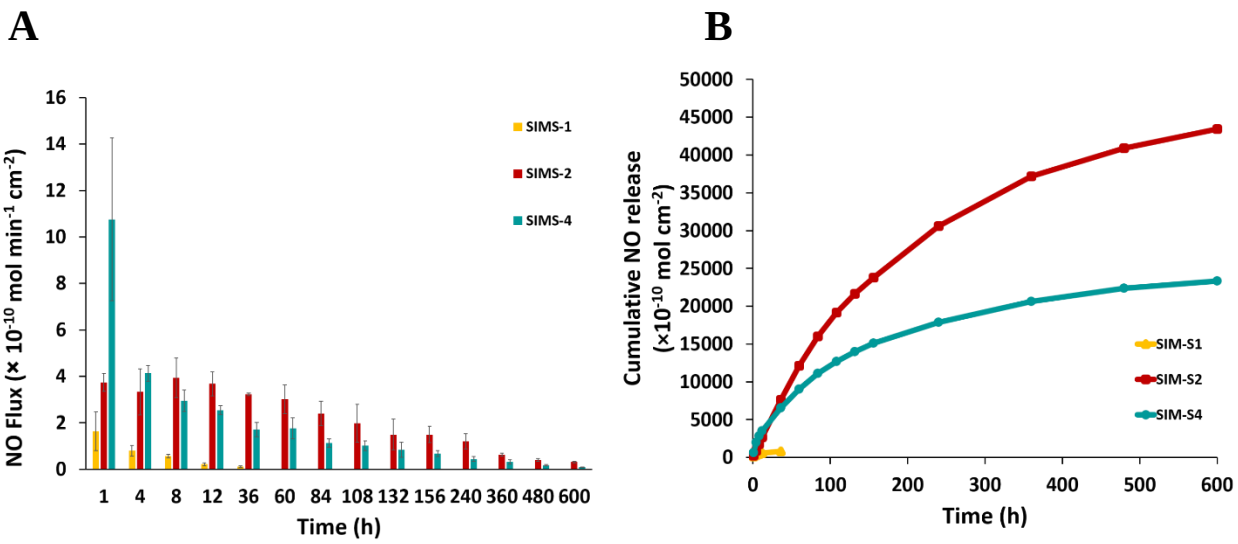

Figure 4.2: A) Comparison of day by day NO release measurements between SIM-S1, SIM-S2, and SIM-S4. (n=3). B) Comparison of cumulative NO release from SIM-S1, SIM-S2, and SIM-S4. (n=3)

Assessment of the Non-fouling nature of various SIM surfaces against protein, bacteria, and platelet rich plasma

One common method for assessing the fouling of materials *in vitro* is to examine the ability of the material to resist non-specific protein adhesion, or if intended for blood contacting applications more specifically, fibrinogen (Fg). The adsorption of Fg to the material surface greatly aids in the ability for activated platelets or bacteria to bind to the surface, leading to higher risks of thrombus formation or infection.[6] While the orientation of Fg adsorption has been shown to determine the degree of platelet adhesion, limiting protein adhesion regardless of orientation is generally considered to be an improvement in the hemocompatibility of a material.[7] Developing NO-releasing materials that can reduce protein adsorption could provide drastic improvements in the overall hemocompatibility and antibacterial nature of these materials. To examine if the surface immobilized NO donors (both nitrosated and non-nitrosated) can provide a decrease in protein adhesion observed on NO-releasing materials, 2 h exposure to FITC-labeled fibrinogen (2 mg mL^{-1}) was conducted at 37°C (Figure 4.3 A, Table 4.2). While minimal changes in contact angle were observed, increasing the branched nature of the surface grafted NAP groups decreased the degree of Fg adsorption, and is hypothesized to result from increases in steric hindrance.[34] However, altering the chemistry of the linkages to the amine functionalized surface could greatly increase the non-fouling ability of these materials. Overall, reductions in protein adsorption were observed to reach 65.8 ± 8.9% for SIM-S2 when compared to the unmodified SR. It is also interesting to note that the release of NO from the surface had no significant effect on the amount of adsorbed Fg. Previous reports have suggested that increasing NO release levels from other NO donors lead to increased fibrinogen adsorption, where additions of 1 and 9.2 wt.% N-diazeniumdiolated dibutyl-hexanediamine were added to polyvinylchloride

films.[39] The NO release levels of 10 x10^{-10} mol cm^{-2} and 15 x10^{-10} mol cm^{-2} were shown to increase protein adsorption compared to PVC (226 ± 99% and 2334 ± 496%, respectively). However, extensive studies regarding the interaction of proteins and various NO donors have yet to be studied, specifically the differences between S-nitrosothiols and diazeniumdiolates, as well as a broader examination of the levels of NO release. However, the immobilized SIM-S surfaces demonstrate the effectiveness of the surface immobilized NO donors as providing active NO release while decreasing protein adsorption.

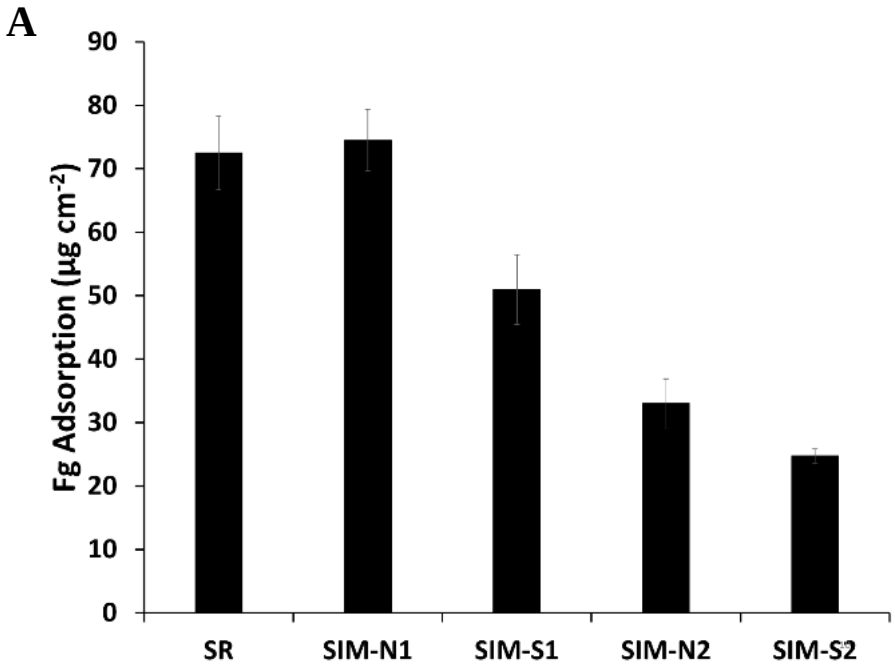

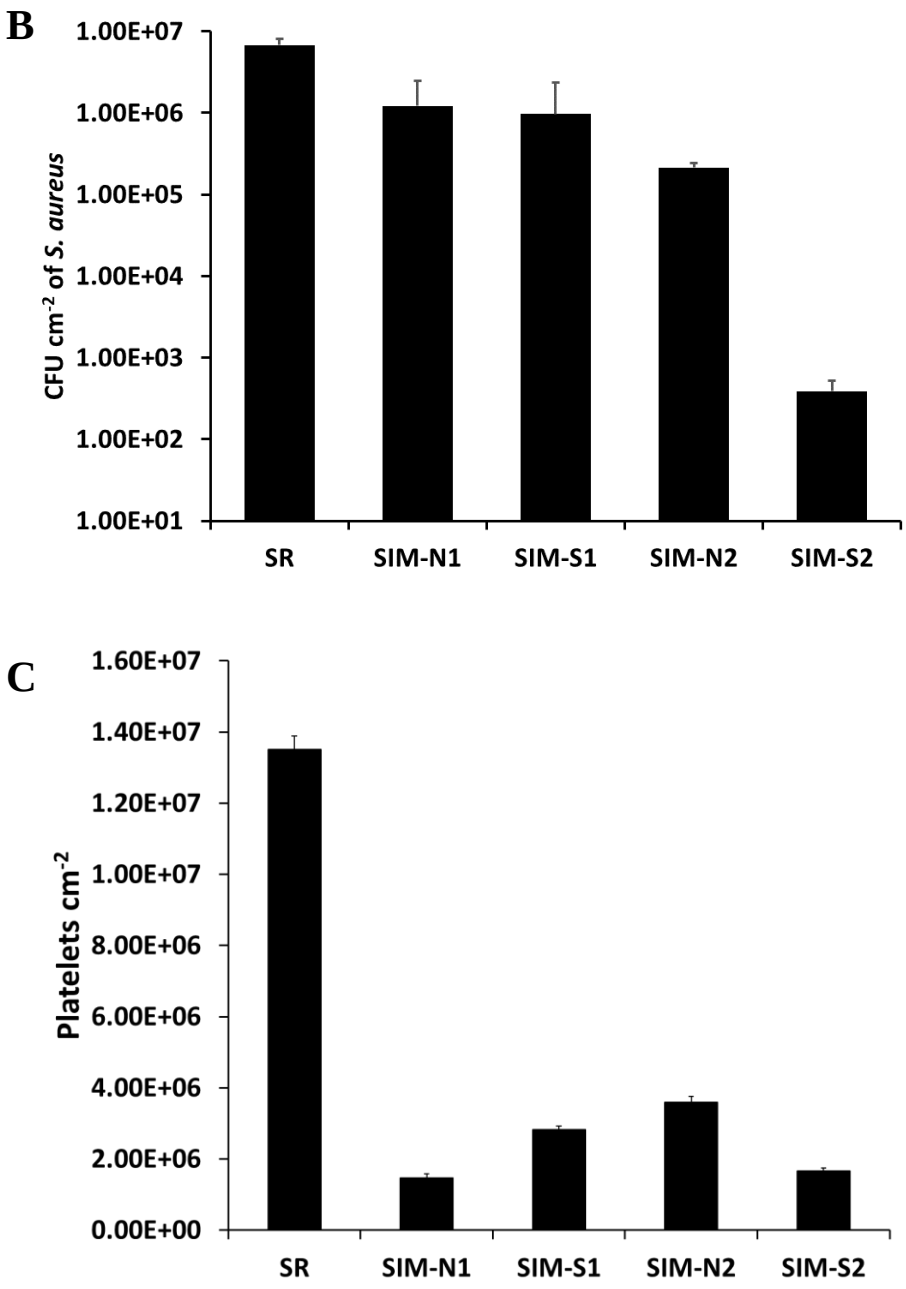

Figure 4.3: A) Adsorption of fibrinogen to modified SR surfaces over a 2 h period. Values are expressed as mean ± standard error. Measurements were conducted using n=8 per group. B) SIM-S2 was able to reduce bacteria adhesion by ~4 log when compared to control samples. C) Comparison of adsorbed platelets per surface area between SR, SIM-N1, SIM-S1, SIM-N2 and SIM-S2.

Table 4.2: Ability of various surface modified SR substrates to reduce nonspecific protein adsorption over 2h.

	SR	SIM-N1	SIM-S1	SIM-N2	SIM-S2
Fg Adsorption (μg cm^{-2})	72.4 ± 16.4	74.5 ± 13.7	51.0 ± 15.5	33.0 ± 11.0	24.7 ± 3.2
Reduction (%)	-	-	29.6 ± 26.7	54.4 ± 18.3	65.8 ± 8.9
p value vs control	-	NS	0.024	1.94×10^{-4}	6.59×10^{-5}
p value vs SIM-S2	6.59×10^{-5}	1.43×10^{-5}	0.027	NS	-

Bacterial adhesion, which ultimately results in biofilm formation, is a predominant issue for implanted devices aided by the moist and microbiome sustaining milieu. Coupled with fouling proteins, implants can become hosts to several pathogens that ultimately leads to medical device failure, infection (including bloodstream infection), and sometimes death.[8] Antimicrobial efficacy of the designed non-fouling antimicrobial coating SIM-S materials was compared to the SR control samples to confirm their superior bacterial repulsion properties. The samples were incubated in bacterial solutions containing ~10^8 CFU mL^{-1} of *S. aureus*, which is one of the most commonly found nosocomial infection bacteria.[35, 40] These infections are most commonly associated with catheters, stents, and prosthetic devices among other implants. As mentioned in the Introduction Section, our hypothesis was that the immobilized structure was expected to repel proteins and bacteria while simultaneously releasing NO to actively kill bacteria, thus enhancing the biocompatibility of the material even after all the NO load was depleted. The antimicrobial efficacy of the SIM-S surfaces was clearly observed after 24 h of incubation, the crucial time for initiation of bacterial adhesion on the surface that leads to infection. The CFU cm^{-2} of viable *S.*

aureus adhered to each sample was determined by plate counting (Figure 4.3 B**)**. SIM-S2 showed the highest bactericidal efficiency with a reduction of 99.99 ±0.002 % (Table 4.3) when compared to the SR samples, where a growth of ~10^8 CFU cm^{-2} was observed. This reduction is higher as compared to samples with only NAP thiolactone functionalization (SIM-N1= 82.14 ±22.20 % and SIM-N2= 96.86 ±0.50 %) and SIM-S1 (85.71 ±24.74 %). It can also be concluded from the results that NAP thiolactone functionalized surfaces alone only reduces bacteria adhesion because it cannot kill bacteria as it does not have any bactericidal property. However, the presence of protein is also known to drastically increase the bacterial adhesion, particularly those associated with medical devices. To further demonstrate the robustness of the antimicrobial activity of NO-releasing SIM-S surfaces and compare to only non-fouling SIM-N surfaces, in the presence of protein attachment like the methods described by Smith *et al.* (details in Supplementary section, Figure S3).[41] These surfaces functionalized with NO-releasing moieties make effective bactericidal-releasing coatings which significantly enhance the antimicrobial efficacy. From the protein and bacterial adhesion assays, the varying effects of the modifiable NO-release kinetics from SR surface were observed which in turn can help significantly reduce dire clinical consequences of a medical implantation.

Table 4.3: Ability of various surfaces to decrease bacterial adhesion over 24 h.

	SR	**SIM-N1**	**SIM-S1**	**SIM-N2**	**SIM-S2**
Average CFU of *S. aureus* cm^{-2}	6.81 x10^6	1.22 x10^6	9.73 x10^5	2.14 x10^5	3.89 x10^2
Reduction (%)	-	82.14 ± 22.20	85.71 ± 24.74	96.86 ± 0.49	99.99 ± .002
p value vs control	-	0.01	0.01	0.02	0.02
p value vs SIM-S2	0.02	NS	NS	0.01	-

Platelet activation and adhesion are important considerations when determining the hemocompatibility of materials. Upon activation, platelets release several coagulation agonists, such as phospholipase A_2 (which is then converted into thromboxane A_2), which further increase platelet activation, the coagulation cascade, and thrombin generation.[42] One key predecessor of platelet activation is the adsorption of fibrinogen to the materials surface, where changes in the protein conformation allows for binding to the Gp IIb/IIIa receptors on platelets. Therefore, reducing protein adhesion alone can act as a mechanism to reduce platelet activation. The aim of this study was to confirm that while NO-releasing SIM-S materials have been shown to significantly reduce platelet adhesion, the functionality of the modified surface is not lost after all the NO payload has been released. In fact, small molecules with free thiol groups (similar to NAP) have been shown to provide potent thrombolytic effects when administered systemically by binding to von Willebrand factor crosslinks of adhered platelets in arterial thrombi.[43] Both nitrosated and non-nitrosated surfaces were incubated in porcine platelet rich plasma for 90 min, where the degree platelet adhesion was then determined using a lactate dehydrogenase (LDH) assay (Figure 4.3 C). Each variation of the surface modifications was able to provide significant reductions in platelet adhesion when compared to unmodified SR controls (Table 4.4). The SIM-N1 and SIM-S2 modifications provided the highest reductions but were not statistically significant when compared to each other (p value > 0.5). However, as the brush size increased from the SIM-N1 to the SIM-N2 configuration, the ability to prevent platelet adhesion begins to decrease ($p = 0.001$). This may stem from the surface wetting characteristics of the methacrylate and diamine linkages, as a decrease in contact angle from 94.36 to 64.95 ± 11.87 was observed. The hypothesis is that the increase in platelet adhesion stems from the confirmation of fibrinogen adsorption, even though the overall protein adsorption was decreased.[7, 44] While the SIM-S2

configuration did not provide significant reductions in platelet adhesion when compared to SIM-N1 or SIM-S1, the significant increase in NO release can provide increased bactericidal activity for extended durations.

Table 4.4: Platelets adsorbed per surface area over a period of 90 mins.

	Control SR	**SIM-N1**	**SIM-S1**	**SIM-N2**	**SIM-S2**
Platelets cm^{-2} ($x10^6$)	13.5 ± 0.4	1.5 ± 0.1	2.8 ± 0.1	3.6 ± 0.2	1.6 ± 0.1
Reduction (%)	-	89.1 ± 0.9	79.1 ± 1.0	73.4 ± 1.3	87.7 ± 0.7
p value ($x10^6$)	-	0.1	1.7	0.5	0.2

Conclusion

In summary, this study presents a facile method to attach various amounts of the NO-releasing donor, SNAP, to any polymer material in order to provide both bactericidal/antiplatelet activity while adding a non-fouling nature to the material surface. Through the covalent attachments, the NO release characteristics from the modified surface were tunable by varying the branching linkers for NO donating structures. This enabled detailed analysis of the protein repelling, antithrombotic, and antibacterial properties of each of the modified surfaces that had varying degrees of NO release for different spans of time. It is a significant progress towards quantitatively controlling the release of NO and hence use this technique to further study NO-releasing properties for applications including microfluidic devices for high-throughput assays. This method will also be highly applicable for biomedical device materials that are prone to infection- and thrombosis-related failures and can easily be coupled with existing NO-releasing polymers.

References

1. B. D. Ratner, *Biomaterials*, 2007, **28**, 5144-5147.
2. E. J. Brisbois, R. P. Davis, A. M. Jones, T. C. Major, R. H. Bartlett, M. E. Meyerhoff and H. Handa, *Journal of Materials Chemistry B*, 2015.
3. R. E. Cronin and R. F. Reilly, 2010.
4. N. Høiby, O. Ciofu, H. K. Johansen, Z.-j. Song, C. Moser, P. Ø. Jensen, S. Molin, M. Givskov, T. Tolker-Nielsen and T. Bjarnsholt, *International journal of oral science*, 2011, **3**, 55.
5. P. Singha, J. Pant, M. J. Goudie, C. D. Workman and H. Handa, *Biomaterials Science*, 2017.
6. G. W. Charville, E. M. Hetrick, C. B. Geer and M. H. Schoenfisch, *Biomaterials*, 2008, **29**, 4039-4044.
7. B. Sivaraman and R. A. Latour, *Biomaterials*, 2010, **31**, 832-839.
8. P. Singha, J. Locklin and H. Handa, *Acta Biomaterialia*, 2017, **50**, 20-40.
9. L.-C. Xu and C. A. Siedlecki, *Biomaterials*, 2007, **28**, 3273-3283.
10. X. Hou, X. Wang, Q. Zhu, J. Bao, C. Mao, L. Jiang and J. Shen, *Colloids and Surfaces B: Biointerfaces*, 2010, **80**, 247-250.
11. E. Ueda and P. A. Levkin, *Advanced healthcare materials*, 2013, **2**, 1425-1429.
12. L. C. Xu and C. A. Siedlecki, *Journal of Biomedical Materials Research Part B: Applied Biomaterials*, 2017, **105**, 668-678.
13. E. J. Falde, S. T. Yohe, Y. L. Colson and M. W. Grinstaff, *Biomaterials*, 2016, **104**, 87-103.

14. N. MacCallum, C. Howell, P. Kim, D. Sun, R. Friedlander, J. Ranisau, O. Ahanotu, J. J. Lin, A. Vena and B. Hatton, *ACS Biomaterials Science & Engineering*, 2014, **1**, 43-51.

15. D. C. Leslie, A. Waterhouse, J. B. Berthet, T. M. Valentin, A. L. Watters, A. Jain, P. Kim, B. D. Hatton, A. Nedder and K. Donovan, *Nature biotechnology*, 2014, **32**, 1134-1140.

16. M. J. Goudie, J. Pant and H. Handa, *Scientific Reports*, 2017, **7**.

17. N. A. Alcantar, E. S. Aydil and J. N. Israelachvili, *Journal of biomedical materials research*, 2000, **51**, 343-351.

18. K. Holmberg, K. Bergström and M.-B. Stark, in *Poly (Ethylene Glycol) Chemistry*, Springer, 1992, pp. 303-324.

19. C.-G. Gölander, J. N. Herron, K. Lim, P. Claesson, P. Stenius and J. Andrade, in *Poly (ethylene glycol) Chemistry*, Springer, 1992, pp. 221-245.

20. J. H. Lee, H. B. Lee and J. D. Andrade, *Progress in Polymer Science*, 1995, **20**, 1043-1079.

21. J. Andrade, V. Hlady and S.-I. Jeon, *Polymeric Materials: Science and Engineering*, 1993, 60-61.

22. J. M. Harris, *Poly (ethylene glycol) chemistry: biotechnical and biomedical applications*, Springer Science & Business Media, 1992.

23. E. J. Brisbois, H. Handa and M. E. Meyerhoff, in *Advanced Polymers in Medicine*, Springer, 2015, pp. 481-511.

24. T. Kolobow, E. Stool, P. Weathersby, J. Pierce, F. Hayano and J. Suaudeau, *Transactions-American Society for Artificial Internal Organs*, 1974, **20**, 269.

25. M. A. De Groote and F. C. Fang, *Clinical Infectious Diseases*, 1995, **21**, S162-S165.

26. M. J. Goudie, E. J. Brisbois, J. Pant, A. Thompson, J. A. Potkay and H. Handa, *International Journal of Polymeric Materials and Polymeric Biomaterials*, 2016, **65**, 769-778.

27. E. J. Brisbois, T. C. Major, M. J. Goudie, M. E. Meyerhoff, R. H. Bartlett and H. Handa, *Acta Biomaterialia*, 2016, **44**, 304-312.

28. M. W. Vaughn, L. Kuo and J. C. Liao, *American Journal of Physiology-Heart and Circulatory Physiology*, 1998, **274**, H2163-H2176.

29. E. J. Brisbois, T. C. Major, M. J. Goudie, R. H. Bartlett, M. E. Meyerhoff and H. Handa, *Acta biomaterialia*, 2016, **37**, 111-119.

30. E. J. Brisbois, T. C. Major, M. J. Goudie, M. E. Meyerhoff, R. H. Bartlett and H. Handa, *Acta Biomaterialia*, 2016.

31. H. A. Moynihan and S. M. Roberts, *Journal of the Chemical Society, Perkin Transactions 1*, 1994, 797-805.

32. Z. Paryzek and I. Skiera, *Organic preparations and procedures international*, 2007, **39**, 203-296.

33. R. S. Smith, Z. Zhang, M. Bouchard, J. Li, H. S. Lapp, G. R. Brotske, D. L. Lucchino, D. Weaver, L. A. Roth, A. Coury, J. Biggerstaff, S. Sukavaneshvar, R. Langer and C. Loose, *Sci Transl Med*, 2012, **4**, 153ra132.

34. E. J. Brisbois, H. Handa and M. E. Meyerhoff, in *Advanced Polymers in Medicine*, ed. F. Puoci, Springer International Publishing Switzerland, Switzerland, 2015.

35. Q. Liu, P. Singha, H. Handa and J. Locklin, *Langmuir*, 2017, DOI: 10.1021/acs.langmuir.7b02970.

36. M. J. Goudie, J. Pant and H. Handa, *Scientific Reports*, 2017, **7**, 13623.

37. G. L. Ellman, *Archives of Biochemistry and Biophysics*, 1959, **82**, 70-77.

38. J. Pant, M. J. Goudie, S. P. Hopkins, E. J. Brisbois and H. Handa, *ACS Applied Materials & Interfaces*, 2017, **9**, 15254-15264.

39. S. M. Lantvit, B. J. Barrett and M. M. Reynolds, *Journal of Biomedical Materials Research Part A*, 2013, **101**, 3201-3210.

40. S. Y. Tong, J. S. Davis, E. Eichenberger, T. L. Holland and V. G. Fowler, *Clinical microbiology reviews*, 2015, **28**, 603-661.

41. R. S. Smith, Z. Zhang, M. Bouchard, J. Li, H. S. Lapp, G. R. Brotske, D. L. Lucchino, D. Weaver, L. A. Roth and A. Coury, *Science translational medicine*, 2012, **4**, 153ra132-153ra132.

42. J. J. Ferguson, R. A. Harrington and N. A. Chronos, *Antiplatelet Therapy in Clinical Practice*, Taylor & Francis, 1999.

43. S. M. de Lizarrondo, C. Gakuba, B. A. Herbig, Y. Repessé, C. Ali, C. V. Denis, P. Lenting, E. Touzé, S. L. Diamond and D. Vivien, *Circulation*, 2017, CIRCULATIONAHA. 117.027290.

44. L. Zhang, B. Casey, D. K. Galanakis, C. Marmorat, S. Skoog, K. Vorvolakos, M. Simon and M. H. Rafailovich, *Acta biomaterialia*, 2017, **54**, 164-174.

CHAPTER 5

VERSATILE BIOMIMETIC MEDICAL DEVICE SURFACE: HYDROPHOBIN COATED, NITRIC OXIDE-RELEASING POLYMER FOR ANTIMICROBIAL AND HEMOCOMPATIBLE APPLICATIONS[5]

[5] Devine, R., Singha, P., Handa, H. Submitted to *RSC Biomaterials Science*, 03/24/2019.

Abstract

In medical device design, there is a vital need for a coating that promotes treatment of the patient and simultaneously prevents fouling by biomacromolecules which in turn can progress to infections, thrombosis, and other device-related complications. In this work, hydrophobin SC3 (SC3), a self-assembling amphiphilic protein, was coated on a nitric oxide (NO) releasing medical grade polymer to provide an antifouling layer to work synergistically with NO's bactericidal and antiplatelet activity (SC3-NO). The contact angle of SC3 samples were ~30% lesser than uncoated control samples and was maintained for a month in physiological conditions, demonstrating a stable, hydrophilic coating. NO release characteristics were not adversely affected by the SC3 coating and samples with SC3 coating maintained NO release. Fibrinogen adsorption was reduced over tenfold on SC3 coated samples when compared to non-SC3 coated samples. The viable cell count of adhered bacteria (*Staphylococcus aureus*) on SC3-NO was 79.097 ±7.529% lesser than control samples and 49.533 ±18.18% lesser than NO samples. Platelet adherence on SC3-NO was reduced by 73.407 ±14.59% when compared to control samples and 53.202 ±25.67 when compared to NO samples. Finally, the cytocompatibility of SC3-NO was tested and proved to be safe and not trigger a cytotoxic response. The overall favorable results from the physical, chemical and biological characterization analyses demonstrate the novelty and importance of a naturally-produced antifouling layer coated on a bactericidal and antiplatelet polymer, and thus will prove to be advantageous in a multitude of medical device applications.

Introduction

In the biomaterials field, there is an increasing focus on the development of antifouling coatings to improve the biocompatibility of medical implants and devices (vascular stents and

grafts, catheters, biosensors, extracorporeal circuits, etc.).[1-4] Surface fouling is triggered during the first stage of the foreign body response (FBR), when non-specific proteins absorb onto the foreign surface and form a layer of extrapolymeric substance (EPS).[5] This surface EPS layer provides adhesion receptors for inflammatory cells,[5] bacterial cells,[6] and, in blood-contact devices, platelet cells to attach to the foreign surface.[7] Adhesion of these cells to the device surface can lead to device failure due to fibrous encapsulation by the FBR,[8] sepsis as a result of bacteria biofilm formation,[9] and occlusion of blood-contact devices from thrombus formation[7] (respectively). Consequences from these various biological processes can quickly turn lethal as fouling of medical devices is a major contributor to the annual 99,000 deaths from hospital-associated infections (HAIs) in the U.S.,[10] which in turn contributes to an annual expenditure of $28.4 to $33.8 billion in direct medical costs.[11] In the case of blood-contact devices, occlusive thrombus formation can result in surgical complications, local tissue necrosis, or a lethal cardiovascular complication due to thrombus embolism.[12-15] These severe ramifications of EPS formation is the motivation behind the research of versatile "one-for-all" materials that combine both antifouling and antimicrobial actions, which not only prevent physiological responses through prevention of protein absorption and platelet activation but can also actively kill bacteria.

Commonplace strategies to prevent surface fouling of polymer surfaces are steric repulsion,[16, 17] electrostatic repulsion,[18, 19] or increasing surface hydrophilicity through PEGylation or zwitterionic coating.[19-21] These antifouling methods prevent the adsorption of foulants by increasing the thermodynamic energy needed for foulants to bind to the surface of device polymers.[22, 23] While there have numerous promising publications, these methods of antifouling are mostly confined to the research setting as high cost, difficult operating procedure,

and usage of environmental pollutants in the production process has made commercial scaling difficult.[19] Additionally, these materials have no bioactive component and their durability in long-term biological applications has been called into question.[1, 24, 25] Despite the advances in research of antifouling materials, natural biological surfaces still exhibit excellent antifouling characteristics in comparison to current commercially available medical-grade polymers.[25-27] Thus investigation into alternative antifouling methods is warranted, and at the foremost of these efforts should be biomimetic mechanisms which take advantage of the strategies evolved by nature over billions of years.

Since the discovery of nitric oxide (NO) as the endothelium-derived relaxing factor, there has been a great deal of research into mimicking the physiological release of NO from the endothelium as a means of improving *in vivo* medical device biocompatibility.[28] In the cardiovascular system, healthy endothelial cells release a low, continuous flux of NO into the bloodstream ($0.5\text{-}4 \times 10^{-10}$ mol $cm^{-2}min^{-1}$)[29] to maintain blood vessel homeostasis by controlling blood vessel vasodilation[30,31] and inhibiting platelet activation.[31, 32] Additionally, white blood cells are capable of generating high fluxes of NO, which creates a highly nitrosative and oxidative microenvironment, to prevent bacterial infection.[33] Numerous NO donors, such as diazeniumdiolates[34, 35] and S-nitrosothiols,[36, 37] have been produced and successfully integrated into various polymers in order to mimic physiological levels of NO release, thus circumventing the FBR by tricking the body into thinking NO-releasing materials are a part of the natural *in vivo* environment.[28, 38, 39] The main limitation of these NO-releasing materials is that NO release has been shown to encourage the surface fouling of non-specific, physiological proteins.[40] Once adsorbed onto the surface of medical devices, these proteins provide attachment points for cells to bind to the device surface; however, despite the increase in attachment points, NO-releasing

materials have still been shown to inhibit medical device encapsulation by the FBR[38, 39] and significantly reduce formation of both thrombi[41-43] and biofilms *in vivo*.[44-47]

To account for this limitation, utilization of an antifouling surface coating can provide a synergistic improvement in the biocompatibility of NO-releasing materials by passively preventing surface fouling of physiological proteins while actively averting biofilm and thrombus formation. Recent studies combining NO-releasing materials with various antifouling strategies have shown a significant reduction in both biofilm formation and platelet aggregation over NO-releasing control groups;[48-52] however, as previously mentioned, these various antifouling methods all have their own limitations. Thus, investigation into a biomimetic, complementing antifouling mechanism in combination with NO-releasing materials is warranted.

Hydrophobins, a type of protein produced exclusively by filamentous fungi, are considered the most surface-active class of known proteins.[53, 54] An essential part of fungal growth and development,[55, 56] hydrophobin proteins form self-assembled, amphiphilic monolayers at hydrophilic-hydrophobic interfaces, which alters the wettability of surfaces (changing a hydrophobic surface to hydrophilic and vice versa).[54, 57-59] Of the two known classes of hydrophobins, class I hydrophobins adsorb onto surfaces in an extremely stable monolayer that can only be broken apart by high concentrations of very strong acids.[58-61] The amphiphilic layer formed by class I hydrophobins has been shown to block secondary protein absorption,[62] reduce adherent material on polyethylene stents,[63] lower nanoscale surface friction of polymer surfaces,[64] and reduce biofilm formation on polystyrene surfaces.[65] Considering the ease of hydrophobin monolayer assembly, lack of harsh chemical processing, and potential for application-specific genetic or post-translational modification, the antifouling potential of

hydrophobin protein, as a customizable, ecofriendly antifouling option, in combination with NO-releasing materials warrants study.

In this work, we verified the effect of hydrophobin SC3 (mentioned as SC3) concentration on surface wettability of *S*-nitroso-*N*-acetylpenicillamine (SNAP)-incorporated silicone-base films (polydimethylsiloxane (PDMS) and CarboSil® 2080A). SC3 is a class I hydrophobin that is obtained from the wood-rotting fungus *Schizophyllum commune* and it is considered the most widely studied hydrophobin[53, 60, 66-70]. *S*-nitroso-*N*-acetylpenicillamine (SNAP) was chosen as the NO donor due to its low toxicity and high retainability/storage of NO when blended or swollen into polymers.[43, 46, 52, 71] PDMS is a commonly used biocompatible silicone polymer that can be cured at lower temperatures to form a crosslinked polymer capable of sustainable release of NO when swelled with SNAP,[43, 71] and CarboSil® 2080A (mentioned in this work as CarboSil) is a biocompatible thermoplastic silicone-based polycarbonate urethane that can be blended with SNAP to achieve sustained NO release.[49, 50] CarboSil® was initially used for surface characterization measurements as it is more easily spin coated for ellipsometric and contact angle measurements. After confirming an increase in surface hydrophilicity, an SC3 concentration of 100 μg mL^{-1} was used to test the antifouling efficacy of self-assembled SC3 monolayers. Fibrinogen, the protein involved in thrombus formation, was used as the model protein for adhesion tests performed using spectroscopic ellipsometry measurements. Following this, SC3 was then adsorbed onto the surface of SNAP-swelled PDMS at the same 100 μg mL^{-1} concentration. These PDMS samples were then used to measure SC3's effect on NO-donor behavior, through analysis of NO-release kinetics and leaching of SNAP from the polymer, to test anti-bacterial efficacy against the Gram-positive bacteria *Staphylococcus aureus* (*S. aureus*), and to test the antiplatelet activity of samples incubated in platelet rich porcine plasma.

Materials and Methods

Materials

Hydrophobin SC3 (SC3) was acquired from Sigma-Aldrich Chemie GmbH (Steinheim, Germany). N-acetyl-d-penicillamine (NAP), sodium nitrite, concentrated sulfuric acid (H_2SO_4), tetrahydrofuran (THF), sodium phosphate monobasic (NaH_2PO_4), sodium phosphate dibasic (Na_2HPO_4), potassium chloride, sodium chloride, fibrinogen from bovine plasma, and ethylene diamine tetra acetic acid (EDTA) were obtained from Sigma Aldrich (St Louis, MO). Luria Agar (LA) and Luria broth (LB) were purchased from Fischer BioReagents (Fair Lawn, NJ). Concentrated hydrochloric acid (HCl) and methanol were purchased from Fisher-Scientific (Hampton, NH). Potassium phosphate monobasic (KH_2PO_4) was purchased from BDH Chemicals–VWR International (West Chester, PA). CarboSil® 2080A (mentioned as "CarboSil" hereon) was obtained from DSM Biomedical Inc. (Berkeley, CA). Milli-Q filter was used to obtain de-ionized (DI) water for the aqueous solution preparations. *Staphylococcus aureus* (ATCC 6538, *S. aureus*) was used for all bacterial experiments. Mouse fibroblast cells (ATCC 1658) was used as the model mammalian cell for cytotoxicity assays.

Synthesis of NO donor SNAP

Synthesis of SNAP was carried out using a previously reported method.[36] To summarize, a solution of 1:1 NAP in methanol and sodium nitrite was poured into an Erlenmeyer flask. After the solution was mixed, an equimolar ratio of water, 2M HCl and H_2SO_4 was added to the flask and stirred for 30 minutes. Once the solution was sufficiently mixed, the reaction vessel was placed in an ice bath and blown with an air stream to precipitate SNAP crystals. After 8 hours of reaction, the SNAP crystals were collected by vacuum filtration, washed with DI water, dried overnight at room temperature in a vacuum desiccator. All reagents and crystals were protected

from light throughout the reaction process. After synthesis, SNAP crystals were tested for purity and stored at -20°C until their use in the experiment.

Preparation of NO-Releasing Polydimethylsiloxane

Polydimethylsiloxane (PDMS) was chosen to perform the NO release kinetics measurements and bacteria adhesion assessment due to its wide use as a biomedical polymer. A previously developed method was used to impregnate the NO donor, SNAP, into the PDMS samples.[36, 43]

SNAP swelling solution was prepared by dissolving SNAP in THF at a concentration of 125 mg mL^{-1}. 0.79375 cm diameter, 0.3175 cm thick PDMS pieces were soaked in the SNAP swelling solution for 24 h on a test tube rocker. The PDMS pieces were removed, dried for 24 h in a vacuum desiccator to allow excess THF to evaporate, and then briefly sonicated for 10 minutes in PBS with EDTA buffer to remove any non-swelled SNAP present on the surface. The swelling solution and PDMS pieces were protected from light throughout the swelling process. PDMS samples were used for NO release, SNAP leaching, and bacteria studies.

Preparation of NO-Releasing CarboSil® Films

CarboSil®, a copolymer marketed by DSM Biomedical as a combination of silicone elastomers and thermoplastic polycarbonate-urethanes was chosen to be the NO-releasing base for the contact angle measurements and protein adhesion assessments. This is a copolymer that is easily spin-coated on silicon wafers and hence avoids the incorrect readings that the thinnest PDMS spin coated films (usually upwards of 200 nm thickness compared to 50 nm thickness of CarboSil® thin films) can produce on ellipsometry measurements. A thin layer of CarboSil®, with and without SNAP, was deposited on silicon wafers by spin coating. The spin coating solution was prepared by dissolving CarboSil® in THF to achieve a concentration of 1 mg mL^{-1}.

After the CarboSil® was completely dissolved, 10 wt.% of SNAP was added to the CarboSil®-THF solution. This mixture was protected from light and stirred until the SNAP crystals were dissolved completely. Using a CHEMAT Technology KW-4A spin coater, films were spin coated at 2500 rpm for 30 seconds. The resulting films formed were highly uniform with a surface thickness of 40–50 nm. These thin films were used for contact angle measurements using a Krüss DSA100 Drop Shape Analyzer (sessile drop method with deionized water) and for studying protein adhesion using an M-2000 spectroscopic ellipsometer (J.A. Woollam Co., Inc.).

Surface adsorption of Hydrophobin SC3

Solutions of hydrophobin SC3 (SC3) were prepared by sonication of SC3 in DI water. With limited hydrophobin availability, only DI water was investigated as a solvent and low concentrations of SC3 (10-100 µg) were investigated. SC3 was adsorbed onto the surface of CarboSil®-SNAP wafers and the PDMS-SNAP samples by completely covering the samples with a 100 µL aliquot of SC3 solution for 24 hours at room temperature. The thickness of the adsorbed SC3 layers for the CarboSil®-SNAP wafers were measured using an M-2000 spectroscopic ellipsometer (J.A. Woollam Co., Inc.) with a white light source at three angles of incidence (65°, 70°, and 75°) to the silicon wafer normal. This was used as a validation to ensure adsorption of SC3 to the samples as PDMS-SNAP samples were too thick and undefined in the model to be used for ellipsometric measurements.

Contact Angle Measurements

The static contact angle of CarboSil®-SNAP silicon wafers, with and without an adsorbed SC3 layer, were measured using a Krüss DSA100 Drop Shape Analyzer (sessile drop method with deionized water). Care was taken to measure the same area of the films as measured before to avoid any inconsistency in data collection. The durability of SC3 monolayer surface

hydrophilicity in physiological conditions (37°C in the dark) was measured by taking the contact angle of films over a month period.

Scanning Electron Microscopy

To check for hydrophobin adsorption on the surface of the materials and incorporation of the NO donor, SNAP, in the samples, scanning electron micrograph equipped with a large detector Energy dispersive X-ray spectroscopy (EDS, Oxford Instruments) system was performed. An accelerating voltage of 5kV was applied to image the surface. All the samples were sputter coated with gold-palladium (10 nm thickness, Leica sputter coater).

Fibrinogen Adsorption Test

The thicknesses of spin-coated CarboSil® films were measured using an M-2000 spectroscopic ellipsometer (J. A. Woollam Co., Inc.) with a white light source at three angles of incidence (65°, 70°, and 75°) to the silicon wafer normal. Three replicates were used for each measurement. After the initial thickness of each film was measured, a non-saline, 7.41 pH phosphate buffer solution was prepared from 1 M sodium phosphate dibasic and 1 M potassium phosphate monobasic. Samples were incubated in the non-saline phosphate buffer (PBS) for 30 minutes at 37°C. A solution of fibrinogen from bovine plasma and non-saline PBS was prepared to achieve a concentration of 1 mg mL^{-1} once added to the initial non-saline PBS. After the fibrinogen solution was added, the samples were allowed to incubate at 37°C for 90 minutes. After incubation, each sample was washed with 5 mL of non-saline PBS five consecutive times followed by 5 mL of DI water five consecutive times. The slides were then dried gently with air. The thickness of the wafers after submersion in the protein solution was measured again by spectroscopic ellipsometry. Care was taken to measure the same area of the films as previously measured to avoid any inconsistency in data collection.

Nitric Oxide release measurements

Release of NO from SNAP-swelled PDMS samples was measured using a Sievers chemiluminescence Nitric Oxide Analyzer (NOA), model 280i (Boulder, CO). Prior to NO release measurements, SNAP-loaded samples with no SC3 layer were soaked in DI water at room temperature for 24 h to mimic the 24 h SC3 incubation step. PDMS samples were placed in 3 mL PBS buffer with EDTA at 37°C. NO released from the sample was constantly cleared from the buffer and headspace of the sample cell by purging the buffer with a nitrogen gas stream and bubbler. This nitrogen gas stream is then fed into the chemiluminescence detection chamber where NO levels are measured and plotted. The nitrogen flow rate was set to 200 mL min^{-1} with a chamber pressure of 6 Torr and an oxygen pressure of 6.2 psi. The NO release from samples was normalized by the surface area to obtain a flux unit for NO release rate ($\times 10^{-10}$ mol cm^{-2} min^{-1}).

SNAP Leaching

The weight percentage of SNAP leached from swelled PDMS samples were measured by recording the absorbance of buffer solution in time intervals of 0.5 h, 1 h, 4 h, and 24 h at 340 nm. PDMS samples were soaked in 2 mL of PBS with EDTA at 37°C. A UV-vis spectrophotometer (Thermo-Scientific Genesys 10S UV-Vis) was used to measure the absorbance of the buffer solutions at the previously mentioned time points. Absorbance measurements were taken at an optical density of 340 nm to match the UV-Vis absorbance maxima spectra for SNAP. A calibration curve of SNAP in PBS with EDTA was used to interpolate the absorbance measurements recorded from the study and convert them to concentrations of SNAP. This concentration was converted to percentage of SNAP leached by dividing the total amount of SNAP loaded in each sample used. The total SNAP in samples used

was measured by placing the samples in excessive THF to leach out all remaining SNAP. The absorbance of SNAP in THF at 340nm was recorded and results were interpolated into SNAP concentrations using a calibration graph of SNAP in THF. Care was taken to make sure that buffer solution amount for each sample was maintained at the same amount throughout the experiment to avoid any inconsistent readings and three replicates were used for each measurement.

In vitro analysis of inhibition of bacteria adhesion on polymer surface

The anti-bacterial efficacy of absorbed hydrophobin SC3 was assessed using a previously used method.[49] This protocol, based off E2180 American Society for Testing and Materials protocol, is designed to test the antimicrobial efficacy of hydrophobic polymers. The Gram-positive bacterium *S. aureus*, one of the most common causes of HAIs, was used as the model organism to test anti-bacterial efficacy of the fabricated samples.

Bacterial culture preparation:

Luria Broth (LB) medium and agar was prepared following the manufacturer's instructions and was autoclaved prior to use in the study. Using the LB medium, *S. aureus* was cultured overnight in suspension at 37°C and 150 rpm in a shaker incubator. To confirm that the bacteria were in an active growth phase, the optical density (O.D.) of the culture was measured at a wavelength of 600 nm using a UV-vis spectrophotometer (Thermo-Scientific Genesys 10S UV-Vis). The culture was then centrifuged at 4400 rpm for 7.5 min and the supernatant was discarded. *S. aureus* cells were then washed with fresh sterile PBS (pH 7.4), by centrifuging at 4400 rpm for 7.5 min. The supernatant was discarded, and fresh PBS was added to resuspend the cells. Optical density of the resuspended cells was adjusted to get a bacterial density of 10^6-10^8 CFU mL^{-1} of cell suspension.

Bactericidal activity analysis:

Control, SC3, NO, and SC3-NO samples were exposed to 1 mg mL^{-1} of fibrinogen from bovine plasma for 1 hour. After 1 h of protein exposure, the samples were exposed to *S. aureus* cells (10^6–10^8 CFU mL^{-1}) at 37°C for 24 hours at a speed of 150 rpm in a shaker incubator. After 24 hours, the samples were washed with sterile PBS, to remove any unbound bacteria from the sample surface, and moved to fresh PBS. The samples were then homogenized (to remove adhered cells) for 45 seconds, vortexed (to mix cells in the solution) for 20 seconds and *S. aureus* was plated in the LB agar medium after preparing serial dilutions in the range of 10^{-1}–10^{-5}. Plated *S. aureus* cultures were then incubated at 37 °C for 20 hours. After 20 hours, the CFUs were counted with dilutions factored in using Equation 5.1, and the percentage of bacteria reduction between control groups was calculated using Equation 5.2. Five replicates of each sample type were used.

The following formulae were used to calculate average number of cells present on each sample per $cm^2$and reduction percentage:

Equation 5.1)

$$\text{Total CFUs per sample} = \frac{\text{total number of CFUs per sample x dilution factor x suspension in solution}}{\text{suspension volume plated}}$$

Equation 5.2)

$$\%\ \text{Reduction of Bacteria Adhesion} = \frac{\frac{\text{CFU}}{\text{cm}^2}\ \text{on control} - \frac{\text{CFU}}{\text{cm}^2}\ \text{on test}}{\frac{\text{CFU}}{\text{cm}^2}\ \text{on control}}\ \text{x } 100$$

Platelet adhesion assay

In order to measure the effects of surface treatment on platelet adhesion, control samples were exposed to blood plasma with a known quantity of platelets. All protocols pertaining to the

use of whole blood and platelets were approved by the Institutional Animal Care and Use Committee. Freshly drawn porcine blood (Lampire Biological) with 3.9% sodium citrate at a ratio of 9:1 (blood:citrate) was used. The anticoagulated blood was centrifuged at 300 rcf for 12min using a Beckman Coulter Allegra X-30R Centrifuge. The platelet rich plasma (PRP) portion was collected carefully with a pipet as to not disturb the buffy coat. The remaining samples were then spun again at 4000 rcf for 20 min to collect platelet poor plasma (PPP). Total platelet counts of both the PRP and PPP fractions were determined using a hemocytometer (Fisher). The PRP and PPP were combined in a ratio to give a final platelet concentration 2×10^8 platelets mL^{-1}. Calcium chloride ($CaCl_2$) was added to the final platelet solution to reverse the anticoagulant (Na-citrate). The samples were placed in blood tubes and exposed to approximatively 4 mL of the calcified PRP. The tubes were then incubated at 37°C for 90min with mild rocking (25 rpm) on a Medicus Health blood tube rocker. Following the incubation, the tubes were infinitely diluted with 0.9% saline solution. The degree of platelet adhesion was determined using the lactate dehydrogenase (LDH) released when the adherent platelets were lysed with a Triton-PBS buffer (2% v/v Triton-X-100 in PBS) using a Roche Cytotoxicity Detection Kit (LDH). The directions were followed according to the kit's manual. A calibration curve was constructed using known dilutions of the final PRP, and the platelet adhesion on the various tubing samples was determined from the calibration curve.

Cytocompatibility assay

The ability of SC3-NO films to generate a cytotoxic response (if any) was tested on mouse fibroblast cells using cell counting kit-8 (CCK-8) assay in accordance with ISO 10993 standard. The CCK-8 assay is based on the reduction of highly water-soluble tetrazolium salt. WST-8 [2-(2-methoxy-4-nitrophenyl)-3-(4-nitrophenyl)-5-(2,4-disulfophenyl)-2H-tetrazolium

monosodium salt] (the tetrazolium salt) dehydrogenases in viable mammalian cells to give formazan (an orange color product) in direct proportion to the number of viable cells when detected at a wavelength 450 nm. Mouse fibroblast cells were cultured in a humidified atmosphere with 5% CO_2 at 37°C in 75 cm^2 T-flask containing premade DMEM medium (Thermo Fischer) with 10% fetal bovine serum (FBS) and 1% penicillin-streptomycin. After the confluency reached 80–90%, cells were removed from the flask using 0.18% trypsin and 5 mM EDTA, counted using bromophenol blue in a hemocytometer, and then 100 μL of 5000 cells mL^{-1} were seeded in 96 well plates. The leachates from each sample (PDMS, NO, SC3 and SC3-NO) were obtained by soaking each sample in 2mL DMEM medium for 24h at 37°C. 10μL of the CCK-8 solution was added to each well containing fibroblast cells and were incubated for 4 h. Controls cultures containing 5000 cells ml^{-1} were grown in 8 separate wells for reference to compare with the cells treated with leachates. Absorbance values were measured at 450 nm and the relative cell viability of mammalian cells exposed to the respective leachates were compared. 100 μL of the DMEM medium without cells was added in 3 of the wells and used as blank to adjust the background interference from DMEM media. Results were reported as percentage cell viability difference between the leachate treated cells relative to the negative control (without leachate treatment) using equation 3.

Equation 3)

$$\text{Cell Viability \%} = \frac{\text{Absorbance of test samples}}{\text{Absorbance of control samples}} \text{ x } 100$$

Statistical analysis

All data were calculated as mean ± standard deviation. Student's t-test with unequal variance was used to calculate p values. Population standard deviation calculation was used in bacterial, platelet, and cytocompatibility analyses.

Results and Discussion

Characterization of adsorbed surface layer of SC3

During self-assembly onto hydrophobic surfaces, SC3 undergoes an intermediate α-helical state before forming the more stable β-sheet state.[59, 60] Transition to the β-sheet state can be induced by heating the sample in the presence of detergent or low pH, presence of schizophyllan in solution (a polysaccharide also produced by *S. commune*), or a large enough concentration of SC3 in solution for long incubation periods (≥16 h). [59, 60, 69, 70] In this study, formation of the β-sheet state was accomplished by the last listed method as it avoids high-heat processing, which causes NO release by degradation of the SNAP reservoir and does not require extra reagents.

SNAP-swelled PDMS samples were incubated in SC3 concentrations of 10, 25, 50 and 100 μg mL^{-1} for 24 h at room temperature. In its spherical, α-helical state SC3 has a diameter of ~3 nm, which elongates to a length of 7-10 nm upon formation of the cylindrical, β-sheet state.[53, 60, 65, 69, 70] Therefore, any change in thickness detected by ellipsometry that is greater than 7 nm signals formation of the β-sheet state. As shown in Figure 5.1, all SC3 concentrations less than 100 μg mL^{-1} failed to elongate to the β-sheet state (thicknesses between 2.00 ± .205 nm and 3.36 ± .152 nm); whereas SC3 at a concentration of 100 μg mL^{-1} exhibited a significant increase in surface thickness on both Control and NO samples (thicknesses of 9.54 ± .286 for Control and 9.91 ± .156 nm for NO), which indicates successful formation of the β-sheet state. SEM images

of the surface of NO and SC3-NO samples (Figure 5.2) were used to verify the surface coating of the SC3 on samples. From these images, it can be inferred that the SC3 coating was successfully able to coat the polymeric surface without adversely affecting the surface roughness of samples. This is a benefit of SC3 monolayer assembly as it's known that SC3 is able to lower the friction of polymeric surfaces, and that smoother surfaces adsorb less proteins than rougher surfaces.[64,72] Thereafter, the contact angle of all samples was recorded in order to validate an increase in surface hydrophilicity (Figure 5.3 a). Non-SC3 surfaces exhibited hydrophobic behavior (106.9 ± 0.74^{o} and 107.6 ± 1.18^{o} for Control and NO surfaces, respectively), which was altered to a hydrophilic surface upon incubation with 100 µg mL^{-1} SC3 (74.2 ± 0.81^{o} and 76.12 ± 0.93^{o} for SC3-Control and SC3-NO, respectively). After confirmation of the formation of the β-sheet state and an increase in surface hydrophilicity established, an SC3 concentration of 100 µg mL^{-1} was used in all remaining studies. Additionally, the ability of adsorbed SC3 to retain its hydrophilicity in physiological conditions over a month period was measured by taking contact angle measurements every other day (Figure 5.3 b). Over this month period, the SC3 layer showed no significant loss of hydrophilicity.

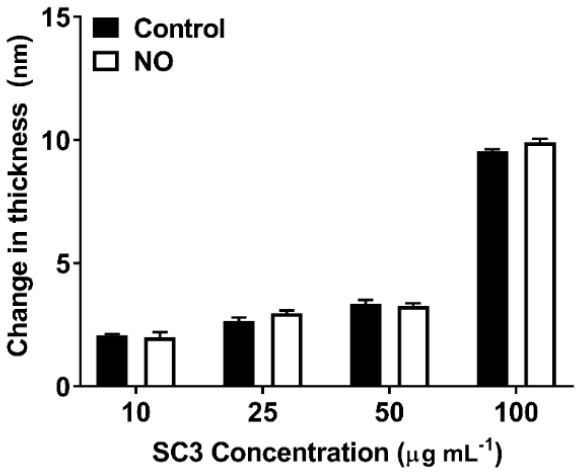

Figure 5.1: Thickness of SC3 layers after incubation in varying concentrations of SC3 for 24 hours. A thickness of 7-10 nm suggests formation of the β-sheet state. Data shown represents mean ± SD (n = 3).

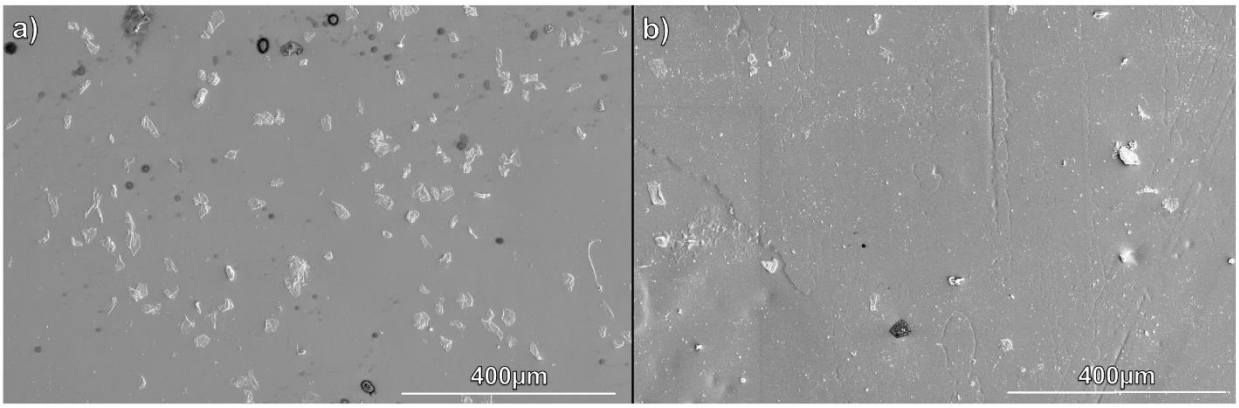

Figure 5.2: SEM images to show morphology of the SNAP-swelled PDMS surface uncoated and coated with SC3. A) SNAP B) SC3-SNAP.

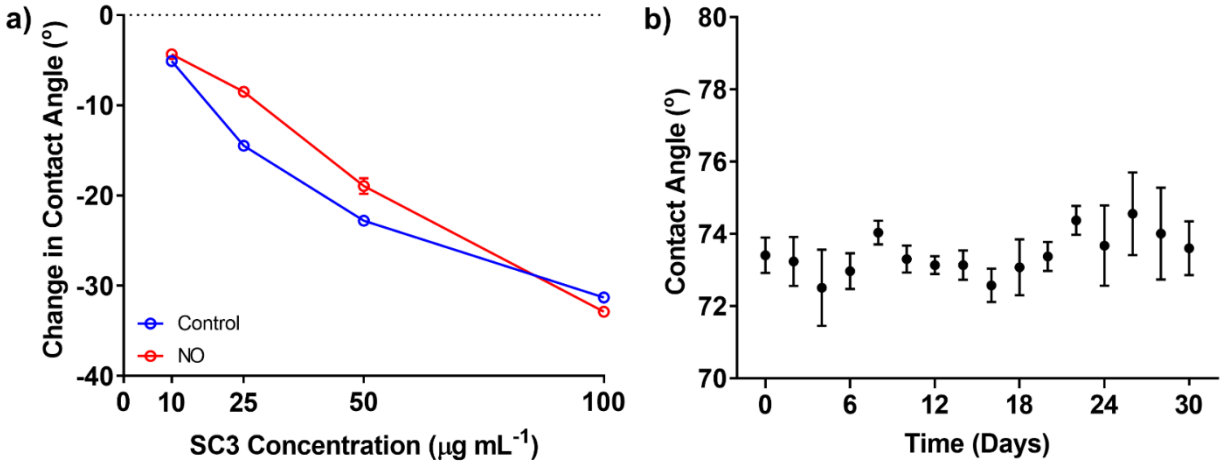

Figure 5.3: Wettability after SC3 coating and storage for one-month. a) Change in contact angle after incubation in varying SC3 concentration. Data shown represents mean ± SD (SD too small to be depicted for most data points, n = 3). b) Contact angle measurements of SC3 covered surface at 100 μg mL^{-1} for 1 month in physiological conditions (37^{o}C in humid environment). Data shown represents mean ± SD (n = 3).

SC3 effect on NO-releasing kinetics

Before testing the antifouling ability of SC3 monolayers, the effect of SC3 on NO-kinetics of SNAP-swelled PDMS pieces was measured. Previously reported methods of increasing surface hydrophilicty of NO-releasing materials has shown an increase in both NO-release and NO-donor leaching,[45] which can limit application due to depeletion of the NO-donor reservoir. This increase in release and leaching is due to the fact that hydration layer formed can swell the underlying polymer. Therefore, the ideal hydrophilic coating for NO-releasing materials should have no major impact on either NO-release behavior or NO-donor leaching.[49]

As depicted in Figure 5.4 a, freshly made SNAP-swelled PDMS displayed a NO flux of 1.63 ±.233 ($\times 10^{-10}$ mol cm^{-2} min^{-1}). Thereafter, separate samples were placed in either DI water or a 100 μg mL^{-1} SC3 solution for 24 hours at room temperature. After the 24 hours, control NO samples exhibited a NO flux of 0.836 ± .198 ($\times 10^{-10}$ mol cm^{-2} min^{-1}), while SC3-NO samples with an adsorbed SC3 layer had a slightly lower flux at 0.763 ± .155 ($\times 10^{-10}$ mol cm^{-2} min^{-1}). This data shows that the prescence of SC3 does not have a significant impact on the release of NO. After NO release measurements, a SNAP leaching study was performed to determine if the presence of adsorbed SC3 has any effect on the SNAP reservoir. The NO samples were placed in a PBS-EDTA buffer at 37°C. Figure 5.4 b shows that, over the course of 24 h, no significant

difference of SNAP leaching between NO groups with and without adsorbed SC3 could be observed. These results support the notion that presence of a SC3 monolayer, despite the increase in surface hydrophilicity, has no significant effect on NO kinetics, which is a favorable quality in the design of NO-releasing materials. Figure 5.4 c shows a 1-hour NO-release profile of freshly made NO, SC3-NO, and 24-hour incubated NO control samples.

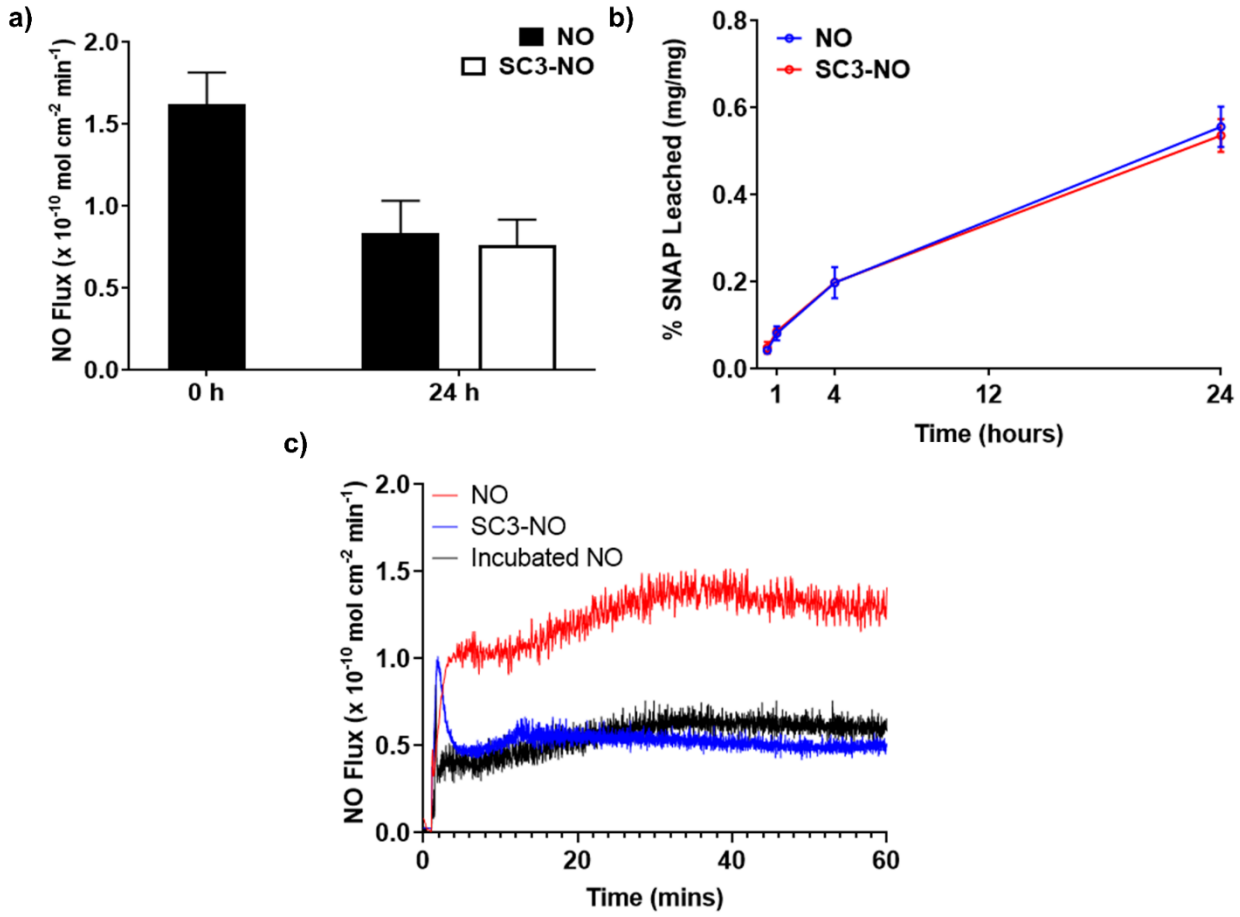

Figure 5.4: NO donor leaching and NO Release Characteristics a) NO-release before and after adsorption of SC3 under physiological conditions (soaked in PBS with EDTA buffer at 37 °C in the dark). Data represents mean ± SD (n = 4). b) SNAP content in PBS buffer due to leaching from NO-releasing polymer. Calculated as a percentage of SNAP leached into the PBS buffer

from the polymer compared to total SNAP loaded. Data represent mean ± SD (n = 3). c) 60-minute NO release profile of freshly made SNAP, SC3-SNAP, and incubated SNAP control.

Assessment of physiological conditions

Fibrinogen is a glycopotein found in the blood of all vertebrates and is the precursor to the fibrin mesh that holds together platelet cells in thrombi.[73, 74] Because of its high surface affinity, fibrinogen is able to replace other proteins (e.g. albumin) already adsorbed onto the surface of materials through the Vroman effect.[75] Once adsorbed onto a foreign surface, fibrinogen undergoes a conformational change that results in a dramatic increase in exposure of adhesion receptors.[73, 74] These adhesion receptors provide binding sites for inflammation,[5] platelet,[7, 74] and bacteria cells[6, 76] to latch onto the device surface. Respectively, the resulting celluar attachment leads to device failure by either FBR encapsulation[8] or thrombus formation[7, 74] while increasing the risk severe infection due to biofilm formation.[76, 77] Fibrinogen's implication in medical device failure and biofilm formation is the reasoning behind its selection as the model protein to measure the anti-fouling capabilites of adsorbed SC3 monolayers.

Spin coated CarboSil films, with and without an adsorbed SC3 layer, were incubated in a non-saline buffer solution of fibrinogen (1 mg mL^{-1}) for 90 minutes at 37°C to mimic the physiological environment. An incubation time of 90 minutes was chosen as the majority of proteins adsorb to medical devices surfaces within the first few minutes of exposure to physiological fluids.[26] After incubation, any unattached proteins were rinsed off from the polymer surfaces by sequential washing with non-saline buffer and DI water. The change in thickness of the films was measured with a spectroscopic ellipsometer at the nanometer scale. Previous microscopic measurements of fibrinogen reveal that it is a very narrow protein with

dimensions of 5–6.5 nm in diameter and 47.5 nm in length.[73, 78] Therefore, for this ellipsometric study, any change in surface thickness above 5 nm would be considered adsorption of fibrinogen.

The data shown in Figure 5.5 a shows the change in the thickness of the spin coated films after incubation in the fibrinogen solution. Control samples without SC3 displayed typical *in vivo* polymeric medical device behavior[26] with a change in surface thickness of 30.78 ± 3.53 nm for the Control group and 48.15 ± 3.34 nm for the NO group, which indicates high levels of fibrinogen adsorption to the polymer surface to both. The significantly larger change in thickness seen in the NO group over the Control group confimed the previously reported notion that NO-releasing materials adsorb more proteins.[40] In comparison, samples with an adsorbed SC3 layer exhibited excellent antifouling behavior with a thickness change of 2.97 ± .299 nm and 4.24 ± .285 nm, which are both lower than the 5 nm diameter of fibrinogen. The over ten-fold decrease in fibrinogen adsorption can be attributed to three phenomena: 1) The stability of the formed SC3 monolayer due to the surface affinity of SC3's hydrophobic portion and hydrophobic:hydrophobic/hydrophilic:hydrophilic interactions between neighboring SC3 proteins 2) The formation of a hydration layer with the surrounding environment on SC3's hydrophilic side which increases the thermodynamic requirement for foulants to adsorb onto the surface 3) The decrease in surface roughness caused by SC3 monolayer assembly over SNAP crystals which lowers the available surface area for foulants to attach onto (Figure 5.2). All of these interactions combine to prevent the removal of SC3 and subsequent adsorption of fibrinogen through the Vroman effect. The slight increase in thickness observed on adsorbed SC3 surfaces could be the result of either slight swelling of the CarboSil® films due to the formation of a hydration layer or prescence of dust particles which, despite our best efforts, could have settled on the surface during handling.

With confirmation of SC3's antifouling ability, the next step is to test SC3-NO's usability as a medical device coating. One of the most fundamental and important antimicrobial evaluation of polymers involves the exposure of the polymer to a specific microbe for a certain period of time followed by plating of the microbial adhesion/growth extracted from the polymer. Previous studies using NO-releasing materials in combination with hydrophilic coatings have shown significant decrease in bacteria adhesion over control groups.[49, 50] Thus, for this study, it was expected that SC3-NO samples would also exhibit greater antibacterial efficacy over controls. This antimicrobial test was performed with *S. aureus*, one of the most commonly found nosocomial pathogens[76, 79] with an exposure time of 24 hours. The initial exposure time is important to consider because this is when bacteria start to release exopolymeric substrates to attach to the surface of the biomaterials. From Figure 5.5 b we can see that there was a reduction of bacteria among all the materials when compared to the untreated control group.

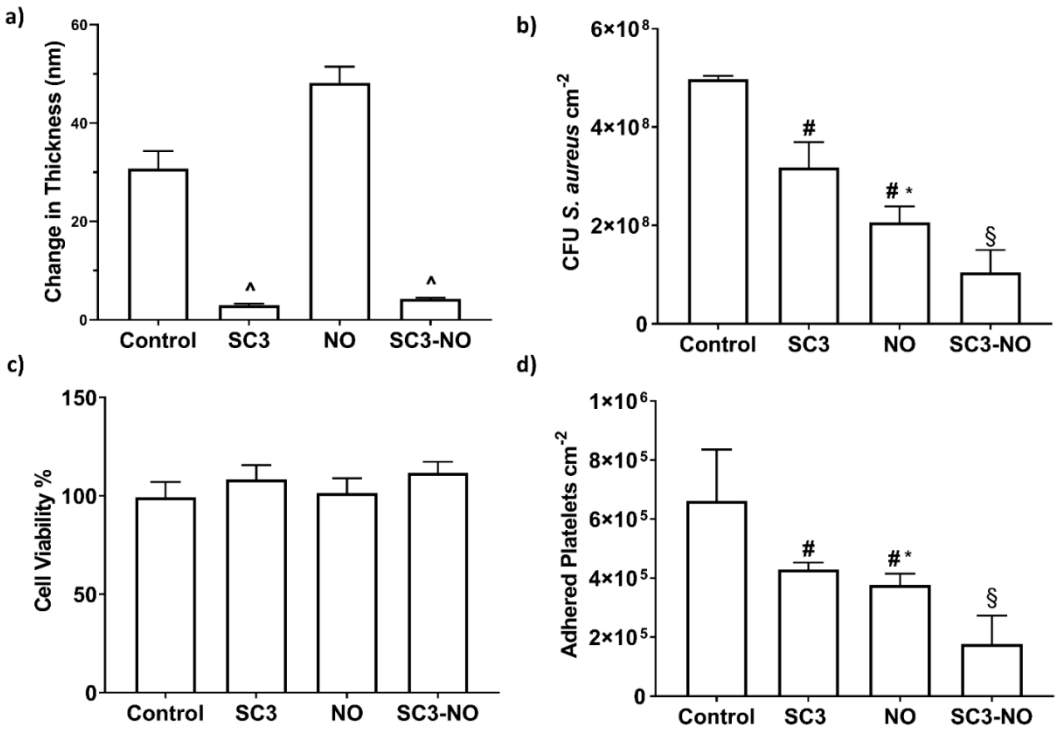

Figure 5.5: Biological characterization of SC3-SNAP samples. a) Thickness of EPS layer after exposure to 1 mg mL^{-1} fibrinogen from bovine serum for 90 minutes. Data shown represents mean ± SD (n = 3). b) Antimicrobial adhesion assay conducted with *S. aureus*. Calculated as a log of the colony forming units (CFU) per cm^2 of surface material. Data represents mean ± SD (n = 5). c) Cytocompatibility assay exposing material leachates to mouse fibroblast cells. Reported as a percent viability compared to control cells not exposed to any material leachates (n=6). d) Adhered platelet counts of samples incubated in porcine platelet rich plasma. Data represented mean ± SD (n = 6). ^ = p < .01 vs Control & NO. # = p < .05 vs Control. * = p <.05 vs SC3. § = p <.01 vs Control, SC3, & SNAP.

When compared to control samples, bacteria adhesion reduced by 36.129 ±8.510% vs. SC3, 58.581 ±5.429% vs. NO and 79.097 ±7.529% vs. SC3-NO (Table 5.1). This result was expected as we normally see bacterial/biofilm growth in polymers with no antibacterial or antifouling polymer within 24 h. This decrease is important to establish the antimicrobial efficacy of all the fabricated surfaces when compared to the control surface. In addition to this reduction compared to control samples, significant difference in bacterial growth between the SC3, NO, and SC3-NO samples was also observed. The demonstrated hydrophilic activity of the SC3 coating from previous studies was validated by the reduced adhesion of bacteria on the SC3 coated samples. The hydration layer formed on the SC3 monolayer surface acted as a passive repulsion layer making it harder for bacteria to attach to the material's surface. Hence, an initial reduction was seen when compared to control samples. However, since NO is an antibacterial agent, the bacterial adhesion reduced by 35.152 ±8.499% when comparing NO to SC3 samples.

The most significant results are perhaps seen by combining the antifouling properties of SC3 monolayers with the bactericidal activity of NO. The synergistic combination of SC3 monolayers and NO significantly reduced bacteria adhesion when compared to both SC3 (67.273 ±11.788%) and NO (49.533 ±18.178%) control groups. This indicates and further establishes the pattern of increased antimicrobial efficacy of NO-releasing materials when combined with antifouling surfaces.

Table 5.1: Comparison of bacterial adhesion in terms of percentage reduction.

	Reduction (%) ± SD	**p value**
Control vs. SC3	36.129 ±8.510	0.003
Control vs. NO	58.581 ±5.429	1×10^{-4}
Control vs. SC3-NO	79.097 ±7.529	4×10^{-6}
SC3 vs. NO	35.152 ±8.499	0.005
SC3 vs. SC3-NO	67.273 ±11.79	1×10^{-4}
NO vs. SC3-NO	49.533 ±18.18	0.005

After 24 hours of exposure to *S. aureus* in physiological conditions, NO release measurements were taken and revealed SC3-NO samples had a slightly higher flux (.476 ± .069 $\times 10^{-10}$ mol cm^{-2} min^{-1}) compared to NO samples (.445 ± .041 $\times 10^{-10}$ mol cm^{-2} min^{-1}). While not stastically significant, considering NO-only samples had a higher NO flux than SC3-NO samples before the bacteria study (Figure 5.4 a), this suggests presence of SC3 monolayer does not negatively affect the NO-release characteristics in the prescense of biological foulants. Therefore, it can be concluded from the results that we were able to demonstrate a more potent antimicrobial surface with the combination of SC3 and NO.

While it has been demonstrated that the combination of SC3-NO reduces unwanted bacterial adhesion, it is of equal importance to establish that the combination does not induce a cytotoxic response when placed inside the physiological environment. To test the combination's

cytocompatibility, a CCK-8 assay was deployed utilizing mouse fibroblast cells as the model mammalian cell. Control, SC3, NO, and SC3-NO leachates were collected in DMEM media and exposed to fibroblast cells. As shown in Figure 5.5 c, there was no significant cytotoxic response observed from any of the control groups, suggesting that the combination of SC3-NO is safe to use in the physiological environment. It should be noted that, while not significant, SC3 and SC3-NO samples exhibited a slightly proliferative effect compared to control (9.086 ±7.254% and 12.36 ±5.715% increase) and NO samples (7.281 ±7.134% and 10.51 ±5.621% increase). Results are reported as a percentage compared to control cultures (not exposed to leachates).

With verification of SC3-NO's cytocompatibility in physiological environments, it is important to also assess the adhesion of physiological cells. Platelet cell adhesion to the surface of blood-contact medical devices, in combination with the conversion of fibrinogen to fibrin, results in the formation of thrombi.[7, 73, 74] Once initiated, thrombi can rapidly form a completely occlusive clot, which can result in a multitude of severe consequences such as tissue necrosis[12] or a cardiovascular event (heart attack, stroke, arrhythmia, etc.) due to an embolism of the thrombus.[15] In order to prevent thrombus formation on blood-contact devices, the systemic administration of the anticoagulant heparin is standardly used; however, due to stripping the blood of its ability to clot, there are a number of complications with the systemic administration heparin that has led to heparinization as the leading cause of clinical drug-related deaths in the United States.[80] Therefore, in order to reduce the risk of device failure and clinical complications, a versatile "one-for-all" biomedical material must be able to not only to prevent the adhesion of bacteria but to also prevent the adhesion of platelet cells.

Control, SC3, NO, and SC3-NO samples were exposed to fresh porcine platelet rich plasma for 90 mins at 37°C under mild rocking. Thereafter, the number of adhered platelets were

detached using a lysing buffer and quantified using a Roche LDH assay (Figure 5.5 d). Similar to the results seen in the bacterial adhesion study, the hydration layer formed on the SC3 monolayer surface and antiplatelet activity of NO release reduced platelet adhesion compared to control samples (35.326 ±3.701% and 43.176 ±5.581%, respectively) (Table 5.2); however, a significant improvement is seen in the combination of mechanisms as SC3-NO samples showed a significant reduction of adhered platelets compared to control samples (73.407 ±14.59%), SC3 samples (58.882 ±22.55%), and NO samples (53.202 ±25.67%).

Table 5.2: Comparison of platelet adhesion in terms of percentage reduction.

	Reduction (%) ± SD	**p value**
Control vs. SC3	35.326 ±3.701	.03
Control vs. NO	43.176 ±5.851	.02
Control vs. SC3-NO	73.407 ±14.59	3×10^{-4}
SC3 vs. NO	12.138 ±9.047	.03
SC3 vs. SC3-NO	58.882 ±22.55	.001
NO vs. SC3-NO	53.202 ±25.67	.003

Conclusion

In summary, the fabrication of a medical device coating containing a natural antifouling protein with NO-releasing base polymer was described for the first time. This work was able to establish the significant synergistic effects of combining passive with active strategies for antimicrobial properties. SC3 was surface coated using a simple physical strategy to provide a green alternative for antifouling method and prevent the drawbacks of NO-releasing medical device coatings. Contact angle measurements and SEM imaging verified the coating and stability of the SC3 surface for a one-month period. 100 µg/mL of SC3 coating was found to be ~9 nm in thickness and hence confirmed the formation of the more stable β-sheet state of SC3. The

resulting SC3 monolayer reduced the contact angle of CarboSil® by ~30 and was maintained for a period of 30 days in physiological conditions which indicates a durable coating. A protein adsorption test with 1 mg/mL of fibrinogen was performed in order to establish the antifouling capability of SC3 coated samples. Negligible thickness change (≤5 nm) in the films with SC3 indicated the antifouling property important for increasing bactericidal efficacy whereas samples with no SC3 showed a thickness change of as much as ~48 nm. NOA characteristics revealed that, despite the layer of hydrophilic SC3 coating, no significant effect on NO kinetics was observed, which is a favorable quality in the design of NO-releasing materials. Next, the bactericidal and antiplatelet properties were demonstrated to be superior for the SC3-NO combination compared to control samples. When comparing SC3-NO samples to control, SC3, and NO controls, bacterial adhesion was reduced by 79.097 ±7.529%, 67.273 ±11.788%, and 49.533 ±18.178% and platelet adhesion was reduced by 73.407 ±14.59%, 58.882 ±22.55%, and 53.202 ±25.67% respectively. Finally, a cytocompatibility test was performed to demonstrate that the leachates from the SC3-NO combination do not induce a cytotoxic response in mammalian cells and is safe to use for *in vivo* applications.

The steady physiological level of NO-release characteristics along with enhanced protein-resistance, bactericidal, antiplatelet, and cytocompatibility properties indicate a possibility of future application of this facile strategy in all medical device coatings. As SC3 is just one protein in the hydrophobin family, this study should serve as a proof-of-concept in using ecofriendly, biologically-derived surface proteins as a means of antifouling. Thus, the results of this study warrant future investigation into SC3 robustness in long-term *in-vivo* applications along with investigation into the antifouling nature other hydrophobin proteins.

References

1. V. B. Damodaran and N. S. Murthy, *Biomaterials research*, 2016, **20**, 18-18.
2. I. Banerjee, R. C. Pangule and R. S. Kane, *Advanced Materials*, 2011, **23**, 690-718.
3. C. Blaszykowski, S. Sheikh and M. Thompson, *Trends in Biotechnology*, 2014, **32**, 61-62.
4. Q. Yu, Y. Zhang, H. Wang, J. Brash and H. Chen, *Acta Biomater*, 2011, **7**, 1550-1557.
5. J. M. Anderson, A. Rodriguez and D. T. Chang, *Seminars in immunology*, 2008, **20**, 86-100.
6. P. S. Stewart and M. J. Franklin, *Nature Reviews Microbiology*, 2008, **6**, 199.
7. M. B. Gorbet and M. V. Sefton, *Biomaterials*, 2004, **25**, 5681-5703.
8. G. S. Wilson and R. Gifford, *Biosensors and Bioelectronics*, 2005, **20**, 2388-2403.
9. R. M. Donlan and J. W. Costerton, *Clinical Microbiology Reviews*, 2002, **15**, 167-193.
10. R. M. Klevens, J. R. Edwards, C. L. Richards, T. C. Horan, R. P. Gaynes, D. A. Pollock and D. M. Cardo, *Public Health Reports*, 2007, **122**, 160-166.
11. R. D. Scott, 2009.
12. J. A. Bittl, *Journal of the American College of Cardiology*, 1996, **28**, 368-370.
13. D. M. J., F. W. F. M. and R. W. B., *The Journal of Pathology*, 1979, **127**, 99-110.
14. M. J. Davies and A. Thomas, *New England Journal of Medicine*, 1984, **310**, 1137-1140.
15. M. D. Silverstein, J. A. Heit, D. N. Mohr, T. M. Petterson, W. O'Fallon, L. Melton and Iii, *Archives of Internal Medicine*, 1998, **158**, 585-593.
16. G. Kang, M. Liu, B. Lin, Y. Cao and Q. Yuan, *Polymer*, 2007, **48**, 1165-1170.
17. C. Perrino, S. Lee, S. W. Choi, A. Maruyama and N. D. Spencer, *Langmuir*, 2008, **24**, 8850-8856.

18. A. J. Alpert, *Analytical Chemistry*, 2008, **80**, 62-76.

19. G.-d. Kang and Y.-m. Cao, *Water Research*, 2012, **46**, 584-600.

20. M. Inutsuka, N. L. Yamada, K. Ito and H. Yokoyama, *ACS Macro Letters*, 2013, **2**, 265-268.

21. M. He, K. Gao, L. Zhou, Z. Jiao, M. Wu, J. Cao, X. You, Z. Cai, Y. Su and Z. Jiang, *Acta Biomaterialia*, 2016, **40**, 142-152.

22. E. Ostuni, R. G. Chapman, R. E. Holmlin, S. Takayama and G. M. Whitesides, *Langmuir*, 2001, **17**, 5605-5620.

23. S. Chen, J. Zheng, L. Li and S. Jiang, *Journal of the American Chemical Society*, 2005, **127**, 14473-14478.

24. J. B. Schlenoff, *Langmuir*, 2014, **30**, 9625-9636.

25. D. Rana and T. Matsuura, *Chemical Reviews*, 2010, **110**, 2448-2471.

26. A. R. Statz, A. E. Barron and P. B. Messersmith, *Soft Matter*, 2008, **4**, 131-139.

27. Y. Chang, S.-C. Liao, A. Higuchi, R.-C. Ruaan, C.-W. Chu and W.-Y. Chen, *Langmuir*, 2008, **24**, 5453-5458.

28. Y. Wo, E. J. Brisbois, R. H. Bartlett and M. E. Meyerhoff, *Biomaterials Science*, 2016, **4**, 1161-1183.

29. M. W. Vaughn, L. Kuo and J. C. Liao, *American Journal of Physiology-Heart and Circulatory Physiology*, 1998, **274**, H2163-H2176.

30. J. O. Lundberg, M. T. Gladwin and E. Weitzberg, *Nat Rev Drug Discov*, 2015, **14**, 623-641.

31. M. Emerson, S. Momi, W. Paul, P. A. Francesco, C. Page and P. Gresele, *Thrombosis and haemostasis*, 1999, **81**, 961-966.

32. D. Salvemini, M. G. Currie and V. Mollace, *The Journal of Clinical Investigation*, 1996, **97**, 2562-2568.

33. T. Akaike and H. Maeda, *Immunology*, 2000, **101**, 300-308.

34. M. M. Reynolds, J. A. Hrabie, B. K. Oh, J. K. Politis, M. L. Citro, L. K. Keefer and M. E. Meyerhoff, *Biomacromolecules*, 2006, **7**, 987-994.

35. Z. Zhou and M. E. Meyerhoff, *Biomaterials*, 2005, **26**, 6506-6517.

36. E. J. Brisbois, H. Handa, T. C. Major, R. H. Bartlett and M. E. Meyerhoff, *Biomaterials*, 2013, **34**, 6957-6966.

37. K. A. Broniowska, A. R. Diers and N. Hogg, *Biochim Biophys Acta*, 2013, **1830**, 3173-3181.

38. E. M. Hetrick, H. L. Prichard, B. Klitzman and M. H. Schoenfisch, *Biomaterials*, 2007, **28**, 4571-4580.

39. S. P. Nichols, A. Koh, N. L. Brown, M. B. Rose, B. Sun, D. L. Slomberg, D. A. Riccio, B. Klitzman and M. H. Schoenfisch, *Biomaterials*, 2012, **33**, 6305-6312.

40. S. M. Lantvit, B. J. Barrett and M. M. Reynolds, *Journal of Biomedical Materials Research Part A*, 2013, **101**, 3201-3210.

41. J. E. Saavedra, G. J. Southan, K. M. Davies, A. Lundell, C. Markou, S. R. Hanson, C. Adrie, W. E. Hurford, W. M. Zapol and L. K. Keefer, *Journal of Medicinal Chemistry*, 1996, **39**, 4361-4365.

42. H. Handa, T. C. Major, E. J. Brisbois, K. A. Amoako, M. E. Meyerhoff and R. H. Bartlett, *Journal of materials chemistry. B*, 2014, **2**, 1059-1067.

43. E. J. Brisbois, T. C. Major, M. J. Goudie, R. H. Bartlett, M. E. Meyerhoff and H. Handa, *Acta Biomaterialia*, 2016, **37**, 111-119.

44. B. J. Nablo, H. L. Prichard, R. D. Butler, B. Klitzman and M. H. Schoenfisch, *Biomaterials*, 2005, **26**, 6984-6990.

45. E. J. Brisbois, J. Bayliss, J. Wu, T. C. Major, C. Xi, S. C. Wang, R. H. Bartlett, H. Handa and M. E. Meyerhoff, *Acta biomaterialia*, 2014, **10**, 4136-4142.

46. Y. Wo, E. J. Brisbois, J. Wu, Z. Li, T. C. Major, A. Mohammed, X. Wang, A. Colletta, J. L. Bull, A. J. Matzger, C. Xi, R. H. Bartlett and M. E. Meyerhoff, *ACS Biomaterials Science & Engineering*, 2017, **3**, 349-359.

47. E. J. Brisbois, T. C. Major, M. J. Goudie, M. E. Meyerhoff, R. H. Bartlett and H. Handa, *Acta Biomaterialia*, 2016, **44**, 304-312.

48. M. J. Goudie, P. Singha, S. P. Hopkins, E. J. Brisbois and H. Handa, *ACS Applied Materials & Interfaces*, 2019, DOI: 10.1021/acsami.8b16819.

49. P. Singha, J. Pant, M. J. Goudie, C. D. Workman and H. Handa, *Biomaterials Science*, 2017, **5**, 1246-1255.

50. Q. Liu, P. Singha, H. Handa and J. Locklin, *Langmuir*, 2017, **33**, 13105-13113.

51. W. L. Storm, J. Youn, K. P. Reighard, B. V. Worley, H. M. Lodaya, J. H. Shin and M. H. Schoenfisch, *Acta Biomaterialia*, 2014, **10**, 3442-3448.

52. M. J. Goudie, J. Pant and H. Handa, *Scientific Reports*, 2017, **7**, 13623.

53. X. Wang, F. Shi, H. A. B. Wösten, H. Hektor, B. Poolman and G. T. Robillard, *Biophysical Journal*, 2005, **88**, 3434-3443.

54. M. B. Linder, *Current Opinion in Colloid & Interface Science*, 2009, **14**, 356-363.

55. H. A. B. Wösten and J. G. H. Wessels, *Mycoscience*, 1997, **38**, 363-374.

56. J. G. H. Wessels, *Mycologist*, 2000, **14**, 153-159.

57. Q. Ren, A. H. Kwan and M. Sunde, *Biopolymers*, 2013, **100**, 601-612.

58. A. Piscitelli, P. Cicatiello, A. M. Gravagnuolo, I. Sorrentino, C. Pezzella and P. Giardina, *Biomolecules*, 2017, **7**.

59. H. A. B. Wösten and K. Scholtmeijer, *Applied Microbiology and Biotechnology*, 2015, **99**, 1587-1597.

60. K. Scholtmeijer, M. L. de Vocht, R. Rink, G. T. Robillard and H. A. B. Wösten, *Journal of Biological Chemistry*, 2009, **284**, 26309-26314.

61. V. Lo, Q. Ren, C. Pham, V. Morris, A. Kwan and M. Sunde, *Nanomaterials*, 2014, **4**, 827.

62. B. von Vacano, R. Xu, S. Hirth, I. Herzenstiel, M. Ruckel, T. Subkowski and U. Baus, *Anal Bioanal Chem*, 2011, **400**, 2031-2040.

63. U. Weickert, F. Wiesend, T. Subkowski, A. Eickhoff and G. Reiss, *Adv Med Sci*, 2011, **56**, 138-144.

64. R. Misra, J. Li, G. C. Cannon and S. E. Morgan, *Biomacromolecules*, 2006, **7**, 1463-1470.

65. M. Artini, P. Cicatiello, A. Ricciardelli, R. Papa, L. Selan, P. Dardano, M. Tilotta, G. Vrenna, M. L. Tutino, P. Giardina and E. Parrilli, *Biofouling*, 2017, **33**, 601-611.

66. X. Wang, H. P. Permentier, R. Rink, J. A. Kruijtzer, R. M. Liskamp, H. A. Wosten, B. Poolman and G. T. Robillard, *Biophys J*, 2004, **87**, 1919-1928.

67. M. I. Janssen, M. B. van Leeuwen, T. G. van Kooten, J. de Vries, L. Dijkhuizen and H. A. Wosten, *Biomaterials*, 2004, **25**, 2731-2739.

68. A. Zykwinska, T. Guillemette, J.-P. Bouchara and S. Cuenot, *Biochimica et Biophysica Acta (BBA) - Proteins and Proteomics*, 2014, **1844**, 1231-1237.

69. M. L. de Vocht, K. Scholtmeijer, E. W. van der Vegte, O. M. H. de Vries, N. Sonveaux, H. A. B. Wösten, J.-M. Ruysschaert, G. Hadziioannou, J. G. H. Wessels and G. T. Robillard, *Biophysical Journal*, 1998, **74**, 2059-2068.

70. M. L. De Vocht, I. Reviakine, W.-P. Ulrich, W. Bergsma-Schutter, H. A. B. Wösten, H. Vogel, A. Brisson, J. G. H. Wessels and G. T. Robillard, *Protein Science : A Publication of the Protein Society*, 2002, **11**, 1199-1205.

71. M. J. Goudie, E. J. Brisbois, J. Pant, A. Thompson, J. A. Potkay and H. Handa, *International journal of polymeric materials*, 2016, **65**, 769-778.

72. Q. An, F. Li, Y. Ji and H. Chen, *Journal of Membrane Science*, 2011, **367**, 158-165.

73. R. F. Doolittle, in *Fibrinogen, Thrombosis, Coagulation, and Fibrinolysis*, eds. C. Y. Liu and S. Chien, Springer US, Boston, MA, 1990, DOI: 10.1007/978-1-4615-3806-6_2, pp. 25-37.

74. S. Kattula, J. R. Byrnes and A. S. Wolberg, *Arteriosclerosis, Thrombosis, and Vascular Biology*, 2017, **37**, e13-e21.

75. C. Fuss, J. C. Palmaz and E. A. Sprague, *Journal of Vascular and Interventional Radiology*, 2001, **12**, 677-682.

76. L. Bonifait, L. Grignon and D. Grenier, *Applied and Environmental Microbiology*, 2008, **74**, 4969-4972.

77. T. Boland, R. A. Latour and F. J. Stutzenberger, in *Handbook of Bacterial Adhesion: Principles, Methods, and Applications*, eds. Y. H. An and R. J. Friedman, Humana Press, Totowa, NJ, 2000, DOI: 10.1007/978-1-59259-224-1_2, pp. 29-41.

78. A. Toscano and M. M. Santore, *Langmuir*, 2006, **22**, 2588-2597.

79. M. Otto, *Annual Review of Medicine*, 2013, **64**, 175-188.

80. G. Shepherd, P. Mohorn, K. Yacoub and D. W. May, *Annals of Pharmacotherapy*, 2012, **46**, 169-175.

CHAPTER 6

COVALENT GRAFTING OF ANTIFOULING PHOSPHORYLCHOLINE-BASED COPOLYMERS WITH ANTIMICROBIAL NITRIC OXIDE RELEASING POLYMERS TO ENHANCE INFECTION-RESISTANT PROPERTIES OF MEDICAL DEVICE COATINGS[6]

[6] Liu, Q., Singha, P., Handa, H., Locklin, J. 2017. *Langmuir*.
Reprinted with permission from the publisher.

Abstract

Medical device coatings that resist protein adhesion and bacterial contamination are highly desirable in the healthcare industry. In this work, an antifouling zwitterionic terpolymer, 2-methacryloyloxyethyl phosphoryl-choline-co-butyl methacrylate-co-benzophenone (BPMPC), is covalently grafted to a nitric oxide (NO) releasing antimicrobial biomedical grade copolymer of silicone-poly-carbonate-urethane, CarboSil, to significantly enhance the biocompatibility, nonspecific protein repulsion and infection-resistant properties. The NO donor embedded into CarboSil is S-nitroso-N-acetylpenicillamine (SNAP) and covalent grafting of the BPMPC is achieved through rapid UV-cross-linking, providing a stable, hydrophilic coating that has excellent durability over a period of several weeks under physiological conditions. The protein adsorption test results indicate a significant reduction (~84−93%) of protein adhesion on the test samples compared to the control samples. Bacteria tests were also performed using the common nosocomial pathogen, *Staphylococcus aureus*. Test samples containing both NO donor and BPMPC show a 99.91 ± 0.06% reduction of viable bacteria when compared to control samples. This work demonstrates a synergistic combination of both antimicrobial and antifouling properties in medical devices using NO donors and zwitterionic copolymers that can be covalently grafted to any polymer surface.

Introduction

The non-specific adsorption of proteins has long been considered a grand challenge in many biomedical applications such as implants, contact lenses, catheters, and biosensors. In addition to medical device failure, the consequences of protein adsorption include thrombus formation, innate immune response, and bacterial infection.[1, 2] Preventing direct microbial contamination is also highly desired characteristic of medical devices, implants, and hospital

equipment.[3-6] Although significant progress has been made in understanding and reducing adsorption and contamination, the Centers for Disease Control and Prevention (CDC) still reported that, in 2011, there were an estimated 722,000 healthcare-associated infections (HAIs) in U.S. acute care hospitals. Additionally, about 75,000 patients with HAIs died during their hospitalization.[7] On any given day, approximately 1 out of every 25 patients in the U.S. contracts at least one infection during their hospital care. Therefore, materials demonstrating antifouling and antimicrobial effects are highly desirable.

In recent years, zwitterionic polymers have attracted attention due to their biomimetic nature, which provides excellent biocompatibility and antifouling properties compared to traditional materials like poly(ethylene glycol) (PEG).[8-10] Zwitterionic polymers, in which both cationic and anionic groups are on the same monomer residue, have a strong hydration ability which accounts for their ultra-low fouling properties.[11-16] The dipole arrangement of water molecules in the hydration shell formed via electrostatic interactions with the charged groups of the zwitterion are closer to free water than the directional arrangement of water molecules in the hydration shell formed via hydrogen bonds in case of PEG.[17] The excellent hydrophilicity of zwitterionic polymers, however, provides a difficult challenge in coating hydrophobic materials, where coating delamination under physiological conditions has so far limited practical application.[18]

To explore the covalent grafting of zwitterionic polymers to various substrates ranging from hydrophilic to hydrophobic, we incorporated the benzophenone (BP) chromophore, a photoactive tethering reagent, into the polymeric backbone.[19-24] The BP group can produce a diradical under low-intensity UV irradiation (350-365 nm) that abstracts an aliphatic hydrogen from a neighboring C-H bond to form a new C-C bond, without intensive UV oxidative damage

to the polymer or substrates.[20] Through this process, network polymer films can be grafted with excellent durability to a broad selection of C-H containing materials and surfaces, and has been used for many applications such as microfluidics,[25, 26] organic semiconductors,[27] redox polymers,[28, 29] anti-icing polymers,[30] and biosensors.[31, 32]

Nitric oxide (NO) is known as a potent and nonspecific bactericidal agent due to its natural broad-spectrum antimicrobial properties with low risk for promoting bacterial resistance.[33-35] NO utilizes several antimicrobial mechanisms including nitrosation of amines and thiols, lipid peroxidation, tyrosine nitration and DNA cleavage.[36] Major classes of current NO donors include organic nitrates, metal-NO complexes, N-nitrosamines, and S-nitrosothiols,[37] *S*-nitroso-*N*-acetylpenicillamine (SNAP), a commonly studied NO donor, exhibits significant antimicrobial and antithrombotic effects.[38, 39] In our previous studies, SNAP has been successfully doped into CarboSil polymer films, and these SNAP-doped polyurethane-based materials can release NO for extended periods (20 days) with very low levels of leaching.[38, 40, 41]

In this work, we synthesized zwitterionic terpolymers (2-methacryloyloxyethyl phosphorylcholine-*co*-butyl methacrylate-*co*-benzophenone, BPMPC) that can be covalently grafted to antimicrobial, NO-releasing CarboSil (silicone-polycarbonate-urethane thermoplastic) upon UV-irradiation. The polymer-coated surfaces are characterized in detail and the zwitterionic stability is assessed under physiological conditions. The protein repellency properties of these coatings are evaluated. At the same time, no SNAP degradation was observed during coating or UV irradiation, and the release profile remained above the physiological level for 2 weeks with the zwitterionic top-coat. Moreover, enhanced antimicrobial activity was demonstrated with bacteria testing.

Experiment Section

Materials

4-vinylbenzophenone (BP) was synthesized according to a previously reported method.[30] 2-Methacryloyloxyethyl phosphorylcholine (MPC), albumin from bovine serum (BSA), fluorescein isothiocyanate labeled bovine serum albumin (FTIC-BSA), *N*-acetyl-*D*-penicillamine (NAP), sodium nitrite ($NaNO_2$), concentrated sulfuric acid (conc. H_2SO_4), tetrahydrofuran (THF), sodium phosphate monobasic (NaH_2PO_4), sodium phosphate dibasic (Na_2HPO_4), potassium chloride, sodium chloride, and ethylenediamine tetraacetic acid (EDTA) were purchased from Sigma Aldrich (St. Louis, MO). 2,2'-azobis(2-methylpropionitrile) (AIBN) and n-butyl methacrylate (BMA) were bought from Alfa-Aesar (Haverhill, MA). Isobutyltrichlorosilane was purchased from Tokyo Chemical Industry (Portland, OR). Concentrated hydrochloric acid (conc. HCl), sodium hydroxide (NaOH), and methanol were bought from Fisher-Scientific (Hampton, NH). Potassium phosphate monobasic (KH_2PO_4) and lysozyme from egg white were purchased from BDH Chemicals - VWR International (West Chester, PA). CarboSil™ 20 80A UR STPU (referred to as CarboSil hereon) was acquired from DSM Biomedical Inc. (Berkeley, CA). Milli-Q filter was used to obtain de-ionized(DI) water for all the aqueous solution preparations. Nitrogen and oxygen gas cylinders were purchased from Airgas (Kennesaw, GA). *Staphylococcus aureus* (ATCC 6538, *S. aureus*) was used for the bacterial experiments. LB Agar (LA), Miller and Luria broth (LB), Lennox were purchased from Fischer BioReagents (Fair Lawn, NJ). All the chemicals were used without further purification.

In brief, CarboSil polymers with 10 wt % SNAP (test samples) and no SNAP content (control samples) were prepared using solvent evaporation and/or spin coating method. These samples were then coated with a zwitterionic copolymer (referred to as BPMPC) which was

covalently bonded to the CarboSil base polymers by UV-crosslinking. Surface analysis was performed on the films pre- and post- UV radiation to understand the crosslinking behavior of the polyzwitterionic system. Test and control samples with the BPMPC coating were analyzed for their NO release behavior. The samples were then tested for protein adhesion for 14 days in physiological conditions (37°C in PBS) to evaluate antifouling properties of the topcoat. Finally, antimicrobial assay of the samples was done using a modified version of ASTM E2180 protocol.

Synthesis of NO donor, SNAP

S-nitroso-*N*-acetylpenicillamine was synthesized using a revised approach for a method previously reported.[38] 1M H_2SO_4 and 1M HCl were mixed with an equimolar amount of NAP, methanol and $NaNO_2$ aqueous solution. This reaction mixture was stirred for 20 minutes and then cooled for 7 hours with a constant flow of air on the mixture. After evaporation of the unreacted portion of the reaction mixture, precipitated green crystals of SNAP were filtered, collected and dried in a covered vacuum desiccator. Dried crystals of SNAP were used for all experiments.

Synthesis of CarboSil Films Doped with SNAP

CarboSil films containing 10 wt % SNAP were prepared using solvent evaporation method. 700 mg of CarboSil was dissolved in 10 mL of THF to make the polymer solutions. 77 mg of SNAP was added to this solution for a final concentration of 10 wt % of SNAP. This polymer-SNAP blend was stirred in dark conditions until the SNAP crystals dissolved completely. The blend was then transferred into Teflon molds and allowed to let the solvent evaporate overnight in fume hood. The overnight dried films were then cut into circular shapes of 0.8 cm diameter each. Each sample was immersed into a CarboSil solution without SNAP (40 mg mL^{-1} of polymer concentration in THF) to coat it (this was repeated thrice for each sample).

The samples were dried overnight and then dried under vacuum for an additional 24 hours. This added drying time was included to eliminate any remaining THF which can affect any following studies. Weight of each film was recorded before the topcoat application for all SNAP leaching behavior tests. The formulated samples were stored in the freezer (-18°C) in the dark between experiments to prevent escape of SNAP or consequent loss of NO. These SNAP-incorporated films were used for NO release, SNAP leaching and bacterial cell viability analyses. All samples used for the tests were less than a week old to ensure integrity of studies.

Synthesis of Zwitterionic Copolymer (BPMPC)

The polymer was synthesized by free radical polymerization. MPC (0.546 g, 1.85 mmol), n-BMA (0.105 mL, 0.66 mmol) and BP (0.027 g, 0.132 mmol) were dissolved in 5.3 mL ethanol (total monomer concentration 1.0 mmol mL^{-1}) with initiator AIBN (0.01 mmol mL^{-1}) and the solution was poured into polymerization tube. After degassed with argon for 30 minutes, the polymerization reaction was carried out under nitrogen flow at 60°C for 16 h. The reaction was stopped by exposing the solution to air, cooled to room temperature, and poured into ethyl ether to precipitate the polymer. The white solid was collected by vacuum filtration and dried under vacuum for 12 h. Yield: 0.552 g, 83%. ^{1}H NMR (D_2O) was taken to confirm the polymer composition (Appendix 6).

Crosslinking of BPMPC with Substrates

Silicon substrates were cut into 2.4cm×2.4cm pieces and sonicated with deionized water, isopropanol, and acetone for 5 min each then dried under nitrogen, followed by plasma (Harrick Plasma PDC-32G) clean and treated with iBTS in toluene overnight before modification with the polymer. CarboSil substrates were coated with polymer without pretreatment.

Two coating method were utilized when applying BPMPC on substrates: spin coating and spray coating. For spin coating, polymer modified film was developed on functionalized silicon substrate by using 0.5 mL BPMPC/ethanol solution (10 mg mL^{-1}) at 1000 rpm for 30 seconds. Spray coating was applied for CarboSil films with and without SNAP. BPMPC/ethanol solution (2 mg mL^{-1}) was sprayed using a spray gun from a distance of 10 cm onto vertically placed substrates to achieve uniform coating upon drying. We used spin coating in the protein adsorption experiments, and spray coating in SNAP/NO release and bacterial experiments, based on method that afforded the smoothest, pin-hole free coating on different forms of substrate. Then the BPMPC substrates were irradiated with UV light (UVP, 254 nm, 6.5 mW cm^{-2}) for 1 min to covalently bond the BPMPC to the surface. The substrates were rinsed with abundant ethanol to remove unattached BPMPC then dried under nitrogen.

Characterization of the polymer coatings

The surface wettability was characterized by measuring the static water contact angle, which obtained from a DSA 100 drop shape analysis system (KRŰSS) with a computer-controlled liquid dispensing system. 1 μL DI water droplets were deposited onto substrate surfaces, and the water contact angles were measured within 10 seconds through the analysis of photographic images. The cross-linking kinetics of BPMPC coating was investigated by a UV-vis spectroscopy (Varian) with 254 nm UV light. The thickness of the spin-coated polymer layer on the silicon substrates and CarboSil substrates were measured by M-2000V Spectroscopic Ellipsometer (J.A. Woollam co., INC.) with a white light source at three incident angles (65°, 70°, and 75°). The thickness of the modified layer was measured and calculated using a Cauchy layer model. Infrared spectroscopy studies of polymer coated films were done using a Thermo-

Nicolet model 6700 spectrometer equipped with a variable angle grazing angle attenuated total reflection (GATR-ATR) accessory (Harrick Scientific).

SNAP Leaching Study and NO-Release Profile

The percentage of SNAP discharged from the samples were quantified by noting the absorbance of the PBS solutions (used to soak the samples) at 340 nm (characteristic absorbance maxima of S-NO group of SNAP). Each sample was weighed before coating with non-SNAP polymer solutions to determine the initial amount of SNAP in each film. The films were then immersed in vials containing PBS (pH 7.4 with 100 µM EDTA to prevent catalysis of NO release by metal ions) and stored at 37°C. A UV-vis spectrophotometer (Thermoscientific Genesys 10S UV-vis) was utilized to quantify the absorbance of the buffer solutions in the required time intervals. The readings were converted to wt% of SNAP in the buffer utilizing the initial amount of SNAP present in each sample. 1 mL aliquots of the PBS solution in which the samples were soaked was used for each sample absorbance measurement to avoid any inconsistent readings and three replicates were utilized for each quantification. The calibration graph with known amounts of SNAP in PBS (with EDTA) was used to interpolate the absorbance quantifications recorded from the study and convert them to concentrations of SNAP in the quantified sample.

SNAP incorporated in the polymers release NO in physiological conditions and this release was measured and recorded in real time for the study using Sievers chemiluminescence NO analyzers® (NOA 280i, GE Analytical, Boulder, CO, USA). The sample holder maintained dark conditions for the samples to prevent catalysis of the NO production by any light source. It was filled with 5 mL of PBS (pH 7.4 with 100µM of EDTA) to soak the samples. EDTA acted as a chelating agent to prevent catalysis of NO production by metal ions in the PBS. This buffer

solution was maintained at 37°C by a temperature-regulated water jacket placed around the sample holder. Once a baseline of NO flux without the sample is established, the sample is then placed in the sample holder. Nitric oxide released by the sample in the sample holder was pushed and purged towards the analyzer by a continuous supply of nitrogen gas maintained at a constant flowrate of 200 mL min^{-1} through the sweep and bubble flows. The NO released by the sample is pushed towards the chemiluminescence detection chamber where the reactions shown on Appendix 7 take place.

The voltage signal produced is converted to concentration of NO and displayed on the analyzer's screen. Using the raw data in ppb form and NOA constant (mol ppb^{-1} s^{-1}), the data in ppb is normalized for surface area of the sample and converted to NO flux units (x 10^{-10} mol cm^{-2} min^{-1}). Data was collected in the time intervals mentioned and samples were stored in a PBS (with EDTA) solution at 37°C in dark conditions between measurements. The PBS was replaced daily to avoid any accumulation of SNAP leached or NO released during the storage time. The instrument operating parameters were a cell pressure of 7.4 Torr, a supply pressure of 6.1 psig and a temperature of −12°C. Three replicates were used for each measurement.

Protein Adhesion Assay

Protein adsorption test is a significant important method for evaluating the blood adhesion. Therefore, the thickness change of substrates before and after incubation in protein solutions was monitored, as an indication of protein adsorption. Coated substrates were incubated in fibrinogen (1 mg mL^{-1}) and lysozyme (1 mg mL^{-1}) in PBS (pH 7.4, 0.01 M) solutions up to 14 days, followed by thickness measurement every day.

In the second approach, fluorescein isothiocyanate-bovine serum albumin (FITC-BSA, 2 mg mL^{-1}) in PBS solution was used to evaluate the protein adsorption behavior on the surface of

CarboSil substrate modified by BPMPC.[42, 43] Substrates were immersed in FITC-BSA solution for one and half hour at 37℃, then rinsed with distilled water and dried with nitrogen. The substrates with protein then analyzed by Nikon Eclipse NI-U fluorescence microscope (Nikon Instruments, Inc.), using a 5x objective lens, with filter set (Ex/Em 470/525nm). To confirm the long-term resistance to protein adsorption, the substrates were incubated in BSA (1 mg ml^{-1}) PBS solution for up to 7 days at 37℃ before putting in FITC-BSA solution.

Bacterial Assay

Bacterial adhesion for each of the samples was calculated in terms of the bacterial cell viability using serial dilution after an incubation period of 24 hours. The method used to perform this assay was based on a modified version of the American Society for Testing and Materials E2180 protocol. *S. aureus* was used for antimicrobial evaluation of the samples. Bacteria were cultured in LB Broth (Lennox) at 37°C and grown to ~10^6 colony-forming units (CFU) per mL as measured by optical density. The resulting overnight culture was collected by centrifugation (2500 g, 7 min) and resuspended in PBS. This resuspended bacterial suspension was used for incubation of polymer samples for 24 hours.

After incubation with the bacterial solution, samples were washed gently with PBS to remove any unbound bacteria. The samples were then placed in 1 mL of PBS and homogenized for 1 minute each to transfer any adhered bacteria to this new PBS solution. After homogenization, homogenate samples were serially diluted and plated onto LB Agar nutrient plates (37°C). Bacterial viability was determined by counting the colonies on each plate manually. Calculation of bacterial adhesion was done by counting number of colonies per cm^2 of each sample.

Statistical Analysis

All data are quantified as mean ± standard deviation with an $n \geq 3$ for all trials. The results between the control and test films were analyzed by a comparison of means using student's *t*-test. Values of p were obtained for the data analyzed and $p<0.05$ was considered significant.

Results and Discussion

The zwitterionic polymer (BPMPC) was synthesized by radical polymerization in ethanol (Figure 6.1). The copolymer composition was confirmed by ^{1}H NMR spectroscopy and consisted of 74:18:8 (MPC:nBMA:BP), which roughly matched the monomer feed ratio. This ratio provided the optimal anti-fouling result (discussed below) along with the most uniform coating on both hydrophobic and hydrophilic substrates. The polymer synthesis is simple and straightforward, no further purification is required besides precipitation, which makes large-scale production feasible. BPMPC is a hydrophilic polymer due to the high concentration of MPC and has a high solubility in aqueous and alcohol solutions. The butyl methacrylate component in the terpolymer aids in uniformity and substrate wetting (both hydrophobic and hydrophilic), along with providing additional photochemical cross-linking sites. As described above, the benzophenone component of BPMPC acts as a cross-linker between the hydrophilic polymer and any organic substrate through C-H activation.

The cross-linking kinetics of BPMPC was investigated by UV-vis spectroscopy on isobutyltrichlorosilane (iBTS) functionalized quartz substrates. The polymer solution (10 µL, 10 mg mL^{-1}) was drop cast on alkylated quartz and the solvent allowed to evaporate. The UV crosslinking reaction was monitored by UV-vis, where the decreasing absorbance of the BP group at 255 nm occurs with increased irradiation time. Figure 6.2 shows the UV-vis spectra,

where the absorbance maxima at 255 nm decreased dramatically from 0 to 120 s, and after 240 s, no further absorbance change was observed, even after prolonged irradiation. This result demonstrates that BPMPC crosslinking occurs with rapid kinetics, and only a few seconds are needed to covalently bond BPMPC to a variety of different substrates.

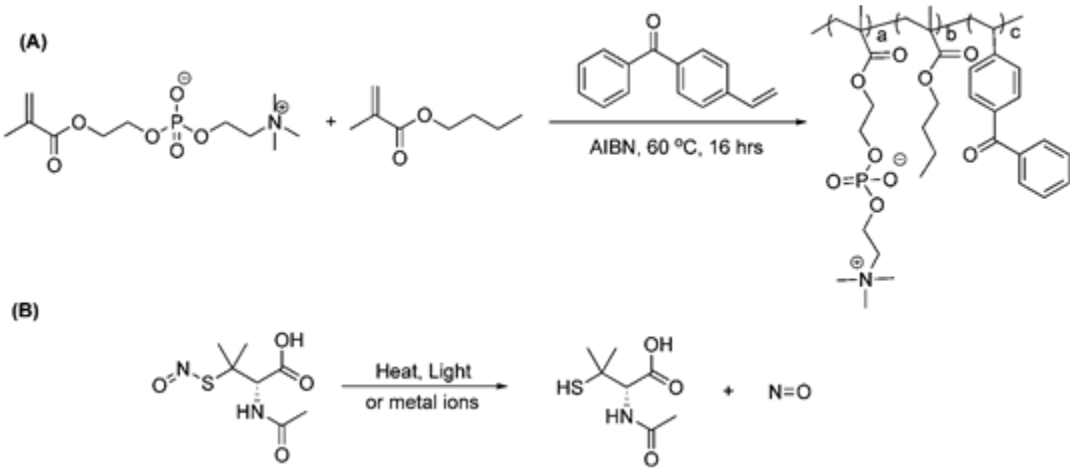

Figure 6.1: (**A)** Synthesis of the BPMPC copolymer. (**B)** Chemical structure of SNAP and NO decomposition along with innocuous N-acetylpenicillamine byproduct.

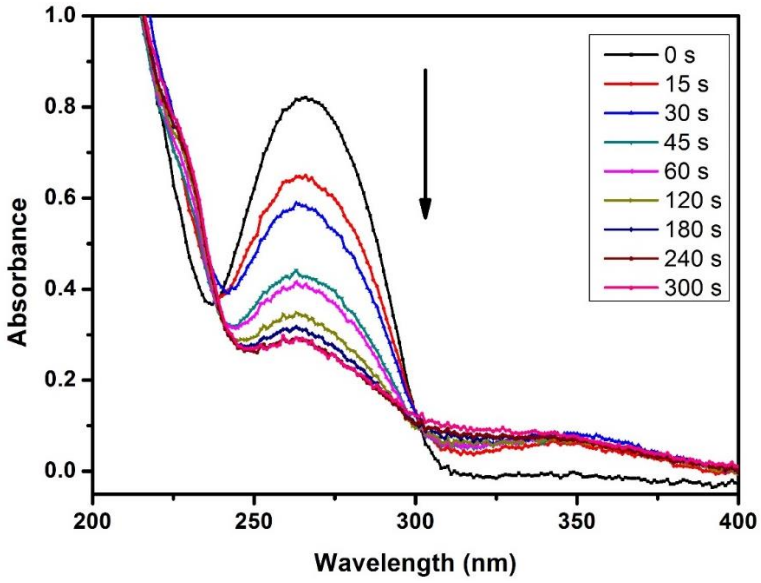

Figure 6.2: UV-vis absorption spectrum of BPMPC drop-cast onto a quartz substrate as a function of photochemical irradiation time at 254 nm (6.5 mW cm^{-2} intensity).

To further confirm the deposition and cross-linking of the BPMPC polymer, FTIR was conducted on coated substrates. In the IR spectra (Appendix 8), absorption peaks of the carbonyl (1720 cm^{-1}) and PC groups (1240, 1080, and 970 cm^{-1}) were observed and assigned to the MPC units. The peak at (1650 cm^{-1}) represents the C=O stretch of BP ketone. A significant reduction of this peak after irradiation further supports the formation of a network polymer of covalent linkage between BP and substrate.

To test the stability and durability of the coating, we monitored the water contact angle of the BPMPC coated silicon samples up to 14 days. The coated substrates were immersed in PBS solution and stirred in an incubator at 37°C, subsequently rinsed with H_2O and dried with nitrogen before measuring the water contact angle (Figure 6.3). The initial static contact angle for the bare CarboSil substrate is about 110°. A significant decrease in contact angle was observed after coating with BPMPC, from 110° to 50°, and this value of contact angle was maintained over a period of 14 days immersed in an agitated PBS solution, which suggests the BPMPC coating was covalent bonded to the substrates and does not delaminate under physiological conditions.

The control samples used to test NO release behavior were coated only with CarboSil (the same polymer used to incorporate SNAP) while the test samples were coated with CarboSil and BPMPC. The samples were tested in lightly agitated conditions to simulate physiological conditions. The samples were tested for a period of two weeks to demonstrate sustainable release of NO from the combination of hydrophobic and hydrophilic polymers.

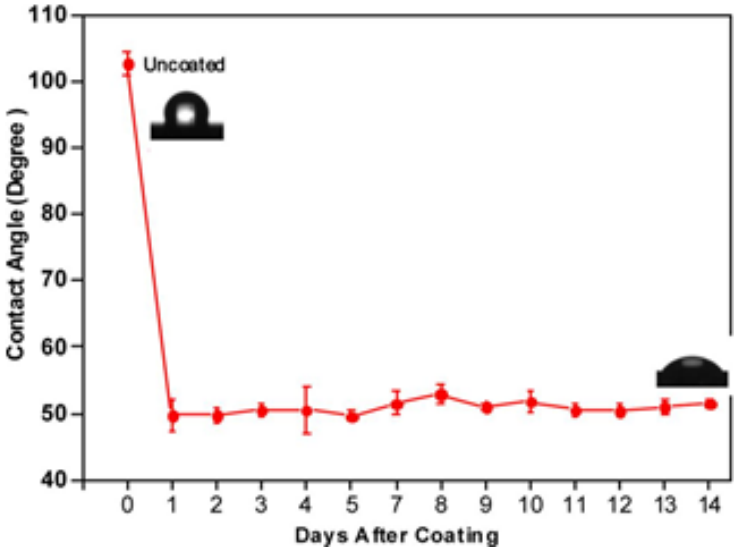

Figure 6.3: Contact angle measurement as a function of time for CarboSil coated with BPMPC and incubated at 37°C in PBS under mild agitation.

A SNAP leaching study was conducted first to measure the retention of SNAP in the control and test polymer films during the study. Measurements were recorded every other day for 2 weeks of soaking in PBS (Figure 6.4 A). A high amount of SNAP retention in the polymers ensures sustained release of NO from the polymer matrix and minimizes the risks (if any) associated with SNAP leaching.[44] As seen in Figure 3A, for the initial measurement (Day 0 on graph of Figure 3A) of leaching after one hour of storage in 37°C in PBS, a loss of 0.39 ± 0.06 % and 0.47 ± 0.26 % was recorded for the control and BPMPC-coated substrate, respectively. This initial higher leaching for the BPMPC-coated substrate is likely due to the hydrophilicity of the surface. However, SNAP leaching is almost identical between the control and test samples as supported by the data from 1 and 3 days of storage in 37°C for BPMPC-coated test films (0.96 ± 0.26 % and 1.44 ± 0.26 % for day 1 and day 3, respectively) and control films (0.96 ± 0.05 % and 1.55 ± 0.07 % for day 1 and day 3, respectively).

This trend of lower leaching of the SNAP molecules from the test films was observed over a 14-day period. It is also to be noted that at no point during the 14-day period were the samples kept at a temperature below 37°C or in dry conditions. This was done to closely simulate physiological conditions for a continuous duration. The leaching for both the control and test samples remained very low (<3.5 %) over the experiment duration but it is worth noting here that despite the expectation that the hydrophilic coating could cause a higher leaching of SNAP molecules from the NO donor containing polymer by attracting water molecules to the polymer surface, this was not the case. This is likely due to the ultrathin nature of the coating, which influences the aqueous interface, but not the bulk of the polymer film.

NO release measurements of the control and test samples were also carried out for a period of 14 days (Figure 6.4 B). Measurements with a Sievers chemiluminescence NO analyzer is the standard characterization methodology accepted for polymers that release NO.[45-47] It measures NO release in real time via the measurement of voltage produced by the photons on the reaction of NO with ozone. In this study, samples were stored at a constant temperature of 37°C and in PBS to simulate physiological conditions.

The results indicated a general trend of higher NO release from the test samples (SNAP-containing material coated with CarboSil and BPMPC) compared to the control samples (SNAP-containing material coated with only CarboSil). Day 0 measurements indicate that the test samples had a flux of 7.75 ± 3.26 (x 10^{-10}) mol cm^{-2} min^{-1} while control samples had 3.76 ± 1.50 (x 10^{-10}) mol cm^{-2} min^{-1} (Table 6.1). This burst of NO release from test samples results from the hydrophilicity of the topcoat which attracts water molecules to the sample surface. Water molecules on the surface can accommodate release of NO as SNAP is more soluble (and prone to S-N=O bond cleavage) in aqueous conditions. After a day of storage, the control samples show a

sharp decrease in NO flux ($0.34 \pm .03 \times 10^{-10}$ mol cm^{-2} min^{-1}). This is seen because of the initial loss in SNAP molecules on day 0 and but inability to maintain a hydrated state for day 1. In contrast, BPMPC-coated substrates show three times the NO flux at $1.02 \pm 0.02 \times 10^{-10}$ mol cm^{-2} min^{-1}. This difference in NO flux can result from the hydrophilic topcoat of test samples that maintains a hydrated surface layer, which facilitates the release of more NO. This trend of higher NO flux from test samples when compared to control samples can be seen through the 14-day study in Table 6.1 and the graph in Figure 6.4 B.

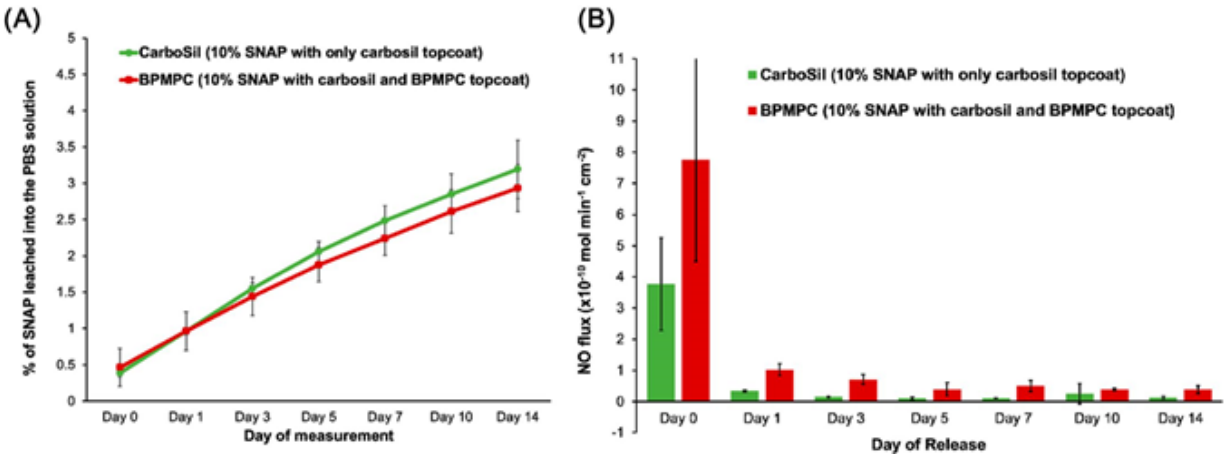

Figure 6.4: (A) SNAP leaching measured using UV-vis over 2 weeks and (B) Nitric oxide release measured over 2 weeks (n = 3) using chemiluminescence.(n=3 for both)

Table 6.1: Comparison of nitric oxide release kinetics between control and coated samples

	10% SNAP with only CarboSil topcoat (NO flux ($x10^{-10}$ mol min^{-1} cm^{-2})	10% SNAP with CarboSil and BPMPC topcoat (NO flux ($x10^{-10}$ mol min^{-1} cm^{-2})
Day 0	3.759 ± 1.491	7.746 ± 3.263
Day 1	0.335 ± 0.032	1.016 ± 0.198

Day 3	0.141 ± 0.023	0.706 ± 0.157
Day 5	0.110 ± 0.045	0.395 ± 0.208
Day 7	0.105 ± 0.008	0.498 ± 0.173
Day 10	0.247 ± 0.324	0.383 ± 0.040
Day 14	0.127 ± 0.035	0.380 ± 0.125

At the end of the 14-day study, test samples (0.38 ± 0.13 (x 10^{-10}) mol cm^{-2} min^{-1}) still release three times the NO flux compared to the control samples (0.13 ± 0.03 (x 10^{-10}) mol cm^{-2} min^{-1}). This propensity of higher release of NO from CarboSil top-coated with BPMPC along with the reduction in leaching of SNAP is very beneficial and combines the material properties of CarboSil (low SNAP leaching) with a higher, sustained release of NO due to the hydrophilic BPMPC topcoat.

As mentioned earlier, the BPMPC coating has excellent hydrophilicity, which helps inhibit the adsorption of proteins from solution. Fibrinogen and lysozyme were used as model proteins to evaluate the antifouling properties of the BPMPC coatings. Fibrinogen is a large (340 kD, pI = 6.0) protein, and a key biomacromolecule in the coagulation cascade that rapidly adsorbs to foreign surfaces and binds to and activates platelets. Lysozyme is a small protein (14 kD, pI = 12) that is positively charged under physiological pH. Figure 6.5 A shows the adsorption thickness increase of Fibrinogen on CarboSil, CarboSil with 10% SNAP, BPMPC coated CarboSil, and BPMPC coated CarboSil with 10% SNAP substrates respectively. On the bare CarboSil films used as a control, the thickness increased about 3 nm after incubation for 24 hours and increased to over 30 nm after 2 weeks. The similar phenomenon was observed for CarboSil with 10% SNAP films, which indicated a high amount of protein adsorption on surface, and protein accumulation over time. On the other hand, for the CarboSil films coated with

BPMPC, the adsorption amount is significantly lower, only a 2 nm increase was observed after incubation for 2 weeks. The large difference in adsorption thickness confirmed that BPMPC coating has an excellent protein resistance property, even after UV activation. As expected, the BPMPC coated CarboSil with 10% SNAP films also shows low adsorption for Fibrinogen. Moreover, similar behavior was observed when films were subjected to lysozyme solution (Figure 6.5 B). The thickness increase in control group was over 14 nm, while the coated group was less than 3 nm. The protein adsorption results indicate that the hydrophilic BPMPC surface layer provides excellent protein-resistant properties.

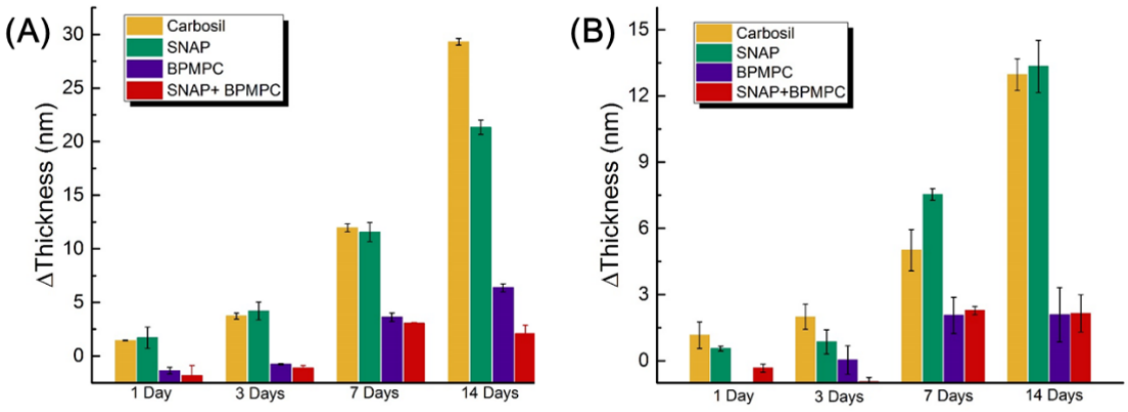

Figure 6.5: Thickness increase after incubation in (A) Fibrinogen solution and (B) in Lysozyme solution.

To further confirm the antifouling effectiveness of the durable BPMPC coating, fluorescence microscopy was utilized to evaluate the protein adsorption on the uncoated and coated CarboSil films using FITC labeled BSA protein. The fouling levels were compared between uncoated and BPMPC coated CarboSil films using the same excitation light intensity and exposure time. Figure 6.6 A indicates protein adsorption on the control samples, and

enhanced fluorescent signal (Figure 6.6 B-C) was observed in the samples pretreated with BSA PBS solution. These results demonstrate that after incubation in protein solution, a large amount of BSA was attached to the CarboSil samples, which facilitate the aggregation of FITC-BSA. On the contrary, protein adhesion to the surface of BPMPC modified samples was not observed (Figure 6.6 D-F), even after incubation in BSA solution for 7 days (Appendix 9). From all these results collectively, the control films demonstrate large amounts of protein adsorption, while the BPMPC coated films display excellent antifouling properties.

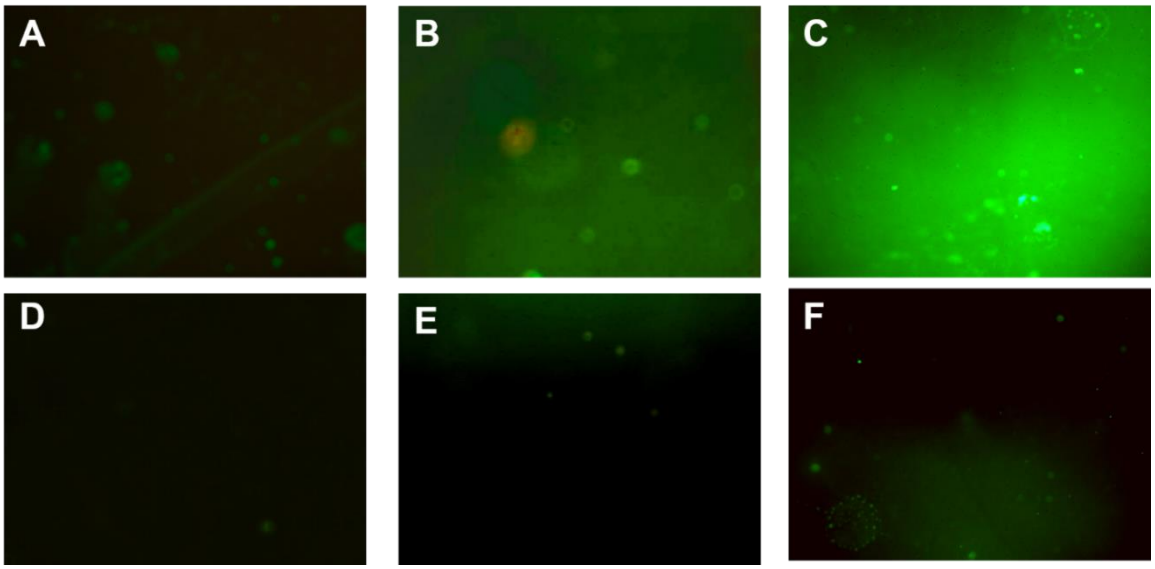

Figure 6.6: Fluorescence micrographs (magnification 10x) of uncoated films after (A) 90-minute incubation, (B) 1 day in BSA PBS solution before incubation, and (C) 7 days in BSA PBS solution before incubation in 2 mg/ml FITC-BSA solution. (D-F) are the coated film measured under the same experimental conditions.

Bacterial adhesion, which often results in biofilm formation, is a prevalent issue in moist and humid environments, including implanted devices. The basic nutrients important for

bacterial growth may be resourced from the device material, bodily proteins that attach post-implantation, or other bodily macromolecular contaminants that adhere to the surface of the device. Antimicrobial efficacy of the designed test samples was compared to the control samples to confirm their superior bactericidal and bacterial repulsion properties.

The samples were soaked in bacterial solutions containing ~10^6 CFU/mL of *S. aureus*. *S. aureus* is a commonly found nosocomial infection bacteria. It has been increasingly linked with healthcare-associated infections in the last two decades.[48] They are most commonly associated with cardiac devices, intravascular catheters and urinary catheters, among other prosthetic devices. This high prevalence of *S. aureus* along with its known affinity to proteins [49, 50] that foul medical devices has made it a very important pathogen used to evaluate the antimicrobial efficacy of medical device materials. For these reasons, bacterial adhesion study of the antifouling-biocide releasing polymer developed was done with *S. aureus*.

As mentioned in the introduction, the NO molecules liberated by the decomposition of SNAP actively kill bacteria while the zwitterion topcoat repels protein adsorption, leading to enhanced antimicrobial efficacy. After 24-hours of incubation, the antimicrobial effect of the test samples was clearly observed. NO releasing polymers with a top-coat of BPMPC showed a bactericidal efficiency of 99.91 ± 0.06 % (~3 log reduction, Figure 6.7) compared to the control samples where a growth of ~10^6 CFU/cm^2 was observed. This reduction is greater compared to films with only a BPMPC topcoat (70.15 ± 14.13 %) and films with only NO-releasing moieties (98.88 ± 0.54 %). It can also be concluded from the results that BPMPC alone only reduces bacteria adhesion. However, because NO is not a contact active antimicrobial but a diffusing biocide, the SNAP-loaded samples also reduce bacterial adhesion significantly.

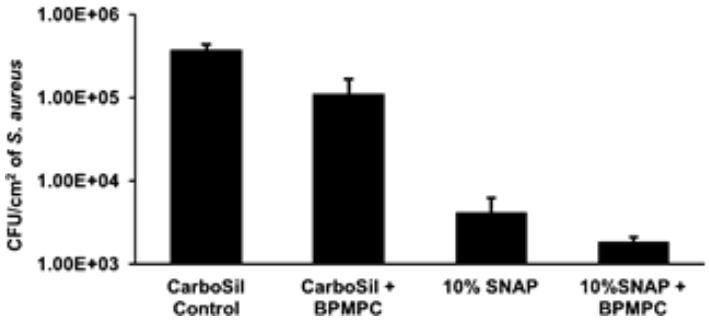

Figure 6.7: Antimicrobial efficacy of NO-releasing BPMPC coated samples relative to controls (n=3).

These results are consistent with the theoretical expectations underlying the surface chemistry of BPMPC and bactericidal properties of NO. In summary, the synergistic effect of the modifiable NO-release kinetics from CarboSil's surface and prevention of protein and/or bacterial adhesion due to BPMPC's surface chemistry will significantly reduce undesired clinical consequences for implanted medical devices.

Conclusions

In conclusion, we have demonstrated a combination of NO release and BPMPC can produce a material with antimicrobial ability and excellent antifouling properties. The formation of the covalent polymer network is rapid (less than 1 min) under mild UV conditions, and can be applied to various substrates, from hydrophilic to hydrophobic. More importantly, even though the BPMPC coating is around 50 nm, it resists moderate abrasion for over a week with retention of its antifouling property. Moreover, the NO release profile indicated a higher NO release form the BPMPC coated sample when compared to the control, with lower leaching of SNAP. The coatings were also challenged with protein adsorption tests for an extended time (up to 2 weeks), where antifouling properties remain. It is noteworthy that, the high killing efficiency of SNAP to

S. aureus is enhanced by BPMPC coating. This one step photochemical attachment process of an antifouling coating to NO-releasing antimicrobial polyurethanes is a simple and scalable process that has application in both medical devices and other and industrial applications where antifouling and antimicrobial properties are desired.

References

1. B. K. Woo Kyung Cho, Insung S. Choi, *Langmuir*, 2007, **23**, 5678.
2. A. T. Nguyen, J. Baggerman, J. M. Paulusse, C. J. van Rijn and H. Zuilhof, *Langmuir*, 2011, **27**, 2587-2594.
3. R. Kenawy el, S. D. Worley and R. Broughton, *Biomacromolecules*, 2007, **8**, 1359-1384.
4. R. Dastjerdi and M. Montazer, *Colloids Surf B Biointerfaces*, 2010, **79**, 5-18.
5. E. M. Hetrick and M. H. Schoenfisch, *Chem Soc Rev*, 2006, **35**, 780-789.
6. J. Yatvin, J. Gao and J. Locklin, *Chem Commun (Camb)*, 2014, **50**, 9433-9442.
7. S. S. Magill, J. R. Edwards, W. Bamberg, Z. G. Beldavs, G. Dumyati, M. A. Kainer, R. Lynfield, M. Maloney, L. McAllister-Hollod, J. Nadle, S. M. Ray, D. L. Thompson, L. E. Wilson, S. K. Fridkin, I. Emerging Infections Program Healthcare-Associated and T. Antimicrobial Use Prevalence Survey, *N Engl J Med*, 2014, **370**, 1198-1208.
8. S. Lowe, N. M. O'Brien-Simpson and L. A. Connal, *Polym. Chem.*, 2015, **6**, 198-212.
9. S. Jiang and Z. Cao, *Adv Mater*, 2010, **22**, 920-932.
10. W. G. Wayne R. Gombotx, Thomas A. Horbett, Allan S. Hoffman, *J. Biomed. Mater. Res.*, 1991, **25**, 1547-1562.
11. Q. Shao and S. Jiang, *Adv Mater*, 2015, **27**, 15-26.
12. Z. Zhang, T. Chao, S. F. Chen and S. Y. Jiang, *Langmuir*, 2006, **22**, 10072-10077.
13. A. Hucknall, S. Rangarajan and A. Chilkoti, *Advanced Materials*, 2009, **21**, 2441-2446.

14. J. Ladd, Z. Zhang, S. Chen, J. C. Hower and S. Jiang, *Biomacromolecules*, 2008, **9**, 1357-1361.

15. R. E. Holmlin, X. X. Chen, R. G. Chapman, S. Takayama and G. M. Whitesides, *Langmuir*, 2001, **17**, 2841-2850.

16. Y. He, J. Hower, S. F. Chen, M. T. Bernards, Y. Chang and S. Y. Jiang, *Langmuir*, 2008, **24**, 10358-10364.

17. P. Singha, J. Locklin and H. Handa, *Acta Biomaterialia*, 2017, **50**, 20-40.

18. P. F. Ren, H. C. Yang, H. Q. Liang, X. L. Xu, L. S. Wan and Z. K. Xu, *Langmuir*, 2015, **31**, 5851-5858.

19. N. J. Turro, *Modern Molecular Photochemistry*, Benjamin/Cummings Pub Co., Menlo Park, CA, 1978.

20. A. A. Lin, V. R. Sastri, G. Tesoro, A. Reiser and R. Eachus, *Macromolecules*, 1988, **21**, 1165-1169.

21. M.-K. Park, S. Deng and R. C. Advincula, *Journal of the American Chemical Society*, 2004, **126**, 13723-13731.

22. H. Higuchi, T. Yamashita, K. Horie and I. Mita, *Chemistry of Materials*, 1991, **3**, 188-194.

23. C. Braeuchle, D. M. Burland and G. C. Bjorklund, *The Journal of Physical Chemistry*, 1981, **85**, 123-127.

24. X. Lin, K. Fukazawa and K. Ishihara, *ACS Appl Mater Interfaces*, 2015, **7**, 17489-17498.

25. J. D. J. S. Samuel, T. Brenner, O. Prucker, M. Grumann, J. Ducree, R. Zengerle and J. Rühe, *Macromolecular Chemistry and Physics*, 2010, **211**, 195-203.

26. S. Hu, X. Ren, M. Bachman, C. E. Sims, G. P. Li and N. L. Allbritton, *Analytical Chemistry*, 2004, **76**, 1865-1870.

27. A. Virkar, M.-M. Ling, J. Locklin and Z. Bao, *Synthetic Metals*, 2008, **158**, 958-963.

28. C. Bunte, O. Prucker, T. Konig and J. Ruhe, *Langmuir*, 2010, **26**, 6019-6027.

29. C. Bunte and J. Ruhe, *Macromol Rapid Comm*, 2009, **30**, 1817-1822.

30. J. Gao, A. Martin, J. Yatvin, E. White and J. Locklin, *J. Mater. Chem. A*, 2016, **4**, 11719-11728.

31. K. Abu-Rabeah, D. Atias, S. Herrmann, J. Frenkel, D. Tavor, S. Cosnier and R. S. Marks, *Langmuir*, 2009, **25**, 10384-10389.

32. T. Brandstetter, S. Bohmer, O. Prucker, E. Bisse, A. zur Hausen, J. Alt-Morbe and J. Ruhe, *J Virol Methods*, 2010, **163**, 40-48.

33. E. J. Brisbois, J. Bayliss, J. Wu, T. C. Major, C. Xi, S. C. Wang, R. H. Bartlett, H. Handa and M. E. Meyerhoff, *Acta biomaterialia*, 2014, **10**, 4136-4142.

34. A. Pegalajar-Jurado, K. A. Wold, J. M. Joslin, B. H. Neufeld, K. A. Arabea, L. A. Suazo, S. L. McDaniel, R. A. Bowen and M. M. Reynolds, *Journal of Controlled Release*, 2015, **217**, 228-234.

35. C. J. Backlund, B. V. Worley and M. H. Schoenfisch, *Acta biomaterialia*, 2016, **29**, 198-205.

36. F. C. Fang, *Nitric oxide : biology and chemistry / official journal of the Nitric Oxide Society*, 2012, **27, Supplement**, S10.

37. P. G. Wang, M. Xian, X. Tang, X. Wu, Z. Wen, T. Cai and A. J. Janczuk, *Chemical Reviews*, 2002, **102**, 1091-1134.

38. E. J. Brisbois, H. Handa, T. C. Major, R. H. Bartlett and M. E. Meyerhoff, *Biomaterials*, 2013, **34**, 6957-6966.

39. K. A. Broniowska and N. Hogg, *Antioxidants & Redox Signaling*, 2012, **17**, 969-980.

40. P. Singha, J. Pant, M. J. Goudie, C. D. Workman and H. Handa, *Biomaterials Science*, 2017, DOI: 10.1039/C6BM00948D.

41. E. J. Brisbois, R. P. Davis, A. M. Jones, T. C. Major, R. H. Bartlett, M. E. Meyerhoff and H. Handa, *J Mater Chem B Mater Biol Med*, 2015, **3**, 1639-1645.

42. H. S. Sundaram, X. Han, A. K. Nowinski, J. R. Ella-Menye, C. Wimbish, P. Marek, K. Senecal and S. Jiang, *ACS Appl Mater Interfaces*, 2014, **6**, 6664-6671.

43. C. Diaz Blanco, A. Ortner, R. Dimitrov, A. Navarro, E. Mendoza and T. Tzanov, *ACS Appl Mater Interfaces*, 2014, **6**, 11385-11393.

44. R. Scatena, P. Bottoni, A. Pontoglio and B. Giardina, *Curr Med Chem*, 2010, **17**, 61-73.

45. Y. Wo, Z. Li, E. J. Brisbois, A. Colletta, J. Wu, T. C. Major, C. Xi, R. H. Bartlett, A. J. Matzger and M. E. Meyerhoff, *ACS Applied Materials & Interfaces*, 2015, **7**, 22218-22227.

46. J. M. Joslin, S. M. Lantvit and M. M. Reynolds, *ACS Applied Materials & Interfaces*, 2013, **5**, 9285-9294.

47. B. J. Privett, A. D. Broadnax, S. J. Bauman, D. A. Riccio and M. H. Schoenfisch, *Nitric oxide : biology and chemistry / official journal of the Nitric Oxide Society*, 2012, **26**, 169-173.

48. S. Y. Tong, J. S. Davis, E. Eichenberger, T. L. Holland and V. G. Fowler, *Clinical microbiology reviews*, 2015, **28**, 603-661.

49. D. Ní Eidhin, S. Perkins, P. Francois, P. Vaudaux, M. Höök and T. J. Foster, *Molecular Microbiology*, 1998, **30**, 245-257.

50. T. Boland, R. A. Latour and F. J. Stutzenberger, in *Handbook of Bacterial Adhesion*, Springer, 2000, pp. 29-41.

CHAPTER 7

MULTI-PRONGED APPROACH TO COMBAT CATHETER-ASSOCIATED INFECTIONS AND THROMBOSIS BY COMBINING NITRIC OXIDE AND A POLYZWITTERION: A 7-DAY *IN VIVO* STUDY IN A RABBIT MODEL[7]

[7] Singha, P., Goudie, M.J., Liu, Q., Hopkins, S.P., Brown, N.E., Schmiedt, C.W., Locklin, J., Handa, H. To be submitted to *Advanced Healthcare Materials*

Abstract

The development of non-fouling and antimicrobial materials have shown great promise for reducing thrombosis and infection associated with medical devices with aims of improving device safety and decreasing the frequency of antibiotic administration. Here, the design of a antimicrobial, anti-inflammatory and antithrombotic vascular catheter is assessed *in vivo* over 7-d in a rabbit model. Antimicrobial and antithrombotic activity is achieved through the integration of a nitric oxide donor, while the non-fouling surface is achieved using a covalently-bound phosphorylcholine-based polyzwitterionic copolymer top coat. Effect of sterilization on the non-fouling nature and nitric oxide release are presented. Catheters significantly reduced viability of *S. aureus* in long term (7 d CDC bioreactor) studies and inflammation in the 7-d rabbit model. Overall, this approach provides a robust method for decreasing thrombosis, inflammation, and infections associated with vascular catheters.

Introduction

Interaction of bodily fluids with implanted devices such as intravascular catheters, urinary catheters, vascular catheters, and extracorporeal life support circuits is a critical process to the success of the devices.[1] This involves favorable and/or inert interactions with blood along with prevention of fouling by biomacromolecules such as proteins and bacteria.[2] Even for short-term catheterization, any unfavorable phenomena such as extraluminal microbial colonization and thrombosis (leading to embolism) can cause a huge increase in healthcare associated costs and fatality within a week.[3] Within seconds of biomaterials coming in contact with tissues, proteins from blood and interstitial fluids adsorb to the surface.[4, 5] Following the adsorption of proteins on the surface, activation of the coagulation cascade, complement system, platelets and immune cells takes place. Adsorption of blood proteins, like fibrinogen, have also been highly linked to an increase in the adhesion of microbes.[6-8] Once the surface of the catheter has been

"fouled", it can lead to various cascading effects like thrombus formation and microbial infection which can ultimately lead to device failure (due to occlusion) and can even result in patient death if not detected early or if the patient has a compromised immune system and/or is undergoing mechanical ventilation.[3] Fouling of central venous catheters can be particularly problematic as even a small number of bacteria infiltrating the vascular system can cause central line-associated bloodstream infections (CLABSIs), the most costly HAI on a per-case basis at about $46,000.[4] Additionally, according to the Centers for Disease Control and Prevention, 30 100 CLABSI cases are reported every year in the intensive care units and acute care facilities of the US. As such, the development of a thromboresistant and antimicrobial catheter coating material is of utmost importance. However, another consideration for the development of a catheter coating materials is to design a material that would form a 'biocompatible system' when placed in the major vein.[9] The term biocompatible has been defined as 'the ability of a material to perform with an appropriate host response in a specific application'. Therefore, in case of central venous catheters, it is important to also characterize the interaction between the coating materials and the endothelium environment.

Several strategies have been introduced in the past decade to reduce protein attachment.[10-15] However, even though much progress has been made in the fields of antifouling surfaces, antithrombogenic and antimicrobial surfaces separately, very few studies have proven to combine all of these three properties to establish an ideal interaction between vascular catheters and the human body's blood vessels.[16] While all of these three properties can be combined to make a material almost biocompatible, a highly efficient biocompatible polymer system would also exude the least inflammatory response from the hosts' cells. This is where most researchers struggle to succeed since achieving some of the other medical device

sustainability goals like antifouling, antithrombogenic, or antimicrobial properties can elicit an immune response. Therefore, a very careful interplay of characteristics is required to achieve a pristine coating that has all the above-mentioned properties.

In this work we have built on our lab's previous work to combine the antifouling, antithrombogenic and antimicrobial properties of a medical grade polymer that has a nitric oxide (NO) releasing donor (*S*-nitroso-N-acetylpenicillamine, SNAP) and a phosphorylcholine-based polyzwitterionic copolymer (2-methacryloyloxyethyl phosphorylcholine-co-butyl methacrylate co-benzophenone, BPMPC) topcoat.[16] It was the first study to be able to design a facile treatment of phosphorylcholine-based polyzwitterion to covalently attach it to any hydrophobic polymer. Superhydrophilic properties of zwitterion materials are a challenge in coating and can involve several difficult steps to achieve covalent attachment. However, we were able to achieve covalent attachment with a simple terpolymer that utilizes the UV-crosslinking properties of a vinyl benzophenone. Zwitterionic polymers having a phosphorylcholine group have been shown to prevent blood cell adhesion even when the polymers contact human whole blood without an anticoagulant.[17] Besides being a potent antimicrobial agent that is physiologically produced by macrophages and the sinus cavities to prevent infection, NO has also been found to reduce inflammatory response by the reduction of inflammatory cell recruitment.[18, 19] In the past it has been found to have sustained effects on reduction of inflammation as NO-release from biomaterials induce the release of more NO from macrophages.[5] Therefore, the two polymers were combined to synergistically act as a biocompatible system. In brief, 10 wt.% of the NO donor (SNAP) was blended within a medical polymer (CarboSil 2080A from DSM Biomedical) and allowed to form disks of films with the solvent evaporation method. Following this, the samples were spray coated with the BPMPC/ethanol solution. Once spray coated and allowed to

dry, the samples were irradiated with UV light (UVP, 254 nm, 6.5 mW cm^{-2}) for 1 min to covalently bond the BPMPC to the NO-releasing polymer. The fabricated samples were able to achieve antifouling (~84-93% reduction for 14 days) and antimicrobial properties (99.91 ± 0.06% reduction in *Staphylococcus aureus* adhesion for 24 hours).

To further advance the studies and design of the biocompatible system, this paper investigates the *in vivo* characteristics of the biocompatible system previously designed and studied for proof-of-concept. Vascular catheters were first fabricated to test for wettability and presence of zwitterion coatings on the catheters, followed by NO-release measurements over a 7-d period. The catheters were then tested *in vitro* for their antimicrobial efficacy against *S. aureus*. To demonstrate the catheter's robustness in retaining its properties after sterilization, contact angle and NO-release measurements were done pre- and post- hydrogen peroxide vapor sterilization. Finally, sterilized catheters were implanted into rabbits for 7 d and evaluated for clot formation and inflammation. The rigorous tests performed through the study were able to confirm the Z-NO material's superior quality in retaining its antimicrobial and hemocompatibility properties for the preservation of the biocompatible system.

Materials and Methods

Materials

4-vinylbenzophenone (BP) was synthesized as previously published.[16] Sodium chloride (NaCl), potassium chloride (KCl), methacryloyloxyethyl phosphorylcholine (MPC), *N*-acetyl-*D*-penicillamine (NAP), ethylenediamine tetraacetic acid (EDTA), sodium phosphate dibasic (Na_2HPO_4), sodium phosphate monobasic (NaH_2PO_4), concentrated sulfuric acid (conc. H_2SO_4), tetrahydrofuran (THF), and sodium nitrite ($NaNO_2$) were purchased from Sigma Aldrich (St. Louis, MO). 2-2'-azobis(2-methyl propionitrile (AIBN) and n-butyl methacrylate (BMA) were bought from Alfa-Aesar (Haverhill, MA). Concentrated hydrochloric acid (conc. HCl), methanol

(CH_3OH) and sodium hydroxide (NaOH) were obtained from Fisher Scientific (Hampton, NH). Potassium phosphate monobasic (KH_2PO_4) was purchased from BDH Chemicals-VWR International (West Chester, PA). CarboSil™ 20 80A UR STPU (referred to as CarboSil hereon) was obtained from DSM Biomedical Inc. (Berkeley, CA). De-ionized water (DI H_2O) was obtained from in-house Milli-Q filtration system. The bacteria strains for the antimicrobial studies were obtained from American Type Culture Collection. Nitrogen and oxygen gas cylinders were from Air gas (Kennesaw, GA).

Synthesis of S-nitroso-N-acetylpenicillamine (SNAP, NO donor)

The NO donor, SNAP, was synthesized using a previously reported method.[20, 21] Briefly, 1M H_2SO_4 and 1M HCl were added to an equimolar solution of NAP dissolved in methanol. This was followed by addition of DI H_2O. The reaction mixture was allowed to cool to room temperature before adding an equimolar concentration of $NaNO_2$. This reaction was allowed to take place for 8 hours in an ice bath. After obtaining the greenish red SNAP crystals through vacuum filtration, the crystals were allowed to dry overnight before storing it in the freezer for further experiments.

Synthesis of 2-methacryloyloxyethyl phosphoryl-choline-co-butyl methacrylate-co-benzophenone (ZI, zwitterionic terpolymer)

The zwitterionic copolymer was synthesized using a previously reported free radical polymerization method.[16] Briefly, MPC (1.85 mmol), *n*-BMA (0.66 mmol), and BP (0.132 mmol) were reacted in the presence of ethanol as the solvent, and AIBN as the initiator (60°C, 16h). Precipitation of the polymer was done by pouring the reaction mixture into ethyl ether at the end of the 16h. The polymer was collected by vacuum filtration. Finally, the polymer (white

solid) was dried under vacuum for 12h. ^{1}H NMR (dH_2O) was done to confirm the copolymer's synthesis.

Fabrication of Catheters

A dip coating method was employed to fabricate catheters: single layered (no NO or ZI), double layered (ZI catheters), trilayered (NO-releasing catheters) (Figure 7.1 a). A more detailed design of the Z-NO catheter is given in Figure 7.1 b. In this method, solutions with the following polymer concentrations were first made: 10 mg ml^{-1} of BPMPC in ethanol (zwitterion coat), 40 mg ml^{-1} of CarboSil in THF (CarboSil coat), 10 wt.% SNAP in 70 mg ml^{-1} of CarboSil in THF (SNAP solution). Steel rods (outer dia.=1.6 mm) were used to first dip coat with CarboSil coat solution (5x). The coatings were left to dry for 2-3 hours and then coated with the SNAP solution (15x). This was then coated with another 5x of CarboSil coat after overnight drying. The NO-releasing catheters were then additionally coated with a zwitterion topcoat by spray method. The ZI coated catheters were treated with UV light for 2 mins followed by ethanol wash to remove any uncrosslinked zwitterionic polymer. NO-releasing catheters were stored in dark, dry, low temperature conditions to preserve the NO-donor quantity. For convenience, the samples will be called the following from hereon,

Catheter Tested	Composition
Control	25 coats of CarboSil only
ZI	Only ZI, no SNAP (25 coats of CarboSil, 1 coat of 10% ZI)
NO	only SNAP, no ZI (5 coats of CarboSil, 15 coats of 10 wt.% SNAP, 5 coats of CarboSil)
Z-NO	SNAP and ZI (5 coats of CarboSil, 15 coats of 10 wt.% SNAP, 5 coats of CarboSil, topcoated with 10% BPMPC).

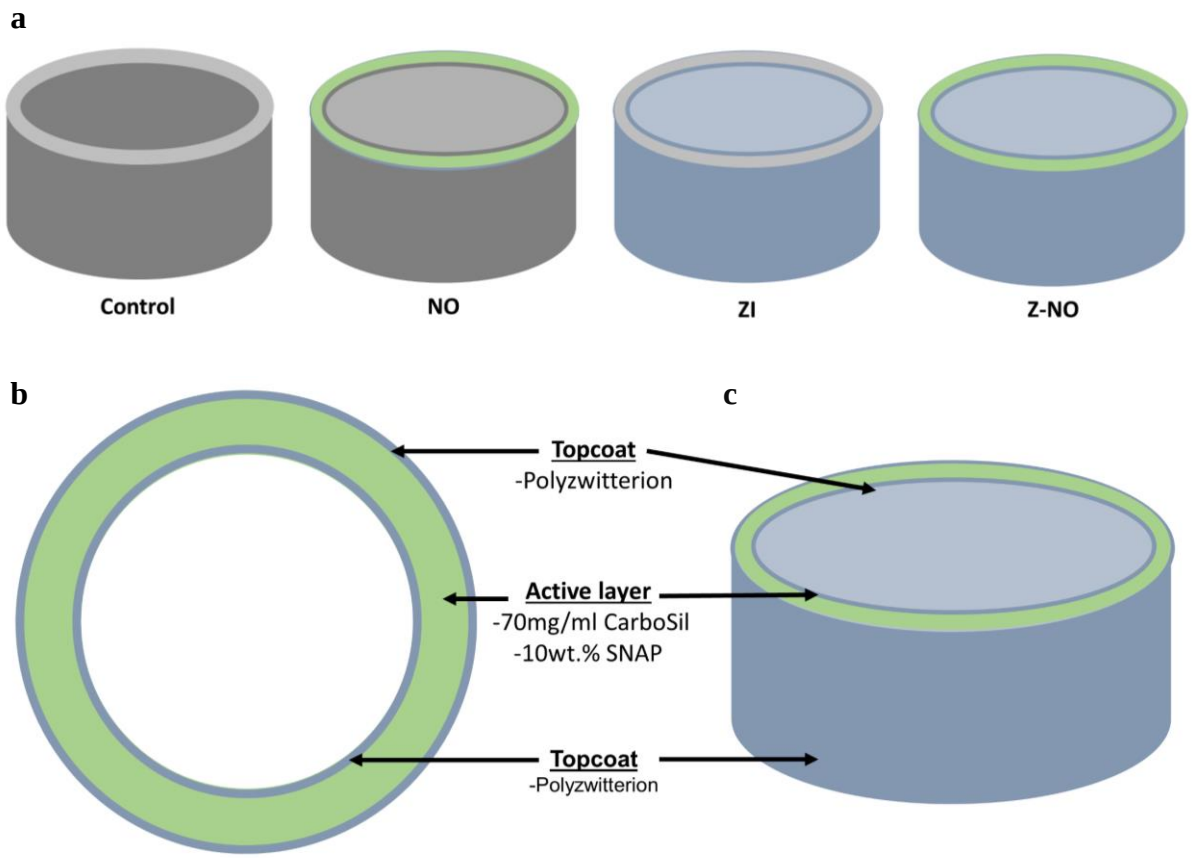

Figure 7.1: Overall design of catheters. a) A representative diagram of the four types of catheters tested in this *in vivo* study. b) Cross-sectional view of Z-NO catheter. c) Isometric view of Z-NO catheter.

Surface Analysis of Catheters

To ensure coverage of the catheters with the BPMPC coat, catheters were cut after coating and static water contact angle measurements were carried out. A DSA 100 drop shape analysis system (Krüss) with a computer controlled dispensing system was used for this purpose. The contact angles were obtained through quick photographic analysis of 1 µl droplets on the substrates.

NO Release Kinetics of Catheters

Once the catheters were fabricated, NO release was measured using a Sievers chemiluminescence nitric oxide analyzer (NOA 280i, GE Analytical, Boulder, CO, USA).[22] It is the gold standard instrument used to measure nitric oxide release with high sensitivity unlike the Griess assay that might falsely detect nitrates and nitrites as nitric oxide release whilst also having the advantage of real-time measurement. All samples were characterized for NO release at 37°C in PBS containing EDTA as the metal ion chelator. Each sample was shielded from light and soaked in 3.5 mL of PBS during the measurement stored in the PBS solution inside a 37°C incubator between measurements. Nitric oxide released by the sample was swept into the analyzer with the help of a constant flow of nitrogen and vacuum supplied by the analyzer. The voltage signal produced was converted to concentration and displayed on the analyzer's screen. Using the raw data in ppb form and NOA constant (mol ppb^{-1} s^{-1}), the data in ppb was normalized and converted to NO flux units ($\times 10^{-10}$ mol cm^{-2} min^{-1}) according to the surface area of the sample used for analysis.

Bacterial Culture and 7-d exposure to Staphylococcus aureus in a "Centers for Disease Control and Prevention" Bioreactor Model

For *in vitro* bacterial adhesion study, a Centers for Disease Control and Prevention (CDC) biofilm bioreactor (model CR 90) from Biosurface Technologies (Bozeman, MT) was used to measure antimicrobial efficacy of the test samples versus control samples over a period of 7 d (Figure 7.2) using a modified version of the ASTM International E2562 – 17 protocol. *S. aureus* was subcultured and grown to a mid-log phase (12-14 hours). This mid-log culture was then centrifuged at 4400 rpm for 7.5 min to extract the bacterial pellet from the growth medium and waste.[20] The bacterial pellet was then suspended in PBS and washed at 4400 rpm for 7 min.

Following this, the optical density of bacterial solution in LB broth was adjusted to 0.1 at 600 nm and used for incubation of the samples in the bioreactor for 2 h. During the 2 h incubation period, the bioreactor was stirred at 100 rpm and not supplied with additional nutrient medium. After 2 h of incubation, nutrient medium (2 g L^{-1} of LB broth) was allowed to flow through the bioreactor at 1.67 ml min^{-1} and the waste allowed to flow into a waste bottle from the outlet of the CDC bioreactor. During the 7-d period of bioreactor study, nutrient was continuously supplied, and waste continuously discharged from the system.

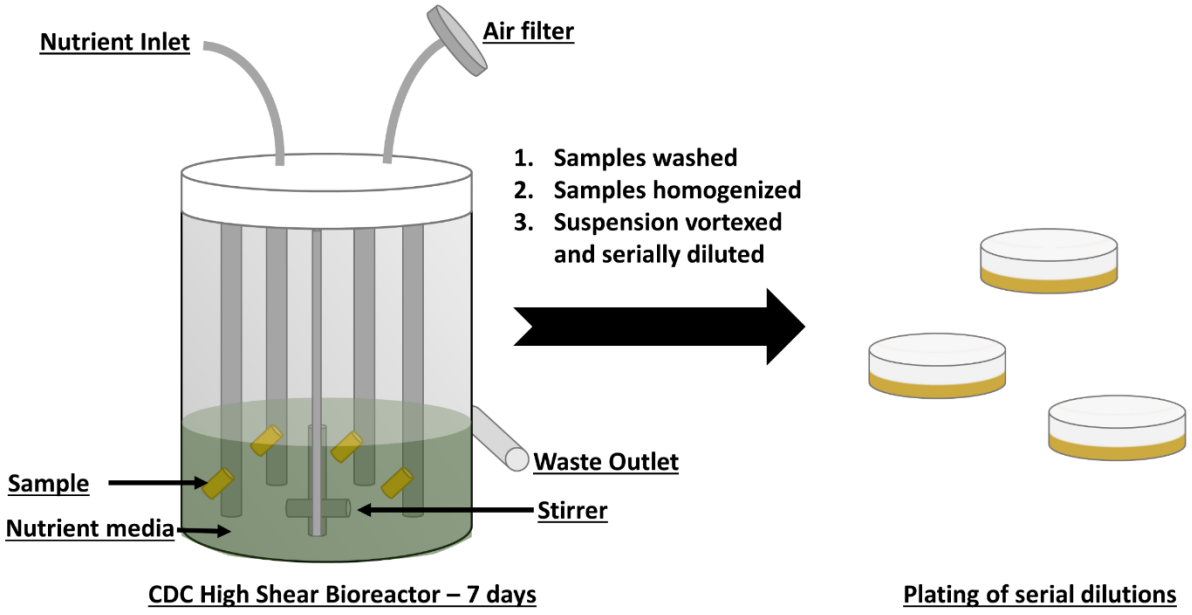

Figure 7.2: A schematic of the 7-d *in vitro* antimicrobial test carried out in a CDC high shear bioreactor.

At the end of the 7-d test period, samples were removed from the bioreactor for colony counting analysis and SEM imaging analysis. For colony counting analysis, samples were gently rinsed with sterile PBS to remove any unattached bacteria and dropped into equal amounts of

PBS. The samples were then homogenized at 25000 rpm to remove the attached bacteria and mix them into the PBS solution. Finally, the solutions were vortexed and serially diluted to be plated on LB agar plates. The colonies were counted post 24 h incubation in 37°C.

The surface characterization of materials after 7-d bioreactor study was performed by a field emission scanning electron microscope (FESEM, FEI Teneo). Before analysis by SEM, materials were washed with PBS to remove any unadhered bacteria. The attached bacteria were then fixed with 3 vol.% glutaraldehyde in PBS, pH 7.4. The fixed samples were dehydrated by gradual water replacement using a series of increasing concentration of ethanol solutions (50%, 60%, 70%,80%, and 90%) in DI water and a final dehydration step with 100% ethanol. The dehydrated materials were then dried using increasing amounts of hexamethyldisilazane and left overnight to dry completely. Once dried, samples were mounted on stubs and gold-palladium coated in vacuum using a sputter coater (Leica sputter coater).

Effect of Hydrogen Peroxide (H_2O_2) Vapor Sterilization

To ensure that H_2O_2 vapor sterilization did not have any significant effects on catheters to be used for *in vivo* study, they were first characterized for their NO-releasing and surface wetting properties pre- and post- sterilization. Sterilization was done using a Sterix VHP MD140X for 28 min, where the chamber is placed under vacuum followed by the injection and vaporization of H_2O_2 to a chamber concentration of 6 mg L^{-1}. Post sterilization, catheters were analyzed for their NO release before and after sterilization. This was done using the chemiluminescence NO analyzer as described previously. Additionally, to ensure the presence of zwitterion coating on the zwitterion and Z-NO samples, static water contact angle was measured before and after sterilization using the drop shape analyzer.

Rabbit Catheter Implantation

All animals were cared for by the standards of the University Committee on Use and Care of Animals (UCUCA) at the University of University of Georgia. The surgical area was sanitized and dedicated to the purpose of performing surgery. All surgical instruments were sterilized using steam sterilization and sterile drapes were used to create a sterile field around the dorsal and ventral sides of rabbit neck. Catheters were sterilized using hydrogen peroxide vapor sterilization at the University of Georgia College of Veterinary Medicine. A total of 16 New Zealand white rabbits (Charles River Laboratories, Wilmington, MA) were used in this study. All rabbits (2.5–3.5 kg) were initially anesthetized with intramuscular injections of 5 mg kg^{-1} xylazine injectable (AnaSed Lloyd Laboratories Shenandoah, Iowa) and 30 mg kg^{-1} ketamine hydrochloride (Hospira, Inc. Lake Forest, IL). Maintenance anesthesia was administered via isoflurane gas inhalation at a rate of 1.5–3% via mechanical ventilation which was done through an A.D.S. 2000 Ventilator (Engler Engineering Corp. Hialeah, FL). Each rabbit's neck region was cleaned with povidone iodine and ethanol prior to incision. Under sterile conditions, a small skin incision (2 cm) was made over the right external jugular vein and the facial vein branch isolated for the catheter insertion. Briefly, the facial vein is ligated proximally and under distal occlusion, a small venotomy is made through which the catheter is introduced into the jugular vein and then advanced into the cranial vena cava (Figure 7.3). About 6 cm of a catheter length is inserted and then fixed to the vein at its entrance by two sterile silk sutures (4-0, Ethicon).[23] By using the facial vein, the external jugular vein blood flow was maintained over the catheter which provided thrombosis assessments. The incision was then closed using uninterrupted stitches (4-0 absorbable suture, Ethicon).

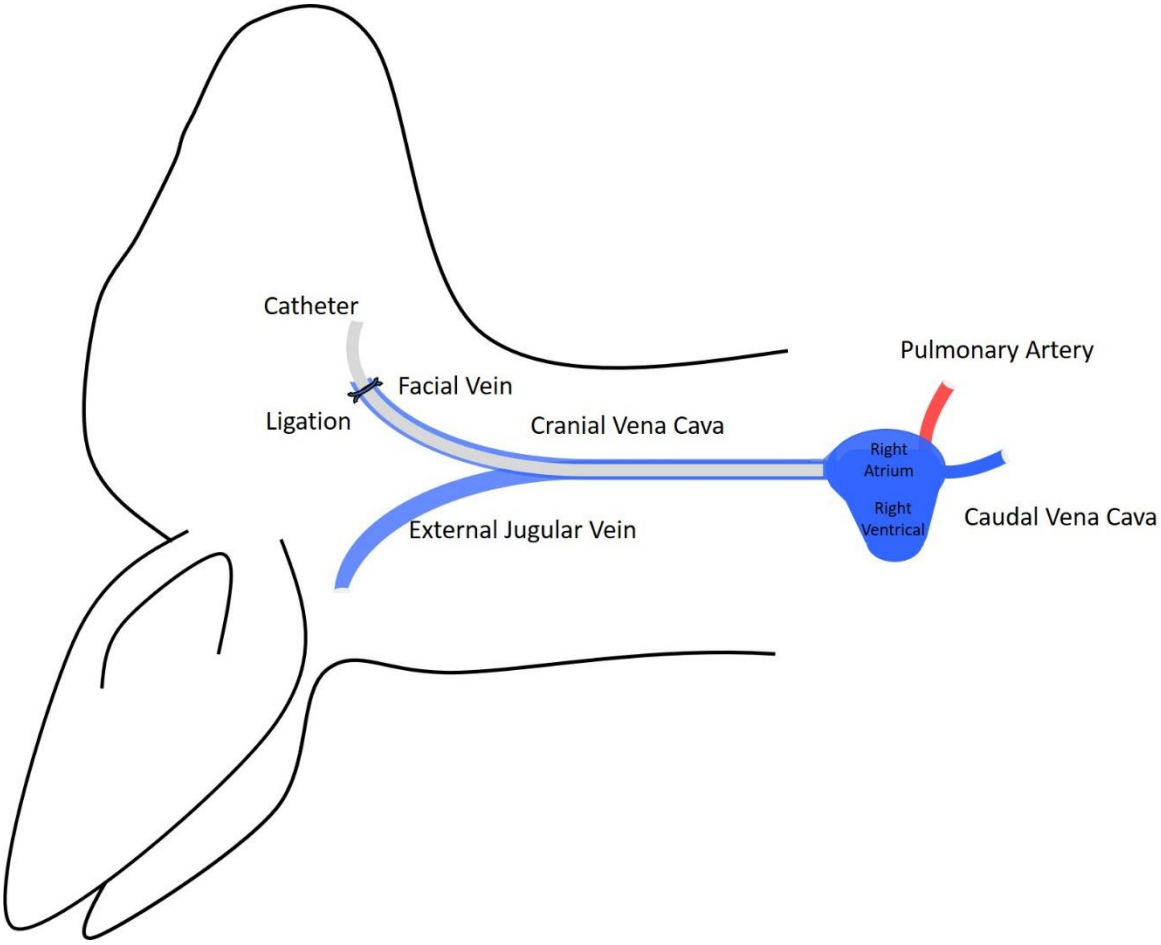

Figure 7.3: A schematic of the *in vivo* rabbit model for 7-day implantation of venous catheter.

Post-operative recovery

After removal from anesthesia, animals were placed in an oxygenated and 37 °C incubator for post-operative recovery. Animals were continuously checked during the 1–2 h recovery period until they were able to maintain sternal recumbency before being transferred to the animal facility. The rabbits that recovered from anesthesia after the catheter placements were housed individually with a respective cage card identifying the animal in the animal facility. Animal health was monitored during routine daily check-ups and weighing, the implanted venous catheters exit site and the skin incision was examined for inflammation (redness). Four

mg kg^{-1} Rimadyl (analgesic) was given for 2 days after surgery and 5 mg kg^{-1} Baytril (antibiotic) was given for 4 days post-surgery. The catheter was flushed with 2 mL of sterile saline every day. After 9 d, rabbits were given 400 IU kg^{-1} sodium heparin just prior to euthanasia to prevent necrotic thrombosis. The animals were euthanized using a dose of Fatal Plus (130 mg kg^{-1} sodium pentobarbital) (Vortech Pharmaceuticals, Dearborn, MI).

Catheter Evaluation and Vein Histological Evaluation

The jugular and facial vein were cut proximal to the catheter, as well as the jugular vein distal to the catheter tip. The vein was then cut longitudinally, and the catheter was carefully removed. Veins were stored immediately in formalin. The left jugular vein (2 cm) was excised to be used as controls for histological imaging. After explanting, the catheters were rinsed in PBS. Pictures were taken of the exterior of the whole catheter. Starting at the distal tip of the catheter, 1 cm sections were cut for SEM, and bacterial adhesion. To quantify the presence of any viable bacteria that might have fouled the surface during surgery, a 1 cm piece was cut longitudinally and placed in PBS buffer. Explanted veins were flushed with PBS and immediately placed in 10% buffered formalin for 48 h. After immersion fixation, veins were rinsed in cold water for 5 min and stored in PBS at 4°C. The fixed veins were then dehydrated in ethanol and cleared in xylenes before finally being cut into 3-4 mm segments, placed within tissue cassettes, and embedded in paraffin wax. The veins were then cut into 10 µm sections and stained with hematoxylin and eosin (H&E) per facility SOPs. Images were taken using an EVOS FL inverted microscope.

Results and Discussion

Surface analysis of catheters

Once the catheters were fabricated, surface analysis was done to confirm the deposition and durability of the ZI coating. The NO releasing polymer, CarboSil, is a hydrophobic polymer

with a contact angle of approx. 100° and hence a drop in the contact angle was expected on the ZI-coated catheters. The wetting properties of the ZI coated catheters were analyzed using a drop shape analyzer which is seen on Figure 7.4. Further characterization of the surfaces and kinetics of the zwitterion's polymerization have been previously demonstrated in a published study by our group.[16] As seen from the wetting characteristics, the ZI was well-coated on the insides and the outsides of the NO-releasing catheters.

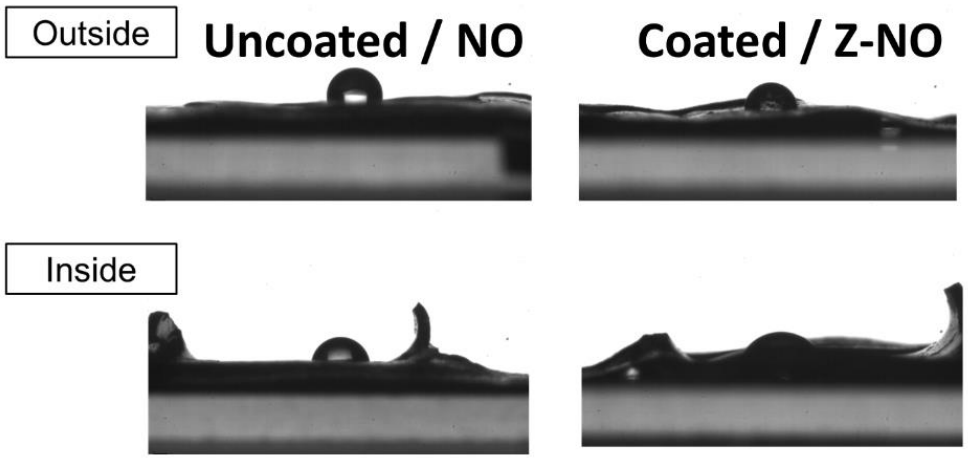

Figure 7.4: Contact angle measured before and after coating with zwitterionic polymer.

In vitro NO-Release Kinetics from catheters

As we have previously stated, one of the desirable properties of the Z-NO materials was to have sustained NO release for the application period of the catheters. This would indicate that the catheters are suitable for antithrombotic and antimicrobial applications. Nitric oxide is released from *S*-nitrosothiols upon exposure to heat, moisture, metal ions (e.g. copper and zinc) or light irradiation (340 and/or 590 nm, S-nitroso adsorption bands).[24-26] For the catheters fabricated in this study, NO release is catalyzed by heat (physiological temperature of 37 °C) and

moisture upon contact with bodily fluids (blood). To minimize burst release of NO, which was seen in our previously published study,[16] the catheters were fabricated via a dip coating method in which several layers of NO-releasing CarboSil were topcoated with five layers of CarboSil and the final topcoat of zwitterion (as shown in Figure 1). This eliminated the possibility of a loss of SNAP, the NO donor. There is also little apprehension regarding the low possibility of leaching of SNAP, NAP (the parent thiol and used to clinically treat heavy metal poisoning), or NAP disulfide from the catheters as none of them would result in any toxicity issues. *S*-nitrosothiols, like SNAP, release NO through their spontaneous decomposition which yields a disulfide (RSSR) product and NO. This NO release from the catheters was measured and monitored using chemiluminescence NO analyzers (NOA, Sievers, Boulder, CO), the gold standard for measuring nitric oxide release, over a period of 7 d. The catheters were incubated in PBS with EDTA at 37°C for the entirety of the study. Unlike the previously published study wherein the samples exhibited a high NO release on the first day because of initial water uptake and leaching of SNAP,[16] no such burst release of NO was observed on these catheters (NO: 1.393 ±.612 and Z-NO: 1.289 ±.625 ($\times 10^{-10}$ mol cm^{-2} min^{-1})). This is desirable as it means that SNAP storage is optimal, and the NO release is gradual and can be expected to remain around physiological levels for a long period of time. However, it is also important to note here that a higher NO release would not be a problem as besides NO's short half-life due to its swift scavenging by hemoglobin, the catheter surface area in blood vessels is significantly lesser than the surface area of blood vessels which are continuously releasing NO at endogenous levels.[1] The results indicated a general trend of comparable NO release from both NO and Z-NO catheters as seen on Figure 7.5. It's also important to note here that despite the presence of a hydrophilic topcoat like zwitterion, NO release was not significantly higher for Z-NO samples.

This demonstrates the robustness of layering NO-releasing polymers to have a gradual NO release instead of burst release. Just as seen on day 1 of the study, day 3, 5, and 7 show comparable NO-release profile from both NO and Z-NO samples (Table 7.1). This trend of comparative NO-release is desirable as it means that even adding a hydrophilic zwitterion topcoat to promote antifouling characteristics does not result in losing the beneficial properties of sustained NO release.

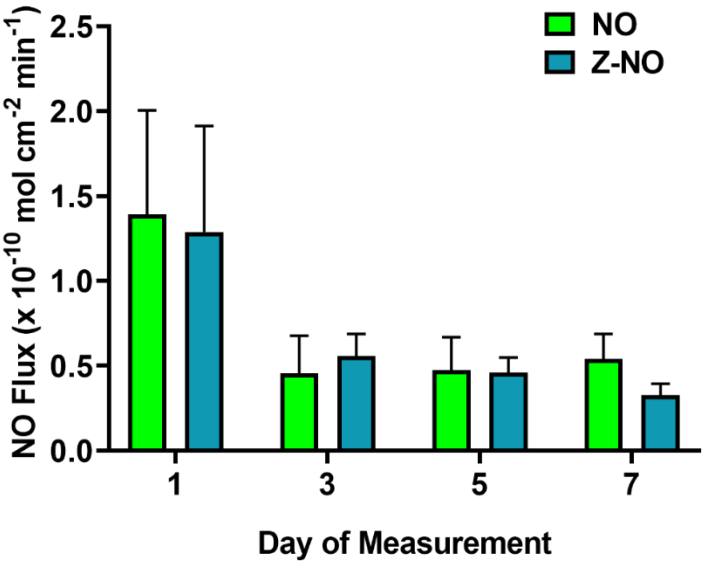

Figure 7.5: NO release kinetics over a 7-day period. (n=3)

Table 7.1: NO-Release Characteristics of materials for a 7-day period (n=3)

Day of Measurement	NO Flux (× 10^{-10} mol cm^{-2} min^{-1})	
	NO	Z-NO
1	1.393 ±.612	1.289 ±.625
3	0.456 ±.221	0.559 ±.129
5	0.476 ±.193	0.462 ±.086
7	0.543 ±.145	0.328 ±.067

Antimicrobial efficacy in a continuous flow "Centers for Disease Control and Prevention" biofilm bioreactor over 7 d

Antimicrobial materials can be developed through passive and active strategies. While a passive method (e.g. PEG, zwitterion) involves the use of strategies that do not release any biocidal agents into the environment, active strategies (e.g. silver nanoparticles, quaternary ammonium ions, nitric oxide) involve the use of agents that actively kill microbes.[27] The Z-NO catheters combine both passive and active strategies through the incorporation of a zwitterion topcoat on a NO-releasing polymer. While the zwitterion topcoat provides protection from the contamination of proteins (as demonstrated in the previous publication), the NO-releasing polymer acts as a biocidal agent releasing polymer that does not have the risk of antibiotic resistance and acts locally. Nitric oxide's antimicrobial mechanisms include lipid oxidation, deamination of DNA, and denaturation of enzymes so the possibility of bacteria developing resistance is minimal.[19] Catheters fabricated via dip coating were tested in a Centers for Disease Control and Prevention (CDC) bioreactor (model CBR 90) over 7 d with *S. aureus* culture (initial inoculum of ~10^8 CFU $mL^{-}1$) to demonstrate their antimicrobial efficacy. *S. aureus* is a Gram-positive bacterium that is a leading pathogen known for causing bacteremia and endocarditis.[28]

Figure 7.6 a represents the surface of the catheter samples after a 7-d exposure to S. aureus in the CDC bioreactor. As expected, a high amount of growth and a well-formed biofilm is seen on the control catheters (A and B). This growth of biofilm is dense and shows a well-connected layer of exopolysaccharide that provides nutrition and protection to the bacterial cells present within the network. In contrast, NO catheters represented on image B and F show little biofilm formation. However, a layer of protein is seen on the catheters as NO cannot prevent the adsorption of protein produced by the bacteria that are able to encounter the surface and use

proteins to attach themselves. The reduction of intact bacteria present on the surface is clearly visible through the SEM images. The ZI catheters represented on image C and G show the structure of the coating on the catheter along with the presence of few bacteria on the surface. The pores seen on the surface could be due to the quick evaporation of the ethanol solvent that is used to coat the zwitterion polymer. The surface of the ZI catheters clearly show a reduction in the protein coverage unlike the NO catheters. Z-NO catheters on the other hand demonstrate both improved surfaces and highest reduction in protein and bacteria attachment (image D and H). A more detailed discussion of the bacterial results will be discussed in the next few paragraphs with the quantitative results.

Figure 7.6 c represents the results from the 7-d antimicrobial study carried out in the continuous flow CDC bioreactor. The continuous flow CDC bioreactor is an ideal design to study vascular catheters materials as the shear rate is high and it provides an ideal platform to continuously supply nutrients and remove waste without exposing the materials to an unsterile environment (as expected in implantation). Several studies have been carried out to monitor biofilm growth and efficacy of antimicrobials with the continuous flow CDC bioreactor.[29-32]

In this study, Z-NO was expected to have a higher reduction of bacteria compared to the other materials (ZI and NO) (Table 7.2). This was due to the additive effects expected from the antifouling nature of the zwitterion topcoat along with the bactericidal effects of NO. As observed, the presence of a zwitterion alone reduces the adhesion of *S. aureus* by 85.039 ±7.375%($p=0.015$) after the 7-d exposure in the bioreactor. This reduction is attributed to the zwitterion's hydrophilic nature which in turn prevents the attachment of proteins and other biomacromolecules produced by bacteria for the formation of biofilms. Thus, the repulsion property of zwitterion itself can provide significant protection from biofilm formation. Similarly,

a reduction of 88.235 ±4.251% (p=0.013) is seen on NO catheters which is attributed to the bactericidal property of NO. As seen from NO release measurements in the range of 0.543-1.393 ($\times 10^{-10}$ mol cm^{-2} min^{-1}) flux, the consistent NO release at physiological levels helps in this reduction. An even more significant reduction is seen with Z-NO catheters. At 97.271 ±1.326%(p=0.009) reduction compared to the control catheters for a 7-d bioreactor, Z-NO catheters establish the additive antimicrobial action of the zwitterion and NO components of the catheters. This is a greater reduction compared to the single modifications on the ZI and NO catheters and hence increases the chances of prevention against microbial infections. It is important to note here that though these are promising results; further studies need to be carried out with longer term *in vitro* and *in vivo* bacterial infection models.

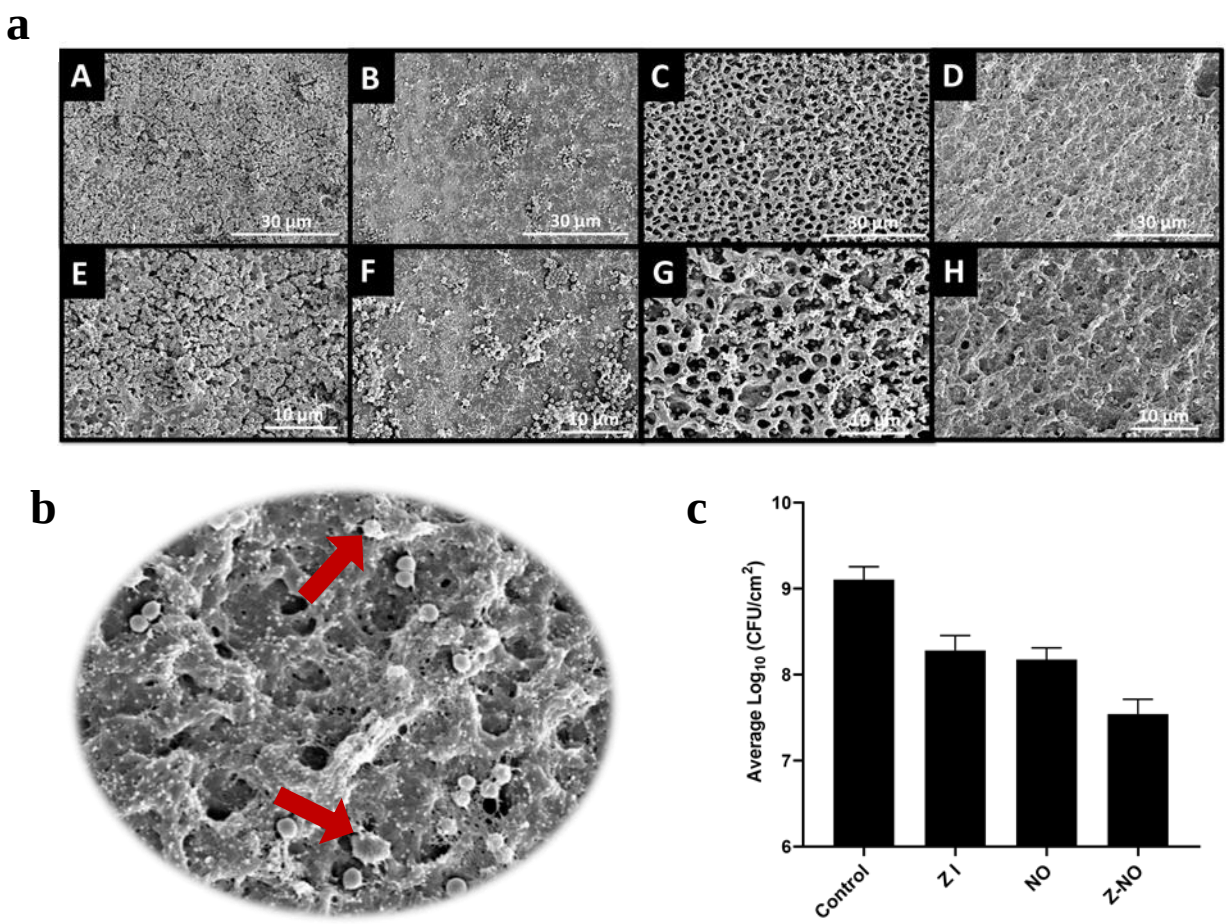

Figure 7.6: Quantitative and qualitative results from 7-day exposure to infection level CFU mL^{-1} of Gram-positive bacteria, *S. aureus*. a) Scanning electron micrographs of materials exposed to *S. aureus* for 7 d. b) Magnified section of SEM image from Figure 6a(H) showing disrupted cells with red arrows c) Log_{10} CFU cm^{-2} counts of bacteria present on each material after 7 d exposure to *S. aureus* in a high shear CDC bioreactor.

Table 7.2: Antimicrobial efficacy comparison between control and Z-NO catheters in a 7-day CDC Bioreactor Model.

	Control	**ZI**	**NO**	**Z-NO**
Avg CFU of *S. aureus* cm^{-2}	1.275×10^9	1.908×10^8	1.500×10^8	3.480×10^7
Reduction % compared to Control		85.039 ±7.375	88.235 ±4.251	97.271 ±1.326
p value vs. Control	-	0.015	0.013	0.009
p value vs Z-NO	0.009	0.031	0.010	-

Effects of hydrogen peroxide vapor sterilization on fabricated materials

Sterilization or biodecontamination is a necessary step required before any medical implants are introduced into living beings for *in vivo* testing. It is also imperative that medical devices withstand sterilization process to be used clinically. The University of Georgia's College of Veterinary Medicine provides the facilities for both sterilization and *in vivo* tests. The sterilization instrument uses low temperature for biodecontamination of temperature sensitive devices and hence is ideal for sterilizing heat-sensitive NO-releasing materials. Another advantage of this sterilization is that it uses hydrogen peroxide in its vapor state and has no condensation of active ingredient onto surfaces, therefore making sure that the only antimicrobial

present post-sterilization is NO itself. Hydrogen peroxide vapor sterilization is slowly replacing ethylene oxide as the main low temperature sterilization technique due to its turnaround time and device compatibility.

The NO flux for pre-sterilized materials was 1.39 and 1.28 ($\times 10^{-10}$ mol cm^{-2} min^{-1}) flux for NO and Z-NO samples, respectively. For post-sterilized materials, the NO flux was 1.65 and 1.01 ($\times 10^{-10}$ mol cm^{-2} min^{-1}) for NO and Z-NO samples, respectively. From NO release analysis of the samples, the NO release for Day 1 is only minutely different for both NO and Z-NO pre- and post-sterilized samples. This is a desirable result since it indicates that the NO donor in the catheter is not affected by the sterilization process and H_2O_2 vapor sterilization is a safe method. It is also an expected result since we know from previous studies that only heat affects the NO content.[22] From Table 7.3, it is seen that contact angle remains the same and does not change pre- and post-sterilization. This demonstrates that the zwitterion coating is not affected by the sterilization method. Hence, both the analyses validate the H_2O_2 vapor sterilization technique as an ideal biodecontamination method for the samples used in this study.

Table 7.3: Pre- and post-sterilization wetting properties of fabricated coatings.

Material	**Pre-sterilization Contact Angle (°)**	**Post-sterilization Contact Angle (°)**
Control	102.83 ±1.70	100.57 ±0.54
ZI	49.75 ±2.36	58.72 ±0.12
NO	97.84 ±2.97	97.23 ±1.28
Z-NO	61.83 ±3.67	61.36 ±0.62

Antithrombogenicity efficacy in an in vivo model over 1 week

Central venous catheters were prepared via dip coating and implanted for 7 d in rabbit cranial vena cava (1 catheter per rabbit) without systemic anticoagulation. After the 7-d period, the catheter and vein were explanted to evaluate the various materials to reduce thrombosis via imaging and scanning electron microscopy (Figure 7.7 a and b). The control CarboSil catheters showed the highest levels of thrombus formation, with large amounts of both fibrin formation and platelet and red blood cell attachment.

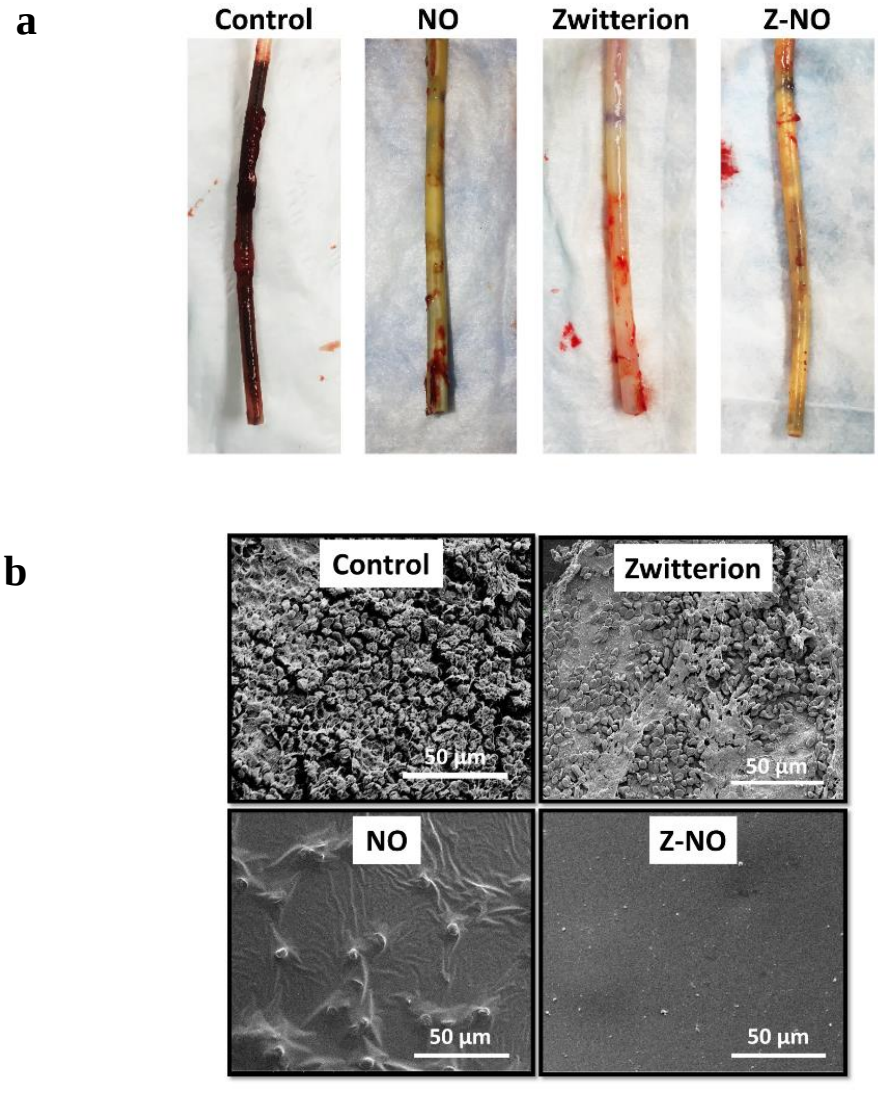

Figure 7.7: Images of catheters post-explantation from 7-day implantation in rabbit model. a) Digital images comparing blood clots on the surface of catheters implanted within the vena cava of rabbits for 7 d. b) Scanning Electron micrograph Imaging of thrombus formation in catheters implanted in in vivo rabbit model for 7 d.

The NO-releasing surfaces showed a dense layer of protein on the surface, with minimal cell adhesion. These results coincide with previous findings of NO releasing materials in central venous catheters after 9 d in a sheep model.[33] While the NO release levels of the previous work are on the higher range of physiological levels, similar reductions in thrombus formation and degree of protein adhesion are observed when compared to the respective controls. While it is estimated the physiological range is between 0.5 - 4 × 10^{-10} mol min^{-1} cm^{-2}, the correlation of NO release levels to the degree of thrombus formation have yet to be determined, including the differences in flow conditions for venous and arterial thrombi.

The zwitterionic coating was also able to significantly reduce thrombus formation when compared to the CarboSil control. However, small localized regions of thrombus formed. This may be the result of the adhesion and activation of platelets on the catheter surface, which then can provide a substrate for fibrinogen adhesion and fibrin formation. This small location can then grow over time despite the non-fouling nature of the material surface.

The combination of the zwitterionic coating along with NO release showed the lowest level of thrombus formation, with minimal protein and cell attachment when viewed on SEM. With there no significant difference in the NO release rates from NO and Z-NO, this demonstrates the importance of both the platelet and protein contributions to thrombus formation. While similar results have been reported on the effect of non-fouling coatings with NO release *in vitro,* this is the first study to investigate their ability to prevent thrombus

formation in a long term *in vivo* application.[34, 35] Overall, the combination of the non-fouling zwitterionic coating coupled with the active release of nitric oxide demonstrate a strong potential for limiting thrombosis associated with central venous catheters for long term applications.

In addition to the surface analysis of the catheters by SEM for the presence of any thrombus formed, the catheters were also tested to check for any bacterial adhesion due to possible contamination via the surgical site. All the catheters were found to have no bacteria growth. This is desirable because it indicates a good sterile environment in which the surgery was performed, and surgical site was maintained with no contamination through the course of the 7-d implantation of the catheters.

Histology Assessment of Foreign body response in an in vivo model over 1 week

Implantation of a CVC can cause a variety of anatomical changes to the venous wall that lead to further complications that can jeopardize the health of the patient. Direct vascular wall damage immediately occurring from the surgical procedure can be unavoidable, often leading to smooth muscle cell (SMC) proliferation. After implantation, any further disturbance to the inner lumen of the vein from the CVC will only accelerate this problem.[36] Blood moving around the catheter also has a high chance of clotting onto the endothelium. There are several types of thrombotic occlusions that occur from implanted CVCs, which originate from the fibrin sheath that initially forms on the catheter surface. The two specific types that typically occur are mural thrombosis, where a blood clot adheres to the catheter and vein wall but does not completely prevent blood flow through the vein, and complete venous thrombosis, where the clot that forms stops all blood flow.[37]

While SMC proliferation is primarily an issue for long term implanted CVCs, early stages of SMC migration to the pericatheter fibrin sheath that forms have been shown to be present within

one week.[38] Explanted veins were stained with H&E to observe the foreign body response to the implanted catheters and are shown in Figure 7.8. Specifically, the formation of mural thrombosis on the vein adjacent to the catheter implantation site was investigated. Catheters without zwitterionic coatings or NO release demonstrated high thrombus formation along with SMC proliferation at the catheter-vein interface. This was anticipated as the previously shown clotting on the surface of the untreated catheters was much more significant compared to ZI or NO functionalized catheters. The combination of ZI-NO showed little clotting as well as a decreased amount of SMC proliferation on the vein endothelium. While the NO was able to inhibit most of the clotting on the catheter surface, it was able to diffuse within the bloodstream and prevent most of the mural thrombosis as well. Since the ZI coating prevents or slows the formation of the fibrin sheath that intensifies the thrombotic complications of CVCs, it was expected that its combination with NO shows even less occurrences of thrombus formation around the adjacent vessel wall.

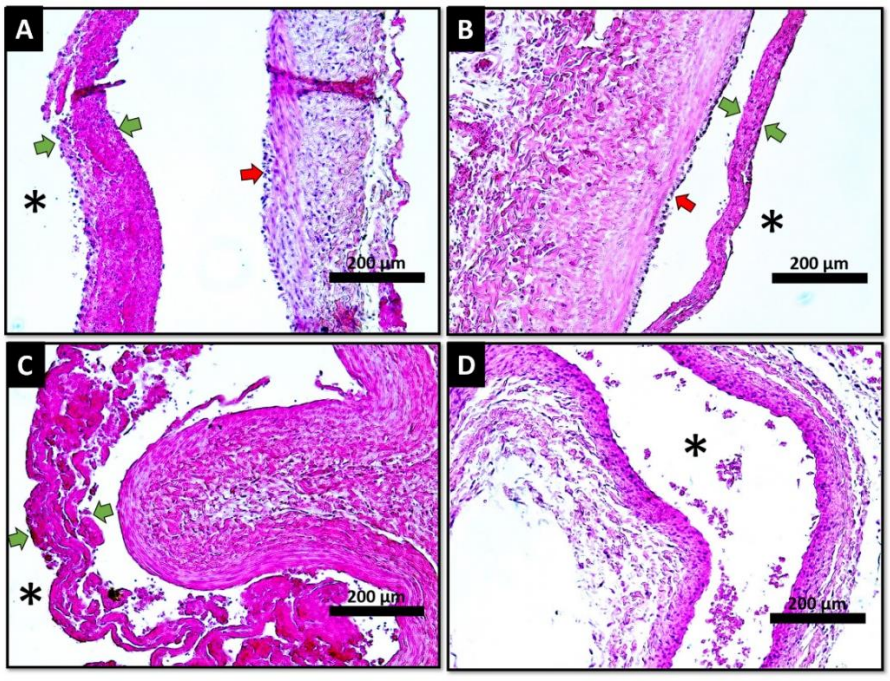

Figure 7.8: Histological imaging with hematoxylin and eosin stains post-explantation after 7 d of implantation in rabbit model. A) Control Catheter – Endothelium and SMC proliferation is seen along with detached thrombus formation B) Zwitterion catheter – endothelium and SC proliferation is seen along with detached thrombus formation C) NO catheter – Little to no SMC proliferation present and thrombus formation is seen D) Z-NO catheter – rare occurrences of clotting and little to no SMC proliferation is seen. [* indicates lumen location, Red Arrow = endothelium and SMC proliferation, Green Arrow = detached thrombus formation]

Conclusions

Vascular catheters with non-fouling, antimicrobial, and antithrombotic activity were developed using phosphorylcholine-based polyzwitterionic copolymer (2 methacryloyloxyethyl phosphorylcholine-co-butyl methacrylate co-benzophenone, BPMPC) topcoat coupled with NO release. Both NO and Z-NO formulations released physiological levels of NO over 1 week. Initial functionalization of the zwitterionic top coat was confirmed via decreases in the contact angle from ca. 100° (control, NO) to 60° (ZI, Z-NO). The presence of the ZI topcoat did significantly affect the release kinetics of NO, and the Z-NO combination demonstrates a 97.2 ± 1.3% reduction in viable *S. aureus* after 7 d in a CDC bioreactor environment. The Z-NO combination withstood hydrogen peroxide vapor sterilization and showed decreases in thrombosis and smooth muscle proliferation *in vivo* over 7 d rabbit model.

References

1. E. J. Brisbois, R. P. Davis, A. M. Jones, T. C. Major, R. H. Bartlett, M. E. Meyerhoff and H. Handa, *Journal of Materials Chemistry B*, 2015, **3**, 1639-1645.

2. L.-C. Xu, J. W. Bauer and C. A. Siedlecki, *Colloids and Surfaces B: Biointerfaces*, 2014, **124**, 49-68.

3. J.-J. Parienti, N. Mongardon, B. Mégarbane, J.-P. Mira, P. Kalfon, A. Gros, S. Marqué, M. Thuong, V. Pottier, M. Ramakers, B. Savary, A. Seguin, X. Valette, N. Terzi, B. Sauneuf, V. Cattoir, L. A. Mermel and D. du Cheyron, *New England Journal of Medicine*, 2015, **373**, 1220-1229.

4. K. G. Neoh, M. Li, E.-T. Kang, E. Chiong and P. A. Tambyah, *Journal of Materials Chemistry B*, 2017, DOI: 10.1039/C6TB03280J.

5. S. Franz, S. Rammelt, D. Scharnweber and J. C. Simon, *Biomaterials*, 2011, **32**, 6692-6709.

6. Z. Zhang, S. Chen, Y. Chang and S. Jiang, *The Journal of Physical Chemistry B*, 2006, **110**, 10799-10804.

7. P. B. Messersmith and M. Textor, *Nature nanotechnology*, 2007, **2**, 138-139.

8. H. Zhang and M. Chiao, *Journal of Medical and Biological Engineering*, 2015, **35**, 143-155.

9. D. F. Williams, *Biomaterials*, 2014, **35**, 10009-10014.

10. P. Kingshott, J. Wei, D. Bagge-Ravn, N. Gadegaard and L. Gram, *Langmuir*, 2003, **19**, 6912-6921.

11. S. Chen, J. Zheng, L. Li and S. Jiang, *Journal of the American Chemical Society*, 2005, **127**, 14473-14478.

12. L. Li, S. Chen, J. Zheng, B. D. Ratner and S. Jiang, *The Journal of Physical Chemistry B*, 2005, **109**, 2934-2941.

13. G. Cheng, Z. Zhang, S. Chen, J. D. Bryers and S. Jiang, *Biomaterials*, 2007, **28**, 4192-4199.

14. H. S. Sundaram, X. Han, A. K. Nowinski, J. R. Ella-Menye, C. Wimbish, P. Marek, K. Senecal and S. Jiang, *ACS Appl Mater Interfaces*, 2014, **6**, 6664-6671.

15. H. S. Sundaram, X. Han, A. K. Nowinski, N. D. Brault, Y. Li, J.-R. Ella-Menye, K. A. Amoaka, K. E. Cook, P. Marek, K. Senecal and S. Jiang, *Advanced Materials Interfaces*, 2014, **1**, n/a-n/a.

16. Q. Liu, P. Singha, H. Handa and J. Locklin, *Langmuir*, 2017, DOI: 10.1021/acs.langmuir.7b02970.

17. K. Ishihara, H. Nomura, T. Mihara, K. Kurita, Y. Iwasaki and N. Nakabayashi, *Journal of biomedical materials research*, 1998, **39**, 323-330.

18. F. C. Fang, *Nitric oxide : biology and chemistry / official journal of the Nitric Oxide Society*, 2012, **27, Supplement**, S10.

19. A. W. Carpenter and M. H. Schoenfisch, *Chem Soc Rev*, 2012, **41**, 3742-3752.

20. P. Singha, J. Pant, M. J. Goudie, C. D. Workman and H. Handa, *Biomaterials Science*, 2017, DOI: 10.1039/C6BM00948D.

21. E. J. Brisbois, H. Handa, T. C. Major, R. H. Bartlett and M. E. Meyerhoff, *Biomaterials*, 2013, **34**, 6957-6966.

22. M. J. Goudie, E. J. Brisbois, J. Pant, A. Thompson, J. A. Potkay and H. Handa, *International Journal of Polymeric Materials and Polymeric Biomaterials*, 2016, **65**, 769-778.

23. P. Klement, Y. J. Du, L. R. Berry, P. Tressel and A. K. Chan, *Biomaterials*, 2006, **27**, 5107-5117.

24. M. C. Frost and M. E. Meyerhoff, *Journal of the American Chemical Society*, 2004, **126**, 1348-1349.

25. M. C. Frost and M. E. Meyerhoff, *Journal of Biomedical Materials Research Part A*, 2005, **72**, 409-419.

26. J. Pant, M. J. Goudie, S. P. Hopkins, E. J. Brisbois and H. Handa, *ACS Applied Materials & Interfaces*, 2017, **9**, 15254-15264.

27. P. Singha, J. Locklin and H. Handa, *Acta Biomaterialia*, 2017, **50**, 20-40.

28. G. R. Corey, *Clinical Infectious Diseases*, 2009, **48**, S254-S259.

29. H. Ren, J. Wu, A. Colletta, M. E. Meyerhoff and C. Xi, *Frontiers in Microbiology*, 2016, **7**.

30. H. Valquier-Flynn, C. L Wilson, A. E Holmes and C. D Wentworth, *Journal of Biotechnology & Biomaterials*, 2017, **07**.

31. S. L. Percival, D. Mayer and A.-M. Salisbury, *Wound Repair and Regeneration*, 2017, **25**, 767-773.

32. K. K. Kandimalla, E. Borden, R. S. Omtri, S. P. Boyapati, M. Smith, K. Lebby, M. Mulpuru and M. Gadde, *Journal of Pharmaceutical Sciences*, 2013, **102**, 2096-2101.

33. E. J. Brisbois, T. C. Major, M. J. Goudie, M. E. Meyerhoff, R. H. Bartlett and H. Handa, *Acta Biomaterialia*, 2016.

34. M. J. Goudie, J. Pant and H. Handa, *Scientific Reports*, 2017, **7**.

35. K. A. Amoako, H. S. Sundaram, A. Suhaib, S. Jiang and K. E. Cook, *Advanced Materials Interfaces*, 2016.

36. D. Z. Xiang, E. Verbeken, A. Van Lommel, M. Stas and I. De Wever, *Eur. Surg. Res.*, 2000, **32**, 236-245.

37. J. L. Baskin, C.-H. Pui, U. Reiss, J. A. Wilimas, M. L. Metzger, R. C. Ribeiro and S. C. Howard, *The Lancet*, 2009, **374**, 159-169.

38. S. Kim, Y. Kim and S.-B. Moon, *J. Pediatr. Surg.*, 2015, **50**, 1928-1932.

CHAPTER 8

CONCLUSIONS AND FUTURE DIRECTIONS

As the research for developing an infection- and thrombo- resistant biomaterial continues, several approaches have been explored to meet the critical requirements of a biocompatible biomaterial. The two broad categories for these approaches are: passive and active. Passive approaches include antifouling strategies such as polyzwitterionic polymers and hydrophilic polymers. Passive approaches involve mechanisms like steric repulsion and low surface energy in which macromolecules do not interact with the material. They are only repelled by the surface. Thus, while not killing bacteria or inactivating proteins, they can still reduce or prevent fouling of the surface. Active surfaces include molecules embedded in them which on interaction with physiological molecules have beneficial effects. Some of the active approaches include heparin, metal nanoparticles, and nitric oxide (NO). In the recent years, NO has become a popular strategy to explore since it has both the beneficial properties of antimicrobial and antithrombotic agents combined.

This dissertation studies and reports results from developing hybrid medical device coatings that have both NO releasing properties and antifouling characteristics. Thus, by combining an active approach (NO) and different passive approaches, these materials impart antifouling, antithrombogenic, and antimicrobial properties to the coatings. To explore increased antimicrobial efficacy, in the first chapter, a NO-releasing material is combined with metal nanoparticles, specifically ZnO nanoparticles, which have catalytic and additive antimicrobial

effects on the NO-releasing polymer. In the following chapters of the dissertation, NO-releasing materials are combined with different antifouling strategies to provide protection from protein fouling, platelet aggregation, and biofilm formation. Thus, the results seen from *in vitro* and *in vivo* studies demonstrate the potential of combining NO releasing materials with other antifouling strategies.

From the perspective of medical device coating fabrication, the work done in this dissertation can be improved upon by including hydrogel materials which have been recently used commercially (Bard catheters) for the dispersal of silver as antimicrobial agents. NO-releasing silica nanoparticles, which have been synthesized by our lab, could be used as a source for NO-release within hydrogel as hydrogels would require a more stable NO donor due to the high-water uptake efficacy. In addition to being immobilized on silicones for medical device coatings, this type of hydrogel based NO delivery would increase the variety of applications that NO could be used for, including wound healing and surgical site or acne treatment topical antimicrobial applications. Another method of medical device coating that could be explored is the layer-by-layer technique to incorporate several other agents for increasing the antifungal properties of these coatings. NO-releasing layers could be alternated with layers containing antifungal agents already available in the market. Since a higher dose of NO is required to kill fungi, these broad-spectrum coatings would provide better protection.

In terms of NO release from materials, it will be important to maintain NO release that is antimicrobial in nature. This will mitigate the problem of antimicrobial resistance development within the body that typically happens due to low dose of antibiotics that does not kill all microbes and hence aids in the survival of resistant microbes. A possible strategy to ensure the required NO release would be to measure NO release through the delivery platform and only use

the platform for the span of time that the FDA approves to be antimicrobial in nature (3 log reduction).

While these results show a promising future for the utilization of NO releasing materials in short term applications (up to 7 days) in both *in vitro* and *in vivo* studies, it sets the groundwork for long term applications, wherein the biological applications remain viable for months or even years. As research continues to synthesize materials for longer sustained NO release, antimicrobial and antithrombotic studies could be carried out for longer periods of time in dynamic flow conditions. In chapter 7, a CDC bioreactor has been used to test the antimicrobial efficacy for a week. This can be further improved upon by including both high shear (CDC continuous flow bioreactor) and low shear (drip flow bioreactor) for use of the materials in different applications (vascular vs. urinary catheters). Another way to study antimicrobial efficacy of the materials fabricated would be to test them against polymicrobial infection causing agents. Most antibiotic therapies are selected to target only one strain of microbes without any consideration for the other microbes present in the same environment. However, most times the presence of one microorganism can provide a niche for other pathogenic microorganisms or the presence of two non-pathogenic microorganism colonies can together cause an infection. These polymicrobial infections have to be taken into account if we want a true representation of the microbial flora in *in vitro* studies for antimicrobial efficacies. Investigations through quantitative studies like flow cytometry, bioreactors, and qualitative analyses like scanning electron microscopy (SEM) will be essential for polymicrobial infections. Additionally, the same quantification methods could be used for devices used in *in vivo* studies for antimicrobial models. For antithrombotic studies, the work in the dissertation is focused mainly on the quantification of adhered platelets and observation of clots with SEM. In the

future, whole blood studies could be performed *in vitro* as this would more closely mimic the physiological vascular environment. Another modification that can be done *in vitro* would be to add a monolayer of endothelium to mimic the endothelium layer present in the vasculature. This would represent the physiology because the endothelium layer would release factors that are normally found in the vasculature whereas the current blood tubes do not mimic the vasculature. Additionally, explanted devices from the *in vivo* studies could be quantitatively analyzed for clot formation and histology by increasing the images taken and labeling for various types of cells and proteins (erythrocytes, thrombocytes, leukocytes, fibrinogen, albumin) found in a thrombus.

In conclusion, while the researches done shines light into the additive and synergistic effects of combining the passive and active approaches, more such combination approaches can be explored in the future while also understanding the mechanisms of their synergistic mechanisms. The investigation of these underlying mechanisms could shed light into the better strategies for long term applications. Additionally, in the future NO releasing materials can be combined with other such therapeutic approaches for wound healing, cancer treatment, and cardiovascular diseases.

APPENDICES

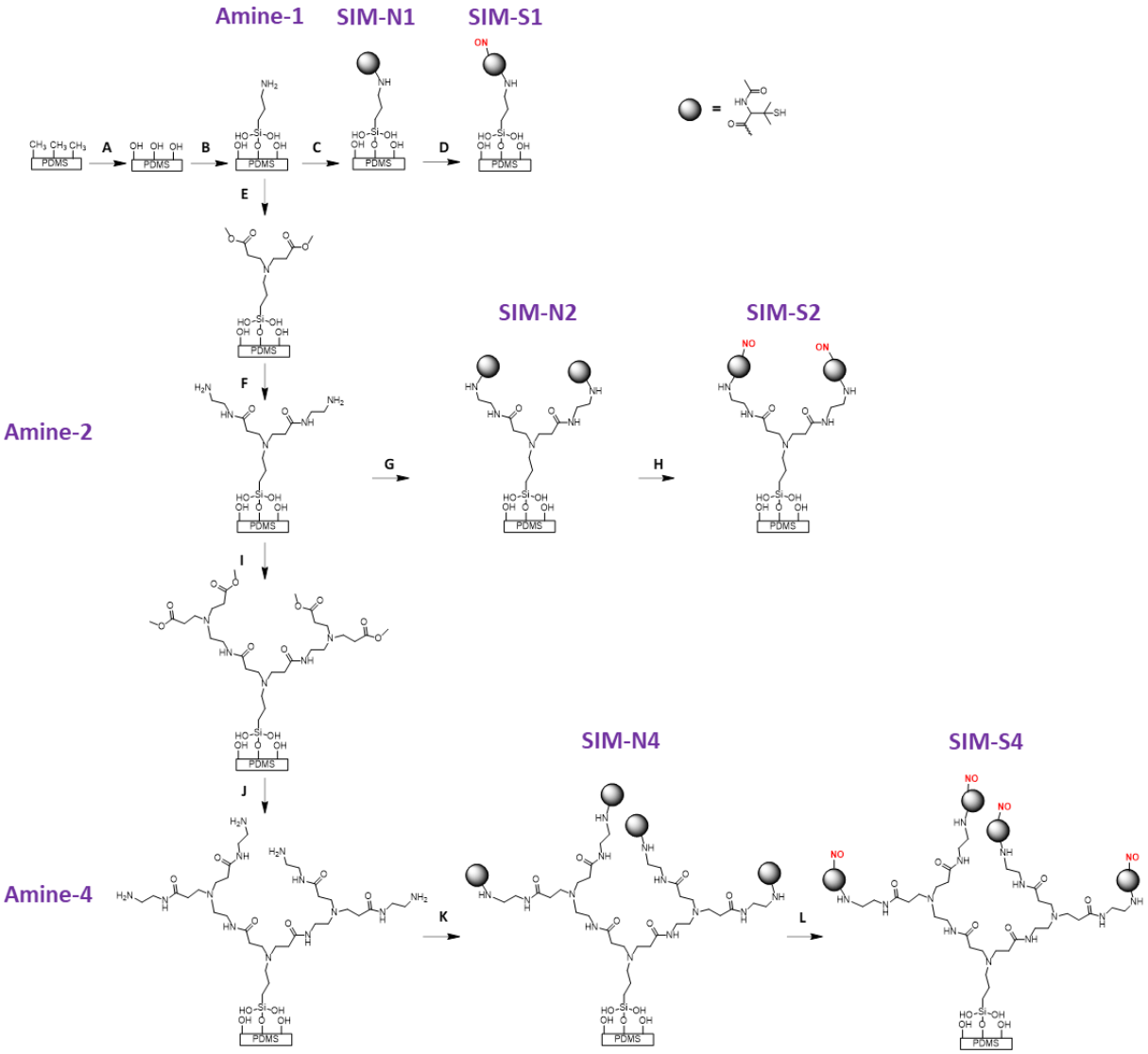

Appendix 1: Detailed schematic of various SIM surfaces.

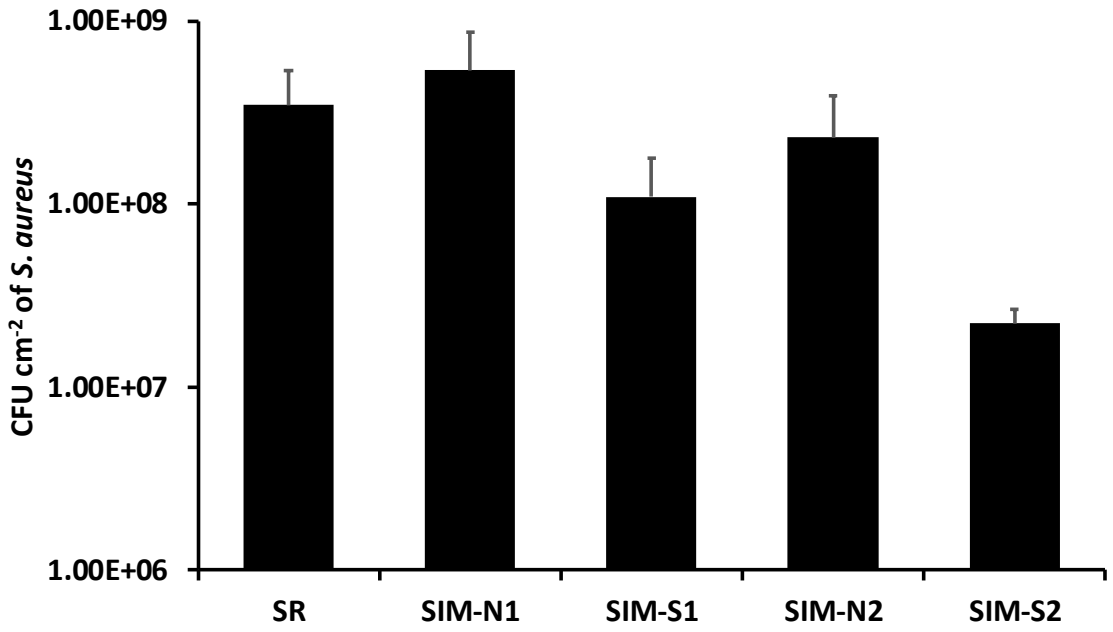

Appendix 2: CFU of *S. aureus* per cm^2 of sample after 24 h exposure to fibrinogen from human serum followed by 24 h of *S. aureus* incubation under physiological conditions (n=5)

Appendix 3: Day by day NO release measurements for 600 h/25 d. (n=3)

NO Flux ($\times 10^{-10}$ mol min^{-1} cm^{-2})	1 h	4 h	8 h	12 h	36 h	60 h	84 h	108 h	132 h	156 h	240 h	360 h	480 h	600 h
SIM-S1	1.633 ± .835	0.795 ± .228	0.566 ± .076	0.216 ± .060	0.108 ± .035									
SIM-S2	3.733 ± .375	3.335 ± .986	3.935 ± .849	3.677 ± .515	3.228 ± .053	3.013 ± .614	2.391 ± .524	1.976 ± .822	1.493 ± .659	1.496 ± .349	1.203 ± .331	.626 ± .060	0.404 ± .049	0.305 ± .032
SIM-S4	10.753 ± 3.509	4.126 ± .338	2.946 ± .466	2.547 ± .186	1.706 ± .317	1.763 ± .449	1.122 ± .180	1.012 ± .204	0.836 ± .324	0.673 ± .132	0.441 ± .096	0.316 ± .090	0.174 ± .027	0.085 ± .008

Appendix 4: Cumulative NO release over 600 h/25 d.

Cumulative NO Release ($\times 10^{-10}$ mol cm^{-2})	1 h	4 h	8 h	12 h	36 h	60 h	84 h	108 h	132 h	156 h	240 h	360 h	480 h	600 h
SIM-S1	98 ±50	316 ±65	479 ±66	573 ±66	807 ±67									
SIM-S2	223 ±22	860 ±179	1732 ±235	2645 ±253	7617 ±253	12110 ±276	16002 ±292	19147 ±327	21645 ±348	23798 ±354	30599 ±359	37183 ±359	40889 ±359	43442 ±359
SIM-S4	645 ±211	1984 ±219	2833 ±235	3492 ±237	6554 ±244	9052 ±257	11129 ±259	12666 ±261	13997 ±268	15084 ±269	17894 ±269	20621 ±270	22386 ±270	23320 ±270

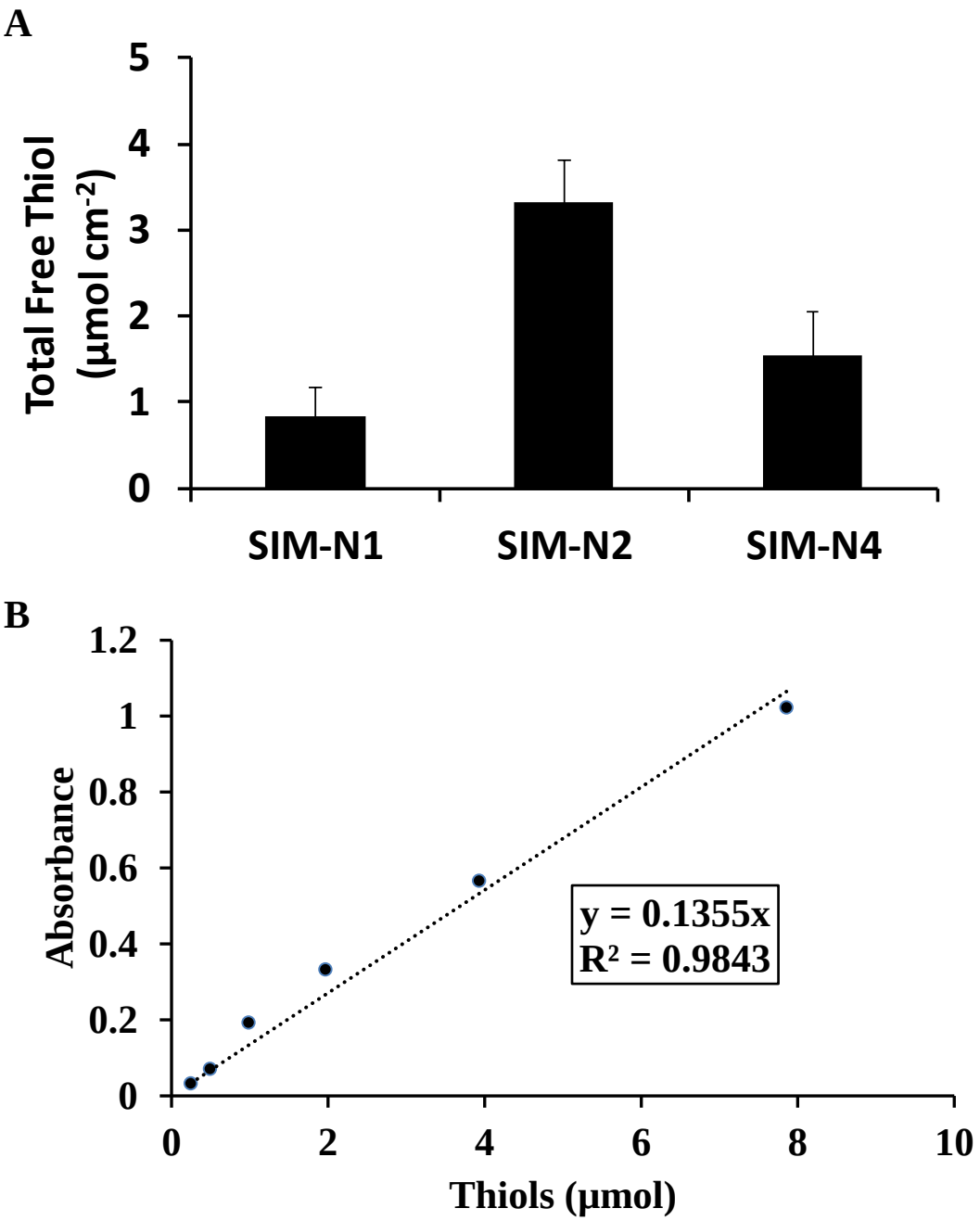

Appendix 5: A) Quantification of free thiols on various SIM surfaces. B) Calibration curve of free thiols.

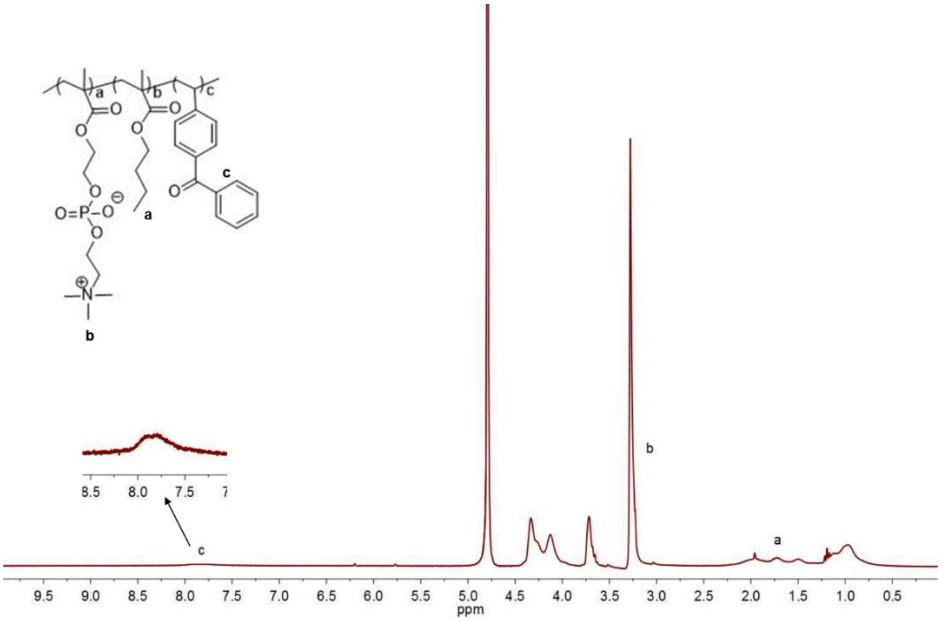

Appendix 6: ^{1}H NMR spectrum of copolymer BPMPC in D_2O

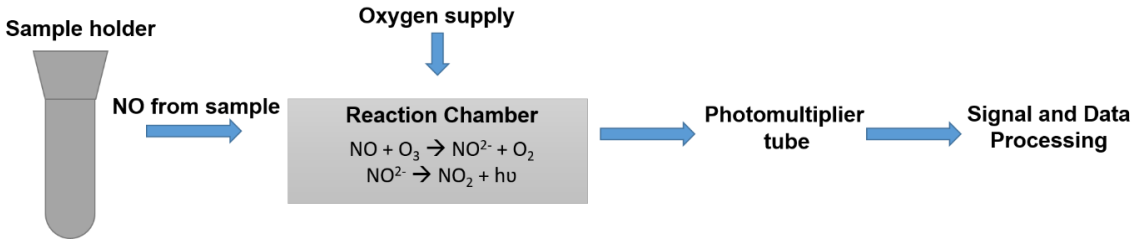

Appendix 7: Nitric oxide chemiluminescence analyzer flowchart

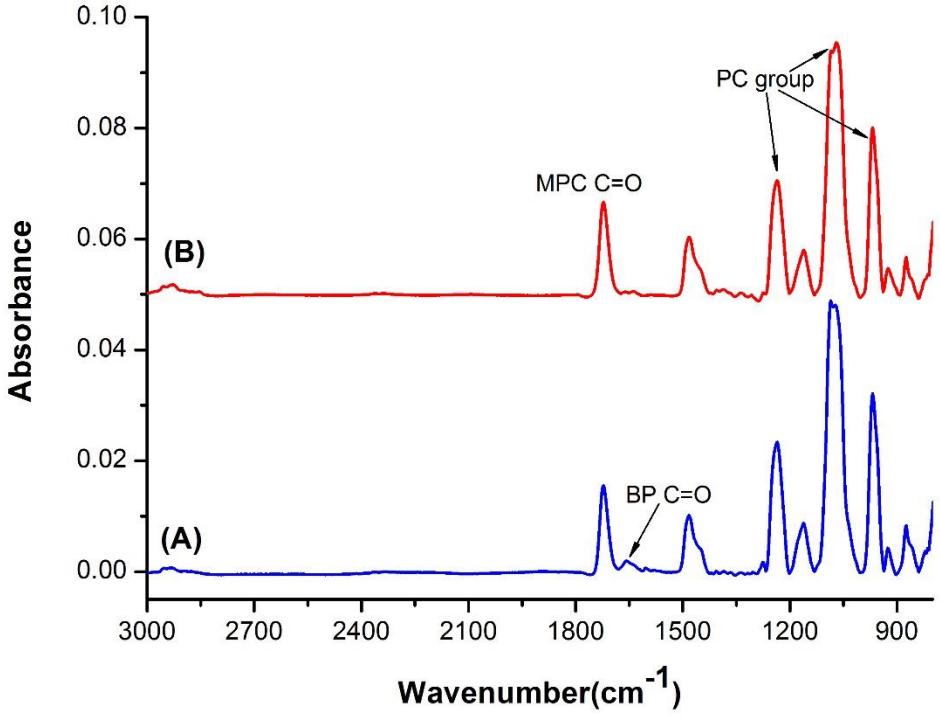

Appendix 8: ATR-FTIR spectra of BPMPC coatings before (A) and after (B) UV exposure.

Appendix 9: Fluorescence intensity analysis of FITC-BSA adsorption images by using ImageJ.

Fluorescence Intensity	90 minutes FITC-BSA	1 Day BSA 90 minutes FITC-BSA	7 Days BSA 90 minutes FITC-BSA
Control	16,612	66,158	173,792
Coated	10,327	21,848	24,241